SPECTRUM SENSING TECHNIQUES IN WIRELESS COMMUNICATION NETWORKS

A thesis submitted to the University of Manchester
for the degree of Doctor of Philosophy
in the Faculty of Engineering and Physical Sciences

2013

By
Abubakar Umar Makarfi
School of Electrical and Electronic Engineering
Microwave and Communication Systems Research Group

Contents

Abstract 12

Declaration 14

Copyright 15

Acknowledgements 16

About the Author 17

List of Abbreviations 19

List of Variables 22

List of Mathematical Notations 25

1 Introduction 27
- 1.1 Spectrum Access Techniques . . . 27
- 1.2 The Cognitive Radio . . . 28
- 1.3 Towards Achieving DSA . . . 30
  - 1.3.1 Policy Issues . . . 30
  - 1.3.2 Standardisation . . . 31
- 1.4 Aims and Objectives . . . 33
- 1.5 Key Contributions . . . 34
- 1.6 Thesis Organisation . . . 38
- 1.7 Publications . . . 39

2 Literature Review 40
- 2.1 Spectrum Sensing . . . 40
  - 2.1.1 Spectrum Holes . . . 41

2.1.1.1 Spatial Dimension 41
2.1.1.2 Spectral Dimension 42
2.1.1.3 Temporal Dimension 42
2.1.1.4 Angular Dimension 42
2.1.1.5 Code Dimension 43
2.1.2 Challenges of Spectrum Sensing 43
2.1.2.1 Sensing Duration and Frequency 43
2.1.2.2 Hidden Terminal Problem 44
2.1.2.3 Detecting Spread Spectrum Primary Users . . 44
2.1.2.4 Aggregate Interference and Noise Uncertainty 45
2.1.2.5 Multi-User Networks 45
2.1.2.6 Hardware Prerequisites 45
2.1.2.7 Regulatory constraints 46
2.1.2.8 Security 46
2.2 Spectrum Sensing Methods 47
2.2.1 Interference Based Detection 47
2.2.2 Transmitter Based detection 49
2.2.2.1 Matched Filtering 49
2.2.2.2 Cyclostationary Feature Detection 51
2.2.2.3 Energy Detection 51
2.3 The Energy Detector 51
2.3.1 The Energy Detector Model 53
2.3.2 Performance Evaluation of the ED 53
2.4 Interference in DSA Networks 55
2.4.1 Interference to the Primary Network 56
2.4.2 Interference to the CR Network 57
2.4.3 Interference Mitigation 58
2.5 Multiple Access and Coexistence Techniques 59
2.5.1 Code Division Multiple Access 60
2.5.1.1 Frequency Hopping Spread Spectrum 61
2.5.2 Random Multiple Access 61
2.5.2.1 CSMA 62
2.6 Chapter Summary 63

3 **Alternate Detection Techniques** 65
3.1 Background . . . 65
3.2 The Power Law Detector . . . 67
3.2.1 Approximations . . . 68
3.2.1.1 The New Approximation . . . 68
3.2.1.2 Gamma Approximation . . . 70
3.2.2 Results and Analysis . . . 72
3.3 Kay's Detector . . . 75
3.3.1 Probability of False Alarm over AWGN Channels . . . 76
3.3.2 Probability of Detection over AWGN Channels . . . 76
3.3.3 Detection Probability under Fading Channels . . . 77
3.3.3.1 Rayleigh Fading . . . 79
3.3.3.2 Nakagami-m Fading . . . 79
3.3.4 Results . . . 80
3.4 Chapter Summary . . . 81

4 **Efficiency of Detectors in the Presence of Co-Channel Interference** 85
4.1 Background . . . 85
4.2 Basic Interference Model . . . 89
4.2.1 The System Model . . . 89
4.2.2 False Alarm and Detection Probabilities . . . 91
4.2.2.1 Detection Probability under Non-Negligible Missed Detections . . . 94
4.2.3 Computation of the MGF . . . 95
4.3 Correlated Active CR Nodes . . . 96
4.3.1 The System Model . . . 97
4.3.2 False Alarm and Detection Probabilities . . . 98
4.3.3 Computation of the MGFs . . . 100
4.3.3.1 Approximation . . . 100
4.3.3.2 Upper Bound . . . 102
4.3.4 Recursive Algorithm . . . 103
4.4 Poisson Field of SU Interferers . . . 104
4.4.1 The System Model . . . 104
4.4.2 False Alarm and Detection Probabilities . . . 105
4.4.2.1 Computation of the MGF . . . 106
4.4.2.2 Exact Solution of P_{f} and P_{d} . . . 107

4.5 The Matched Filter Detector 108
4.5.1 False Alarm and Detection Probabilties 109
4.5.2 Computation of the MGFs 111
4.6 Results 112
4.6.1 Effectiveness against the Gaussian Approximation . . . 112
4.6.2 Effect of Modified Path Loss Model 113
4.6.3 General Detector Performance 114
4.6.4 Effect of Number of Observed Samples 117
4.6.5 Correlated Active CR nodes 120
4.6.6 Comparison against the MFD 123
4.7 Chapter Summary 124

5 Efficiency of Energy Detectors for Wideband Sensing of Frequency Hopping Users 126
5.1 Background 126
5.2 Equal PU-SU Frame Length, Synchronised Time Slot 128
5.2.1 The System Model 128
5.2.2 Detection Analysis 129
5.2.2.1 Subband Detection 130
5.2.2.2 Wideband Joint Detection 131
5.2.3 Transmission Analysis 132
5.3 Equal PU-SU Frame Length, Unsynchronised Time Slot 134
5.3.1 The System Model 134
5.3.2 Detection Analysis 135
5.3.2.1 Subband Detection 135
5.3.2.2 Wideband Joint Detection 135
5.3.3 Transmission Analysis 137
5.4 Unequal PU-SU Frame Length 138
5.4.1 The System Model 139
5.4.2 Detection Analysis 140
5.4.2.1 Subband Detection 140
5.4.2.2 Wideband Joint Detection 142
5.4.3 Transmission Analysis 143
5.4.3.1 Subband Capacity 143
5.4.3.2 Wideband Channel Throughput 144
5.5 Subband Throughput Optimisation 148

5.6 Results and Discussion 149
5.7 Chapter Summary 155

6 Efficiency of Energy Detectors for CSMA based Networks 156
6.1 Background 156
6.2 The Model 159
6.2.1 Transmission and Reception 159
6.2.2 Media Access Control 160
6.3 Performance Analysis 163
6.3.1 Transmission Probability 163
6.3.1.1 PCS-only protocol 163
6.3.1.2 Hybrid PCS and VCS protocol 165
6.3.2 Throughput 166
6.4 Results 167
6.5 Chapter Summary 171

7 Conclusions and Future Work 172
7.1 Conclusions 172
7.2 Future Work 174

References 177

A Mathematical Transformations 195
A.1 Summary of Novel Transformations 195
A.2 Other Important Transformations 196

Word Count: 55,121

List of Tables

5.1 Probabilities of hop scenarios 146

List of Figures

1.1 Simplified cognitive cycle. 29

2.1 An Illustration of the Hidden Node Problem. 44
2.2 Hierarchy of spectrum sensing techniques. 48
2.3 Comparison of various sensing methods. 50
2.4 Overview of multiple access techniques. 60

3.1 PDFs for the sum of i.i.d pth powered Gaussian RVs. $N = 4$ (dashed curves) and $N = 8$ (solid curves). 71
3.2 CDFs for the sum of i.i.d pth powered Gaussian RVs. $N = 4$ and $N = 8$. Exponent $p = 1, 3$ and 4.5 71
3.3 ROC for $p = 1$, $N = 8$. The $P_{\mathrm{f}}^{\mathrm{pld}}$ and $P_{\mathrm{d}}^{\mathrm{pld}}$ are plotted from (3.19) and (3.20), while the gamma approximations are from (3.24) and (3.25). 74
3.4 ROC for $p = 3$, $N = 8$. The $P_{\mathrm{f}}^{\mathrm{pld}}$ and $P_{\mathrm{d}}^{\mathrm{pld}}$ are plotted from (3.19) and (3.20), while the gamma approximations are from (3.24) and (3.25). 74
3.5 ROC curves for an AWGN channel. Both detectors compared. Analytical curves for Kay's detector from (3.31) and (3.32), while ED curves using (2.4) and (2.6). 82
3.6 ROC curves for a Rayleigh faded channel. Both detectors compared. Analytical curves for Kay's detector using (3.31) and (3.45), while ED curves using (2.4) and (2.7). 82
3.7 Probability of detection curves for a Nakagami-m faded channel comparing effect of varying the detection threshold against the parameter m and SNR. Analytical curves for Kay's detector from (3.48). 83

3.8 Probability of detection curves for a Nakagami-m faded channel comparing effect of varying the detection threshold against the parameter m and number of samples N. Analytical curves for Kay's detector from (3.48). 83

4.1 Spectrum sensing node in the presence of multiple secondary user interferers 89
4.2 Variation of false alarm probability P_{f} with changing number of active interferers K_0, comparing the GA method from Eq. (4.75) with the computed exact result obtained by substituting Eqs. (4.23) and (4.22) into (4.11). Detection threshold $\xi = 10$ and SU transmit power $p_{\mathrm{s}} = 1$. 114
4.3 Error probability P_{e} against detection threshold ξ for Poisson interferers illustrating effect of changing interferer density λ and path loss exponent β. SU transmit power $p_s = 1$. 115
4.4 Minimised error probability P_{e} at the optimal threshold ξ_{opt} against interferer density λ [interferer/m^2] for Poisson interferers illustrating effect of different PU signal-to-noise ratio. . 115
4.5 Optimal threshold ξ_{opt} for minimum error against interferer density λ [interferer/m^2] at different PU signal-to-noise ratios. 116
4.6 Complementary ROC curves showing performance of sensing node under different interferer densities λ [interferer/m^2]. . . . 118
4.7 P_{e} against ξ comparing effect of interferer density λ [interferer/m^2] on sensing. $\Pr(H_0) = 0.5$ and $N = 10$. 118
4.8 P_{e} against N illustrating the effect of various interferer densities λ [interferer/m^2] with respect to changing detection threshold ξ. 119
4.9 P_{e} against N, comparing the effect of various interferer densities λ [interferer/m^2] for different $\Pr(H_0)$. 119
4.10 Probability of false alarm against number of secondary users at different detection thresholds ξ. 121
4.11 Error probability against detection threshold 122
4.12 Minimum error probability against potential interferers at optimal detection threshold 122
4.13 ROC curves of an energy detector for varying number of interfering nodes. 123

4.14 ROC curves of a matched filter detector for varying number of interfering nodes. Curves plotted with (4.71) and (4.72). 124

5.1 Illustration of a two primary user system employing frequency hopping to access a wideband channel. $T_{\mathrm{h}} = T$, $W_{\mathrm{h}} = W_{\mathrm{r}}$ 129
5.2 FH misaligned Illustration. τ = sensing frame, $T - \tau$ = transmission frame and $T_{\mathrm{h}} = T$ (but misaligned). 134
5.3 Illustration of unequal PU hop duration T_{h} and ED sensing-transmission time slot T for a single PU network (i.e. $T \neq T_{\mathrm{h}}$). τ = sensing frame of SU and $T - \tau$ = transmission frame of SU. 140
5.4 Achievable throughput against interference for aligned PU hop duration and ED time frames comparing different number of PUs K. Sensing time $\tau = 0.1T$ 150
5.5 Achievable throughput against interference for aligned PU hop duration and ED time frames comparing the effect of varying the sensing time τ. Number of PU $K = 1$ 150
5.6 Throughput performance for misaligned PU hop duration and ED time frames illustrating the effect of misalignment within the ED sensing time $0 < a \leq \tau$. Number of PU $K = 1$. Sensing time $\tau = 0.1T$ 152
5.7 Throughput performance for misaligned PU hop duration and ED time frames showing misalignment within the ED transmission time $(T - \tau) < a' \leq T$. Number of PU $K = 1$. Sensing time $\tau = 0.1T$ 152
5.8 Achievable SU throughput against interference to PU. $K = 1$, $\rho = 0.75$, varying sensing time τ and $T < T_{\mathrm{h}}$. 154
5.9 Achievable SU throughput against interference to PU. $K = 1$, varying ρ, varying sensing time τ and $T > T_{\mathrm{h}}$. 154

6.1 Illustration of the PPP and MH processes generated through simulation. 162
6.2 Transmission probability against detection threshold for both coexistence protocols. Node density $\lambda = 0.01$, path loss exponent $\beta = 3$ and inhibition radius for VCS $r_{\min} = 1$. 168

6.3 Analytical results for transmission probability against node density for both coexistence protocols at different detection thresholds ξ. Path loss exponent $\beta = 3$ and inhibition radius for VCS $r_{\min} = 1$. 168
6.4 Analytical results for throughput against inhibition radius for the combined physical and virtual sensing protocol. Path loss exponent $\beta = 3$, detection threshold $\xi = 1$ and varying traffic densities. 169
6.5 Analytical results for transmission probability against inhibition radius for the combined physical and virtual sensing protocol. Path loss exponent $\beta = 3$, detection threshold $\xi = 1$ and varying traffic densities. 169

Abstract

Recent studies have confirmed that the currently employed spectrum management schemes have brought major inefficiencies in the usage of the frequency spectrum. As a result, dynamic spectrum access (DSA) technologies have been proposed to enable intelligent reuse of the frequency spectrum by secondary users (SUs). However, the SUs should be capable of sensing the surrounding wireless scene, in order to avoid harmful interference to the primary users (PUs) of the network. Several challenges that are generally encountered when conducting spectrum sensing have been identified. Thus, the main focus of this thesis is to address the highlighted coexistence and spectrum sensing challenges, while trying to overcome the shortcomings inherent within the selected sensing technique.

The contributions of this study are explained as follows. The energy detector (ED) was examined under co-channel interference (CCI). The obtained mathematical models are derived using a moment generating function (MGF) approach. This approach provides several advantages over direct approaches, one of which is that it greatly simplifies averaging-out the random variables involved. Furthermore, the problem of detecting spread spectrum users was tackled. This issue was investigated by examining the efficiency of EDs to exploit opportunities resulting from the use of slow frequency hopping by the PUs. In addition, in order to curb the hidden node problem and due to the fact that coexistence etiquettes are not perfect against interference, the efficiency of EDs was further investigated under two simple multiple access protocols that do not require any centralised control.

Furthermore, three other detector types were investigated. Firstly, the power law detector, which is a generalisation of the ED, for which no known exact PDFs exist for the statistics of its decision variable. Hence, approximations are generally relied upon. Here, novel precise approximations for the

PDF and CDF of the PLD's decision variable were presented. Secondly, the performance of Kay's detector for unknown deterministic signals was analysed under AWGN, Rayleigh and Nakagami fading channels by deriving the relevant closed-form analytical expressions. Finally, the robustness of a matched filter detector in the presence of CCI was investigated. For all the detectors, accurate mathematical transformations were derived and their performance compared against the ED.

Declaration

No portion of the work referred to in this thesis has been submitted in support of an application for another degree or qualification of this or any other university or other institute of learning.

Copyright

Acknowledgements

I would like to thank the Almighty for granting me this priceless opportunity to further my studies through a research degree.

The help and support of my supervisor Dr. Khairi Ashour Hamdi, was of immense value and sincerely appreciated. His guidance, encouragement, in-depth knowledge, commitment and confidence in me have been a source of constant motivation during this long and tedious process. I would also like to express my gratitude to my advisor Dr. Emad A. Alsusa for providing his valuable advice and words of encouragement at key times during this study.

I also owe deep gratitude to my loving parents who always showered me with their love, guidance, support, encouragement and prayers. I am sure you will both be proud of my accomplishments. My gratitude also goes to my dear wife Jamila who was always by my side during this entire process, supporting me during difficult times. Much love to my two little ones Muhammad and Hawwa-Jidda for always cheering me up and filling my heart with happiness. I would also like to thank all my siblings for their prayers over the years and my mother-in-law for her continuous support.

Sincere appreciation also to my colleagues, past and present at the research group and in particular Azwan, Fahimeh, Khaled, Javad, Tarla, Maksims, Sarmad, Rashid and Laith. You have helped, encouraged, cheered and even scolded me from time to time and your acquaintance gave me a rich and rewarding experience as a PhD student. My special thanks also goes to Dr. Junaid Ahmed who mentored me from the very beginning and whose support may have even prevented me from quitting and Dr. Ebtihal H.G. Yousif who constantly inspired me academically and otherwise.

Finally, I would like to acknowledge the financial support from the Petroleum Technology Development Fund (PTDF), Nigeria.

About the Author

Mr Abubakar Umar Makarfi received the B.Eng. degree (with first-class honors) in Electrical and Electronic Engineering from the Nigerian Defence Academy, Kaduna, Nigeria in 2001 and the M.Tech. degree in Telecommunications and Electronics Engineering from Obafemi Awolowo University, Ife, Nigeria in 2005.

From 2002 to 2009, he worked with the Nigerian Navy in various capacities as a Communications and Electronics Engineer. He is currently studying towards a Ph.D. degree in Wireless Communications with The University of Manchester, Manchester, U.K with a focus on cognitive radio, spectrum sensing, interference analysis and multiple access techniques.

Mr. Makarfi is a member of IEEE, member of the Nigerian Society of Engineers and a corporate member of the Council for the Regulation of Engineering in Nigeria.

To my dad,
who is not with us today to witness the fruit of our labours.

List of Abbreviations

AFH	Adaptive Frequency Hopping
AP	Access Point
AWGN	Additive White Gaussian Noise
CCI	Co-Channel Interference
CDF	Cumulative Distribution Function
CLT	Central Limit Theorem
CR	Cognitive Radio
CSMA	Carrier Sense Multiple Access
CTS	Clear-to-Send
DCF	Distributed Coordination Function
DoF	Degrees of Freedom
DSA	Dynamic Spectrum Access
DSSS	Direct Sequence Spread Spectrum
EC	European Commission
ED	Energy Detector
FCC	Federal Communications Commission
FH	Frequency Hopping
GA	Gaussian Approximation
GPS	Global Positioning System
IEEE	Institute of Electrical and Electronics Engineers

i.i.d.	Independent and Identically Distributed
ISM	Industrial, Scientific and Medical Band
LBT	Listen-before-Talk
MAC	Media Access Control
MFD	Matched Filter Detector
MGF	Moment Generating Function
OFDM	Orthogonal Frequency Division Multiplexing
PCF	Point Coordination Function
PCS	Physical Carrier Sensing
PDF	Probability Density Function
PER	Primary Exclusive Region
PLD	Power Law Detector
PPP	Poisson Point Process
PU	Primary User
ROC	Receiver Operating Characteristics
RTS	Request-to-Send
RV	Random Variable
SDR	Software Defined Radio
SINR	Signal-to-Interference and Noise Ratio
SLC	Square Law Combining
SNR	Signal-to-Noise Ratio
SS	Spectrum Sensing
SSI	Simple Sequential Inhibition
SU	Secondary User
UWB	Ultra-Wide Band
VCS	Virtual Carrier Sensing

WLAN Wireless Local Area Network

WPAN Wireless Personal Area Network

WRAN Wireless Regional Area Network

xG Next Generation

List of Variables

β	path loss exponent
C_0	capacity of an idle subband
C_1	capacity of an active subband
δ_k	status of the kth node
f_s	sampling frequency
$\overline{\gamma}$	average signal-to-noise-ratio
H_0	null hypothesis
H_1	alternate hypothesis
$i\,(t)$	continuous-time interfering signal
$i\,(n)$	discrete-time interfering signal
m	Nakagami-m shape parameter
M	sampled equivalent of secondary user time frame
N	number of samples received during sensing period
N_0	single sided noise power spectral density
p_k	kth user transmit power
p_p	primary user transmit power

p_{s}	secondary user transmit power
p_{w}	noise power
P_{d}	probability of detection
P_{D}	probability of detection for wideband channel
$P_{\mathrm{d,Nak}}$	probability of detection under Nakagami faded channel
$P_{\mathrm{d,Ray}}$	probability of detection under Rayleigh faded channel
P_{e}	probability of error
P_{f}	probability of false alarm
P_{m}	probability of missed detection
P_{M}	probability of missed detection for wideband channel
Q	number of subbands in a wideband channel
R	total throughput for wideband channel
R_0	total throughput for all idle subbands
R_1	total throughput for all active subbands
S	energy of transmitted signal
$s(t)$	continuous-time transmitted signal
$s(n)$	discrete-time transmitted signal
σ_X^2	variance of random variable X
τ	sensing time
T	secondary user time frame
T_{h}	hop duration of primary user signal

$x(t)$	continuous-time received signal
$x(n)$	discrete-time received signal
ξ	sensing threshold
Ξ	set of active subbands
γ	signal-to-noise ratio
$w(t)$	continuous-time additive white Gaussian noise process
$w(n)$	discrete-time additive white Gaussian noise process
W	bandwidth
W_{h}	primary user hop bandwidth
W_{r}	secondary user hop bandwidth

List of Mathematical Notations

$\exp(x)$	exponential function e^x
$\mathrm{Erf}(.)$	error function
$\mathrm{Erfc}(.)$	complementary error function
$\mathrm{Erfc}^{-1}(.)$	inverse complementary error function
$\mathbb{E}[.]$	expectation of a random variable
${}_1F_1(.;.;.)$	confluent hypergeometric function
$\Gamma(.)$	Gamma function
$\Gamma(.,.)$	upper incomplete gamma function
$\gamma(.,.)$	lower incomplete gamma function
$\Phi_2(.,.,.;.,.)$	Humbert series of the second type
$I_v(.)$	vth order modified Bessel function of the first kind
$J_v(.)$	vth order Bessel function of the first kind
$\log_x(.)$	logarithmic function to base x
$\mathcal{N}(\mu, \sigma^2)$	normal distribution with mean μ and variance σ^2
$\mathcal{CN}(\mu, \sigma^2)$	complex normal distribution with mean μ and variance σ^2
$(.)_n$	Pochhammer symbol
$\Pr(x)$	Probability of x
$Q(.)$	Gaussian Q-function
$Q_m(.,.)$	generalized mth order Marcum Q-function
$\mathcal{R}(.)$	autocorrelation function

$\sinh(.)$	hyperbolic sine function
$\mathrm{var}[.]$	variance of a random variable

Chapter 1

Introduction

THE current boom in the use of wireless communication technologies coupled with the fixed spectrum assignment policy which encourages inefficient spectrum usage, has caused an artificial scarcity of the radio spectrum. Consequently, regulators and entrepreneurs are demanding more spectrum to keep up with the growth and expansion of wireless services [1]. One approach employed in overcoming spectrum scarcity is *spectrum pooling*, which involves multiple spectrum license holders combining or pooling their spectrum allocations for mutual use [2]. Most recently, Dynamic Spectrum Access (DSA) also referred to as NeXt Generation (xG) communication networks have been proposed to solve this problem of inefficient spectrum usage [3]. DSA can more aptly be described as the real-time adjustment of spectrum utilisation in response to changing circumstances and objectives [2]. The efficient application of DSA techniques would enable an effective dynamic spectrum sharing environment for coexistence.

1.1 Spectrum Access Techniques

The effectiveness of spectrum access techniques are influenced by the capability of the devices employed and the regulatory policies that are in place. There are currently two main types of spectrum access techniques in various stages of approval and implementation; *underlays* and *overlays* [3]. Underlays are signals of lower power spectral density and wider bandwidth placed in the same band to overlap traditional communication signals while avoiding

interference at the primary receiver. However, a large number of such devices are likely to raise the noise floor and as a result may adversely affect the licensed user of the spectrum. In 2002, the Federal Communications Commission (FCC) approved new rules permitting the use of ultra-wide band (UWB) underlays at powers equivalent to the unintended emissions allowed for personal computers, while the European Commission (EC) approved UWB underlays for EC member countries in 2007 [4].

On the other hand, overlays involve exploiting free portions of the spectrum at a given time and location, with or without permission so as to avoid harmful interference to the licensed user of that channel [4]. There are basically two approaches to overlays; *cooperative* and *non-cooperative*. In a cooperative overlay system, a conventional radio user agrees to a new user, and in a non-cooperative system, a new user independently determines that the spectrum is available and that its transmission will not cause any harmful interference to the licensed user of the spectrum. This gives rise to opportunistic spectrum access (OSA). OSA is made possible by the use of a software-defined radio (SDR) as the basic platform for the realisation of a cognitive radio (CR).

1.2 The Cognitive Radio

An SDR is a radio in which the properties of carrier frequency, signal bandwidth, modulation, and network access are defined by software. This property of an SDR together with the capability for spectrum management and optimisations, interfacing a wide variety of network resources with a human, while providing electromagnetic resources to aid the human in his or her activities, are what will elevate the SDR to the status of a full CR [5]. A CR is the key technology that enables an xG network to use spectrum in a dynamic manner and should be able to provide efficient utilisation of the radio spectrum and highly reliable communication whenever and wherever needed [6]. A *cognitive radio* can therefore be defined as

> "A radio or system that senses its operational electromagnetic environment and can dynamically and autonomously adjust its radio operating parameters to modify system operation, such as maximise throughput, mitigate interference, facilitate interoperability and access secondary markets [7]."

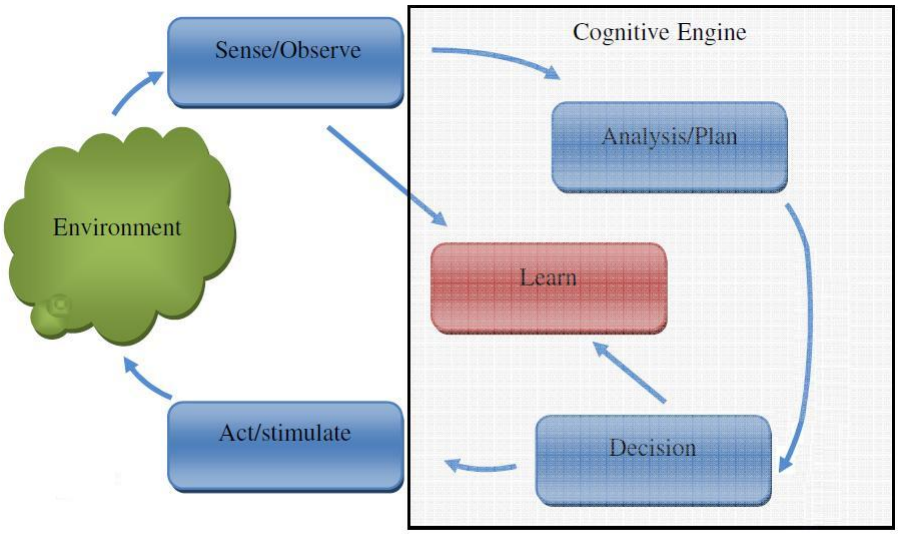

Figure 1.1: Simplified cognitive cycle.

Fig. 1.1 illustrates the various stages of a cognitive cycle.[1] The CR is expected to carry out certain functions which include [3]

- Spectrum sensing: Detecting unused spectrum in order to share the spectrum with other users without harmful interference.
- Spectrum management: Capturing the best available spectrum to meet user communication requirements and ensuring the required quality of service. The management function encompasses *spectrum analysis* and *spectrum decision*.
- Spectrum mobility: Vacating the channel when a licensed user is detected and maintaining seamless communication requirements during the transition.
- Spectrum sharing: Providing the fair spectrum scheduling method among coexisting users.

Spectrum analysis involves examining the characteristics of the detected unused spectrum while spectrum decision entails choosing the appropriate spectrum band according to the spectrum characteristics and user requirements.

[1]Image reproduced from [8].

The functions of spectrum analysis and spectrum decision in conjunction with spectrum sensing, complete the main stages of the cognitive cycle [3].

1.3 Towards Achieving DSA

In June 2013, the FCC via a public notice approved Google, Inc.'s *TV bands database system* to provide service to the public [9]. This is in addition to a prior approval granted to Spectrum Bridge, Inc. and Telcordia Technologies, Inc., thus bringing the CR dream a step closer. These database systems will support unlicensed radio devices that transmit on unused channels in the spectrum bands used by broadcast television (TV white spaces, or TVWS). Notwithstanding, these recent developments, DSA in its different forms still face a few challenges.

1.3.1 Policy Issues

Spectrum allocation models can basically be categorised into *spectrum owned* or *spectrum commons* [10, 11]. The owned model also known as the "property-rights" model is currently the dominating spectrum allocation method which was agreed upon since 1927 [12] and over the years, it has proven to be highly inefficient with spectrum utilisation going as low as 15% in some areas during certain periods [1, 3]. Notwithstanding the seemingly inflexible nature of this model, the "owners" of the spectrum still trade or sub-lease their portion as they wish in a more flexible manner.

In contrast, the spectrum commons model also referred to as the "unlicensed model" involves all communicating parties using the spectrum based upon predefined protocols.

There is an ongoing debate over which policy model will best serve the interest of stakeholders involved. Though it is not likely to have one model satisfying all parties, the two model types are not necessarily irreconcilable. Several attempts have been made to find a middle ground between the two models, among which is the *"end-state regulation"* [13] which in its simplest form encompasses both models with a guarantee of non-harmful interference from unlicensed users and a regulator overseeing the spectrum. Building on this idea, the authors of [11], proposed a model using a spectrum policy

server as a controller/enforcer where both the spectrum access mechanism as well as the market forces are brought to bear in the resulting bandwidth utilisation. Undoubtedly, favourable policies and regulations along with standardised protocols will go a long way in ensuring that this novel concept of DSA/CR becomes a reality.

1.3.2 Standardisation

Standardisation leads to a uniformity in design and policy, thereby allowing multiple independent devices to coexist. Standardisation activities towards the realisation of DSA has been a continuously evolving process over the last decade. In the recent past, the issue of "coexistence" has been addressed in the IEEE 802.11, IEEE 802.15 and IEEE 802.16 standards [14, 15]. For example, under the IEEE 802.15 Wireless Personal Area Network (WPAN) standard, the bluetooth has a feature called adaptive frequency hopping (AFH) to reduce interference in the 2.4GHz unlicensed band. AFH requires a sensing algorithm for determining whether there are other devices present in the Industrial, Scientific and Medical (ISM) band and whether or not to avoid them [16]. Another example is in the 802.11k, which is an extension of the 802.11 standard and deals with improvements on node connection to an access point (AP). Sensing information is used to assign new nodes joining the network to underutilised APs instead of automatically connecting to an AP with the strongest signal (which may already be overloaded). The overall system throughput is therefore better due to more efficient utilisation of network resources. Newer techniques such as dynamic frequency selection and transmit power control have also been added more recently to deal with the coexistence issues [15]. The coexistence techniques incorporated in these standards are similar to the requirements of DSA.

Currently there are two main standards addressing the needs for the CR; IEEE 802.22 and SCC41.[2] The IEEE 802.22 standard is the first worldwide standard based on CR, designed for the Wireless Regional Area Network (WRAN) opportunistic use of the television spectrum [17]. A few issues covered in the

[2]Formerly P1900

standard include coexistence (as well as self-coexistence) mechanisms, spectrum sensing in the MAC and PHY layers and interference mitigation techniques involving the use of two separate antennas; namely, an omnidirectional antenna for sensing and a directional antenna for exchange of information between CR and base station. Furthermore, WRANs are proposed to cover ranges up to 100km, therefore issues regarding propagation delay were considered in the framework. Other companion standards to the 802.22, are the 802.22.1 which seeks to provide enhanced protection to low-powered licensed devices from harmful interference [18] and 802.22.2 which recommends best engineering practices for the installation and deployment of IEEE 802.22 systems.[3]

The IEEE Standards Coordinating Committee 41 (SCC41) is the new governing body inaugurated in early 2007 for all IEEE 1900 standards on Dynamic Spectrum Access Networks (DySPAN). The IEEE 1900.**x** working groups currently encompass seven groups, working on issues relating to (but not limited to) standard definitions, concepts, recommended practices, spectrum sensing, interference and coexistence. The working groups are designated as follows[4]

- **IEEE-1900.1** Definitions and Concepts for Dynamic Spectrum Access: Terminology Relating to Emerging Wireless Networks, System Functionality, and Spectrum Management.
- **IEEE-1900.2** Recommended Practice for the Analysis of In-Band and Adjacent Band Interference and Coexistence Between Radio Systems.
- **IEEE-1900.3** Recommended Practice for Conformance Evaluation of Software Defined Radio (SDR) Software Modules.
- **IEEE-1900.4** Architectural Building Blocks Enabling Network-Device Distributed Decision Making for Optimised Radio Resource Usage in Heterogeneous Wireless Access Networks.
- **IEEE-1900.5** Policy Language and Policy Architectures for Managing Cognitive Radio for Dynamic Spectrum Access Applications.

[3]The objectives of the IEEE 802.22.2 standard can be obtained from http://www.ieee802.org/22/

[4]obtainable from http://grouper.ieee.org/groups/dyspan/

- **IEEE-1900.6** Spectrum Sensing Interfaces and Data Structures for Dynamic Spectrum Access and other Advanced Radio Communication Systems.
- **IEEE-1900.7** Radio Interface for White Space Dynamic Spectrum Access Radio Systems Supporting Fixed and Mobile Operation

A comprehensive breakdown and more in-depth analysis of the various ongoing and completed standards of interest to the DSA/CR technology have been extensively discussed in [10] and [15].

1.4 Aims and Objectives

A two-pronged approach is adopted in this study. Firstly, several challenges that are generally encountered when conducting spectrum sensing have been highlighted from the literature. Such challenges include detecting spread spectrum users, the presence of interference, dealing with uncertainty, multiuser networks, and the hidden terminal problems amongst others. Secondly, energy detectors (EDs) are investigated based on the fact that an ED is favoured for spectrum sensing due to certain advantages inherent within the technique. However, a few of its shortcomings along with those of other alternate sensing techniques are in need of further investigation. Thus, the aim of this study is to analyse the identified spectrum sensing techniques while addressing the highlighted coexistence and spectrum sensing challenges. To achieve this aim, the main objectives of this thesis are:

- To derive the statistics of the decision variables for the highlighted sensing techniques in a multi-user network. These methods are:
  - The energy detector
  - The power law detector
  - Kay's detector
  - The matched filter detector
- To obtain improved mathematical models for the analysis of the highlighted sensing techniques based on the statistics of the decision variables.

- To investigate the performance of a sensing node in the presence of co-channel interference (CCI).
- To propose a framework for sensing a wideband channel when the existing primary user (PU) employs a frequency hopping scheme.

Additionally, the performance of the matched filter detector was compared to that of the energy detector under CCI, while Kay's detector was contrasted against the ED under fading channels.

1.5 Key Contributions

The major points of contribution are highlighted in what follows. However, it is worth noting that part of the contributions outlined below have so far been published in journals and conference proceedings, details of which have been outlined in Sec. 1.7. The key contributions are

- Performance analysis of a spectrum sensing node employing energy detection in the presence of intra-network interference generated by the secondary network. In the model considered, such interference is possible because of the non-zero sensing errors of coexisting secondary users (SU). This situation may arise when the secondary network is non-cooperating and active SUs either missed detecting the presence of the PU and/or the sensing node or were already in operation when the sensing node commenced spectrum sensing. This means SU nodes do not commence and terminate sensing and transmission simultaneously. Several interference models were examined.
  - When missed detection of the PU is assumed very low and therefore negligible. Consequently, sensing errors in this scenario mainly arise from false alarms.
  - When the reference sensing node is in a contention based network of interfering nodes.
  - When the reference sensing node is in the presence of a Poisson field of secondary interferers.
- Derivation of the detector models under interference channels for

  - Energy Detector.
  - Matched Filter Detector (see Sec. 4.5).

- Derivation of novel expressions for the probability of false alarm and detection in terms of the moment generating functions (MGF) of the random interferer powers for both the energy detector and matched filter detector. In particular, the alternative expressions presented have two main advantages; firstly, the new forms of the equations are expressed as single integrals with the limits independent of the argument of the function, so that the argument of the function does not appear in the limits of integration, but only in the integrand. Secondly, the random variables (RVs) appear only in the exponent of the integrand, lending itself to a desired form in terms of the moment generating functions (MGF) of the random interferer powers. Other benefits of this approach include

  - The approach significantly simplifies the arduous task of obtaining the statistics of the aggregate random interference. Direct methods for averaging out the random variables (RV) will require computing several integral operations, which depends on the number of RVs involved and also requires a knowledge of the distribution of the variance.
  - Alternatively, one has to resort to the Gaussian approximation [19], commonly used in the performance analysis of wireless communications in the presence of interference, where the sum of the accumulated interference is approximated by a pure Gaussian random variable with a (non-random) variance. Though the accuracy of this approximation is justified by the central limit theorem (CLT), its validity under certain conditions is questionable [20], which further underpins the need to investigate its accuracy in ED applications.
  - Furthermore, when using direct methods (including the Gaussian Approximation method), significant deviations from practical performances may occur when using the general path loss model $r^{-\beta}$, where r is the distance between transmitter and receiver while β is

the path loss exponent [21]. This occurs because the model manifests a singularity at $r = 0$ and considerably amplifies the transmitted signal in the region $r < 1$.

- For the alternate expressions of the false alarm and detection probabilities of a matched filter detector in terms of the MGF, this required a novel expression for the complementary error function, with arguments in the form $\text{Erfc}\left(\xi\sqrt{\frac{N}{x}}\right)$ (see Appendix A)
- Derivation of closed-form expressions for the MGF of the various interference models discussed. In the case of the contention based model, two solutions were obtained for the MGF, i.e. approximation and tightly bounded expressions (Sec. 4.3).
- An analytical framework for spectrum sensing of a wideband channel. The performance evaluation involves expressions for the detection probability, overall channel throughput of the secondary nodes and interference inflicted on the PU. The model examined is based on a wideband multi-user channel comprising a network of primary users employing slow frequency hopping (FH) signals and secondary users seeking to opportunistically access the channel. Unlike most literature on FH detection that are interested in the FH sequence of the PUs in the channel, the model in this study sought to identify the hopping period of the PU signal, such that secondary nodes can opportunistically transmit in other unoccupied subbands before the PU hop duration elapses. This assumption is possible because slow frequency hopping was assumed for the PU, such that the hop duration is long enough for a combined secondary node sensing and transmission time slot. The PU and SU frame lengths are assumed to be known and equal but the commencement time for the PU frame may not be known. Hence, the following cases are considered:
  - Equal PU-SU frame length, synchronised time slots.
  - Equal PU-SU frame length with time synchronisation errors.
- An analytical framework for wideband sensing with unequal PU-SU frame length. The assumption of equal PU-SU frame length was relaxed to give rise to a model in which nothing is known of the PU frame

length. Note that when the PU hop duration is known, the SU can synchronise its sensing and transmission time frame with PU's hop duration or in the worst case a constant time offset can be maintained (when hop duration is known but the exact hop commencement time is unknown). However, the case of unknown PU hop duration gives rise to several problems. Firstly, the selected SU time frame for combined sensing and transmission could be shorter or longer than the PU hop duration. Secondly, as a result of the unequal PU and SU time intervals, the relative statistics of the SU achievable throughput, detection probability of the PU hop signal and amount of interference inflicted on the PU may change with every hop of the PU.

- Derivation of explicit expressions for the analysis of imperfect physical carrier sensing MAC protocols using the ED under two protocols, i.e. under physical carrier sensing (PCS) and hybrid PCS and virtual carrier sensing (VCS). Analysis is conducted for performance metrics such as the transmission probability and throughput of a node, while the effect of CSMA inhibition zones arising due to neighbour node deactivation by the protocol and other system parameters such as the ED detection threshold, the node density and the radius of inhibition are investigated.

- Performance analysis of the power law detector was conducted. The statistics of the decision variable of this detector type involves the need to compute the sum of arbitrarily powered Gaussian random variables, for which simple but highly precise approximations for the probability density function (PDF) and cumulative distribution function (CDF) were presented. The novel approximations were shown to be an improvement over other current techniques, especially at very low number of samples. For example, it was shown that for very low value of about four summands, the new results showed comparable performance to the CLT approach [22] with 50 summands and the gamma approximation approach with 20 summands [23].

- Performance analysis of Kay's detector for unknown deterministic signals was also conducted under additive white Gaussian noise (AWGN), Rayleigh and Nakagami fading channels, for which the relevant closed-form analytical expressions were derived and the results contrasted

against that of the classic energy detector.

1.6 Thesis Organisation

The thesis is organised as follows.

Chapter 2 presents a literature review on the relevant background fundamentals employed in this thesis. The concepts discussed include spectrum sensing methods and challenges, multiple access techniques and interference issues.

Chapter 3 extends the analysis for two classes of detectors; namely, the power law detector (PLD) and Kay's detector. For the former, simple but highly accurate novel approximations to the PDF and CDF of the decision variable's statistics are presented, while in the case of the latter, the decision variable is derived and the existing study of the detector extended to evaluate the performance in AWGN and certain popular fading channels. The results are compared to the classic energy detector and validated with Monte Carlo simulations in all cases.

Chapter 4 introduces spectrum sensing based on the energy detector and examines some key interference models based on a cognitive radio network. The relevant performance metrics based on these models are derived and the efficiency of the technique is compared against the traditional Gaussian approximation technique. Similar analysis is conducted for a matched filter detector.

Chapter 5 proposes a framework for sensing a primary user employing slow frequency hopping in a wideband. Expressions for the achievable throughput of the secondary network, multi-channel detection probabilities and interference inflicted to the primary users are derived for the various models presented.

Chapter 6 examines the efficiency of employing energy detectors in a multi-user network whose nodes are spatially distributed in a geographic area and employ a MAC protocol to access the channel. Explicit expressions for the performance analysis of a node under physical carrier sensing and hybrid physical and virtual carrier sensing are derived and presented.

Chapter 7 concludes the thesis and prospects for the future extension of the work are outlined.

1.7 Publications

Journals

1. A. U. Makarfi and K. A. Hamdi, "Interference Analysis of Energy Detection for Spectrum Sensing," *IEEE Trans. Veh. Technol.*, vol. 62, no. 6, pp. 2570-2578, Jul. 2013.

Conference Papers

1. A. U. Makarfi and K. A. Hamdi, "Wideband Sensing of Slow FH Primary Users with Unknown Hop Duration," in *proc. IEEE Wireless Commun. and Networking Conf. (WCNC),* Apr. 2013, pp. 3370 - 3375.

2. A. U. Makarfi and K. A. Hamdi, "Efficiency of Energy Detection for Spectrum Sensing in the Presence of Non-Cooperating Secondary Users," in *proc. IEEE Global Commun. Conf. (GLOBECOM),* Dec. 2012, pp. 4934 - 4944.

3. A. U. Makarfi and K. A. Hamdi, "Efficiency of Energy Detection for Spectrum Sensing in a Poisson Field of Interferers," in *proc. IEEE Wireless Commun. and Networking Conf. (WCNC),* Apr. 2012, pp. 1023 - 1028.

4. A. U. Makarfi and K. A. Hamdi, "Wideband Spectrum Sensing Framework for Multiple Slow Frequency Hopping Primary Users," in *proc. IEEE Wireless Commun. and Networking Conf. (WCNC),* Apr. 2012, pp. 2653 - 2658.

Chapter 2

Literature Review

THIS chapter presents a review on the existing literature covering the basics on spectrum sensing methods and challenges, interference/noise uncertainty in Dynamic Spectrum Access (DSA) networks and a synopsis on multiple access and coexistence techniques.

2.1 Spectrum Sensing

As mentioned in the previous chapter, the first and arguably most important task of the CR is spectrum sensing. However, spectrum sensing is not a new phenomenon in wireless systems because it has been integrated in wireless standards prior to the IEEE 802.22 to improve efficiency and quality of service. Sensing involves detecting *spectrum holes* which stands for those subbands of the radio spectrum that are underutilised (in part or in full) at a particular instance in time and/or specific geographic location [24, 25]. However, this is merely a superficial idea of spectrum sensing, and it could be more comprehensively defined as [14]

> "Obtaining the spectrum usage characteristics across multiple dimensions such as time, space, frequency and code. It also involves what kind of signals are occupying the spectrum including the modulation, waveform, bandwidth, carrier frequency etc."

Based on the aforementioned definition, the subtasks of spectrum sensing could be categorised into [25]

- Detecting spectrum holes,

- Identifying the spectral resolution of each spectrum hole,
- Estimating the direction of arrival of interferers using multiple antennas.
- Signal classification.

The ability of the CR to accomplish the subtasks associated with spectrum sensing affords it complete knowledge of the spectrum or *spectrum awareness*, which is a prerequisite for other CR tasks.

2.1.1 Spectrum Holes

The terms *spectrum holes* and *spectrum opportunities* are generally used interchangeably. However, the relationship between the terms is such that obtaining a spectrum hole gives rise to a spectrum opportunity. To maximise the spectrum opportunities available to a CR node, it requires complete spectrum awareness. Exploiting spectrum opportunities in several dimensions including frequency, time and space brings to fore the concept of *multidimensional spectrum awareness* [14]. Other dimensions which could further generate spectrum opportunities are the code and angular dimensions. The level of awareness expected from a CR would determine the capability and ultimately the complexity of the receiver design.

2.1.1.1 Spatial Dimension

The spectrum space in which the CR operates, could be *white*, *gray* or *black* spaces [25]. White spaces are subbands occupied only by white noise and are free of RF interferers. Gray spaces are partially occupied by both noise and interferers while black spaces are completely occupied by the presence of communication signals and noise. The CR's task is to detect spectrum holes within the white and gray spaces of its local environment. The range or radius that is classified as the local space for a CR, would differ between different CRs, depending on the node's receiver capability. In the spatial dimension, spectrum holes could be available to the CR in different locations at the same time and within the same frequency band. The location and distance of primary users (PUs) in space is of utmost importance. Path loss exponent for example, plays an important role in obtaining spectrum opportunities where they otherwise would not have existed. On the other hand, a hidden node

may exist due to the relative positions of a CR node and the PU, which may cause a problem.

2.1.1.2 Spectral Dimension

A spectrum opportunity in the spectral dimension signifies that for a given geographical location and at a particular time, not all the frequency bands may be occupied [14]. This gives rise to spectrum holes and such bands could be exploited opportunistically. Nevertheless, a CR could detect an unoccupied frequency band, but the CR transmissions could result in adjacent channel interference. Therefore, a spectrum opportunity with respect to the frequency dimension could be more aptly defined as a frequency band in which a CR's transmission would not interfere with any primary receivers across all frequencies [24].

2.1.1.3 Temporal Dimension

When a specific frequency band is not continuously in use by the PU, temporal spectrum opportunities may occur during the time intervals of PU absence. Thus, the temporal spectrum opportunity could be simply defined as the period of time that the PU is not transmitting [24]. The FCC's enforcement bureau was able to show satisfactory data across many states in the USA, indicating some frequency bands are left unused for long periods culminating in spectrum underutilisation [1]. Challenges could occur in spectrum sensing particularly when the duration within which detection samples are captured corresponds with a silent period of PU transmission or when the PU resumes after a spectrum hole has been declared by a sensing node. Such challenges give rise to the question of how long and how often should spectrum sensing be performed by CR nodes?

2.1.1.4 Angular Dimension

Conventional sensing methods mainly define spectrum opportunities within the context of the three aforementioned dimensions. However, spectrum opportunities could materialise if the angle dimension is considered. Antenna technologies such as beamforming could create additional spectral space opportunities where angle of arrivals of signals would also be considered [14].

As a result, a CR node could coexist within the same geographical space, time and frequency band. However, this method requires the CR to have more in-depth knowledge about the location and angle of transmission of the PU in order to effectively direct its own transmission and avoid interference.

2.1.1.5 Code Dimension

To exploit spectrum opportunities in this dimension, it is necessary for the sensing node to determine the type of code used in addition to the general spectrum usage parameters. If the knowledge of the PU transmission code is known, the CR could coexist without interference by transmitting orthogonal codes with respect to the PU or implementing direct sequence spread spectrum (DSSS) or frequency hopping (FH) codes. However, if the PU is implementing any form of spread spectrum technique, there would be a difficulty of obtaining the necessary PU code information by the sensing node using conventional sensing techniques [14].

2.1.2 Challenges of Spectrum Sensing

Several challenges plague the current approaches to spectrum sensing. In what follows, a few of the most important issues will be presented and discussed.

2.1.2.1 Sensing Duration and Frequency

Sensing periodicity encompasses both the sensing duration/time and repetition frequency. Sensing repetition frequency captures how often sensing needs to be performed while the sensing duration entails how long each sensing phase would last within a sensing-transmission cycle. The CR will seek to minimise the sensing time so as to increase the data transmission period at its disposal. However, the longer the spectrum can be sensed and detected, the more accurate and reliable the results would be [26] and a longer averaging time reduces the noise power thereby improving signal-to-noise ratio (SNR) for better performance [27]. Hence, the time related parameter needs to be carefully selected as a design trade-off between processing time and performance. In general, if the PU status is known to change slowly like in a TV band, the sensing repetition requirement could be relaxed [14].

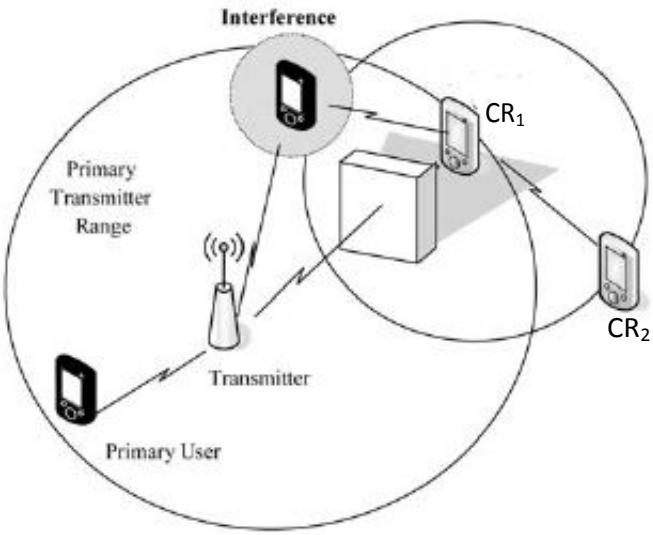

Figure 2.1: An Illustration of the Hidden Node Problem.

2.1.2.2 Hidden Terminal Problem

A CR may miss detecting a primary signal within its detection range, due to channel uncertainties such as severe multipath fading or shadowing. This could result in harmful interference inflicted on the PU hidden to the CR during the sensing phase. In Fig. 2.1, CR_1 is attempting to detect the primary transmitter, but the signal which is intended for the receiver is severely shadowed. As a result, CR_1 decides the absence of the primary transmission and transmits, resulting in harmful interference to the primary receiver. A solution proposed for this problem is for several CR nodes to share spectrum sensing data in a cooperative scheme to improve sensitivity. This is because CR nodes separated by sufficient distances are unlikely to undergo the same channel conditions. For example, in Fig. 2.1 CR_2 is better placed to detect the presence of the transmitter.

2.1.2.3 Detecting Spread Spectrum Primary Users

In contrast to most conventional devices that use a fixed frequency for operation, FH and DSSS devices operate quite differently. The FH device dynamically change its frequency of operation while the DSSS device operates within a frequency band but spreads its signal to occupy a wider spectrum. This makes both forms of signal types difficult to detect. The problem could

be reduced if the sensing node has a knowledge of the hopping sequence or spreading code, which is not likely in an opportunistic scenario. However, in [28–32], attempts have been made to show how energy detectors with no prior knowledge of the hopping sequence or spreading codes could be utilised for primary transmitter detection.

2.1.2.4 Aggregate Interference and Noise Uncertainty

When spectrum sensing is undertaken with certain detector types such as energy detectors, their performance could be seriously hampered at very low SNR levels and noise uncertainty [33]. Moreover, errors in noise power estimation could give rise to reduced accuracy in related parameter calculations such as the detection sensitivity and sensing threshold. Furthermore, aggregate interference uncertainties arising from unknown number of secondary users in operation or other networks beyond the fixed interference ranges could turn out harmful [34]. Hence, more robust interference measurement techniques would be required to overcome the challenge.

2.1.2.5 Multi-User Networks

Realistically, the CR would be in a multi-user environment where cooperation may or may not be implemented. Other CRs may degrade the reliability of sensing, especially if the sensing technique cannot distinguish between the primary signal and other secondary signals. Thus, a few pertinent questions need to be answered. For instance, when collaboration is involved what should be the extent of cooperation and what information needs to be shared in addition to spectrum opportunities, such as location and different user frequencies [35].

2.1.2.6 Hardware Prerequisites

The CR is envisaged as a device with very high capabilities, which would mainly be achieved with complex hardware. The sensitivity of a CR is expected to outperform that of a conventional primary receiver in order to comfortably detect the primary transmitter at longer ranges [27]. CRs would also be expected to be programmable to transmit and receive over different frequencies and should have wider operating bandwidths. Furthermore, there

is a proposal of dual-radio as against single radio sensing architecture with an advantage of a dedicated radio chain for spectrum monitoring [14]. This proposal is similar to that of the IEEE 802.22 requirements of two separate antennas for sensing and transmission [17]. The aforementioned proposals and expectations from the CR would increase design complexity and cost. In general, better functionality for a CR translates into hardware complexity and cost.

2.1.2.7 Regulatory constraints

In addition to the hardware requirements for effective sensing, regulations and standards in place could imply sensing is performed within certain limits. For example, the draft proposal for the IEEE 802.22 standard has outlined various timing related parameters including sensing duration and channel move time for spectrum sensing within the TV band [17]. Also, minimum sensitivity requirements and interference temperature limits, which are decided by regulatory bodies and vary depending on the band. Other bands may have interference ranges and primary exclusive regions or discs within which the CR cannot transmit. These are all regulatory parameters that affect sensing performance.

2.1.2.8 Security

Generally, the CR would be exposed to the security challenges prevalent in a wireless communication environment. But particularly, the CR might be susceptible to further security issues peculiar to a CR network. These issues could mainly be categorised under *reliability* problems and *security attacks* [36]. Several problems inherent in the CR network could contribute to poor reliability such as unknown PU location, lack of common control channels and the requirement for high sensitivity for the CR node. These reliability issues could be exploited by malicious nodes to launch security attacks within the network. In [36], security attacks in CR networks were described as activities that result in unacceptable interference to the PU or brings about a missed opportunity to the SU. One of the more likely security threats in a CR network is PU emulation, where a malicious node could disguise itself as a PU for selfish reasons. This form of threat could be countered by employing public

key encryption based PU identification [14]. However, the encryption techniques can only be used if the SUs have the ability to demodulate the primary signal. An extensive study of various forms of security attacks specific to the different layers of the protocol stack in a CR network and possible solutions were presented in [36].

2.2 Spectrum Sensing Methods

The main approaches proposed by the FCC for obtaining spectrum awareness in CR applications include the use of *geolocation* technology, *beacons* or *local sensing* by the CR [37]. Geolocation involves using Global Positioning System (GPS) or similar technology to store occupied frequency channels in a database from which the CR could make future reference, while beacons involve using separate transmitters (of certain special characteristics) to broadcast occupied channels. Conversely, local CR sensing involves passive sensing of the spectrum by a CR node. While the first two approaches entail some form of assistance by the PU, local CR sensing places the responsibility of obtaining spectrum awareness mainly on the CR.

In order to avoid harmful interference to the PU, the most effective means of local CR sensing should be to actually determine the presence and/or location of a primary receiver. However, this is usually difficult and as a result most sensing techniques concentrate on some form of primary transmitter detection. These techniques may include direct transmitter localisation, interference temperature measurement or cooperation between the CRs to improve efficiency [3]. The relationship between these techniques are illustrated in Fig. 2.2 and are further discussed over the coming sub-sections.

2.2.1 Interference Based Detection

The interference based detection approach entails assessing the radio frequency (RF) environment of interest for a measure of the total RF energy. This energy comprises of thermal noise generated within the receiver, the desired and undesired transmissions from other transmitters. This gives the overall temperature measure or aggregate interference in the band of interest. If the measure is below a certain threshold known as the interference *limit*, a

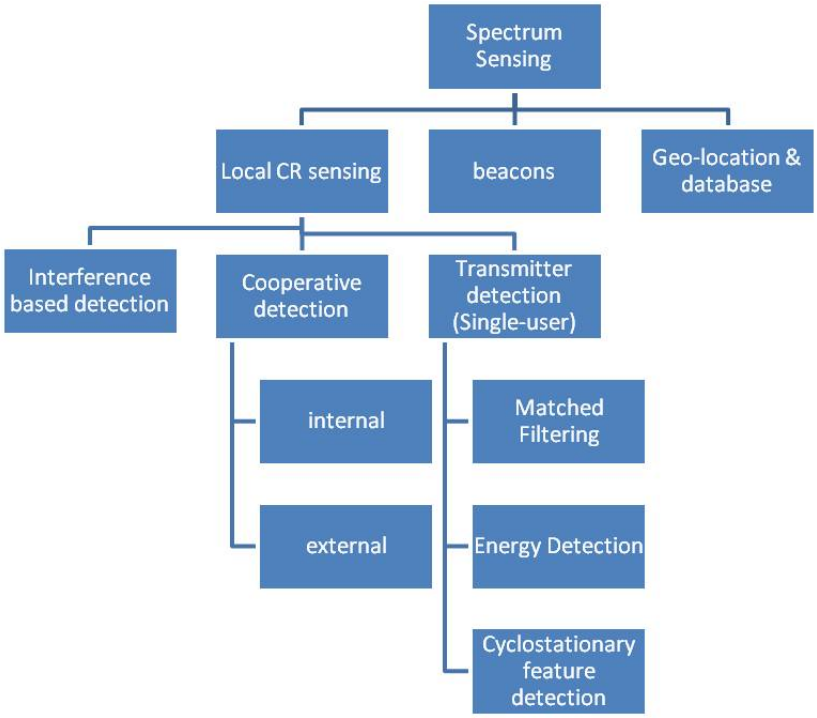

Figure 2.2: Hierarchy of spectrum sensing techniques.

spectrum opportunity is declared for PUs and CRs alike. This is in contrast to direct transmitter detection, where an opportunity is declared for the CR only when the absence of a primary transmitter is ascertained. According to the FCC [38], the interference temperature is calculated as:

> "The power received by an antenna in watts divided by the associated RF bandwidth in hertz and the Boltzmann's constant."

The interference temperature is expressed in Kelvin, while the Boltzmann's constant has a value of $1.38 \times 10^{-23}\mathrm{JK}^{-1}$.

Different approaches may be possible in order to implement detection based on the interference temperature model. First, a single CR node may measure the interference temperature level and make a local decision based on the interference limit for that band. Secondly, the temperature measurements for various bands could be pooled in a centralised unit, and real-time spectrum occupancy data accessed by (or broadcasted to) individual CR nodes in a cooperative manner [38]. In [39], the author analysed two interpretations of the interference temperature model. In the first case, referred to as the generalised model, no assumptions were made to distinguish between

licensed and unlicensed or interfering signals. In the second case, denoted the ideal case, distinction is made between the licensed signal and all other forms of noise and interference. Based on the two models therefore, two separate techniques were proposed for bandwidth selection. Furthermore, the interference temperature model was employed in [40] to present an initial analysis of techniques for improved efficiency in CR networks. In particular, spectrum shaping was utilised in orthogonal frequency division multiplexing (OFDM) and DSSS signals to increase signal bandwidth and take advantage of the noise floor gaps in the prevailing interference environment.

In general, an advantage of interference based detection is that while most other methods try to avoid the licensed user, this scheme tries to coexist with them. Moreover, noise and interference are all regarded as interference and contribute to the Signal-to-Interference ratio. Hence, if implemented there is reduced effect from devices that are difficult to detect. Such devices could be in the form of underlays, which are capable of cumulatively raising the noise floor.

2.2.2 Transmitter Based detection

Spectrum sensing through transmitter detection entails detecting the weak signal from the primary transmitter locally by the CR. A few of such techniques include matched filtering, feature detection, energy detection and waveform based detection. Fig. 2.3[1] illustrates the relative accuracy against complexity of the techniques discussed in this section. The general limitation of the transmitter based detection is that the actual location of the intended receiver may still remain unknown and hence interference could still occur. Moreover, the hidden node problem may still remain unsolved without some form of cooperation between the sensors. Nevertheless, transmitter detection remains one of the most promising techniques for spectrum sensing.

2.2.2.1 Matched Filtering

A matched filter detector (MFD) is a linear filter designed to provide the maximum SNR at its output for a given signal in additive white Gaussian noise (AWGN) [41]. Its two main advantages are that it has a comparatively

[1]Image reproduced from [14].

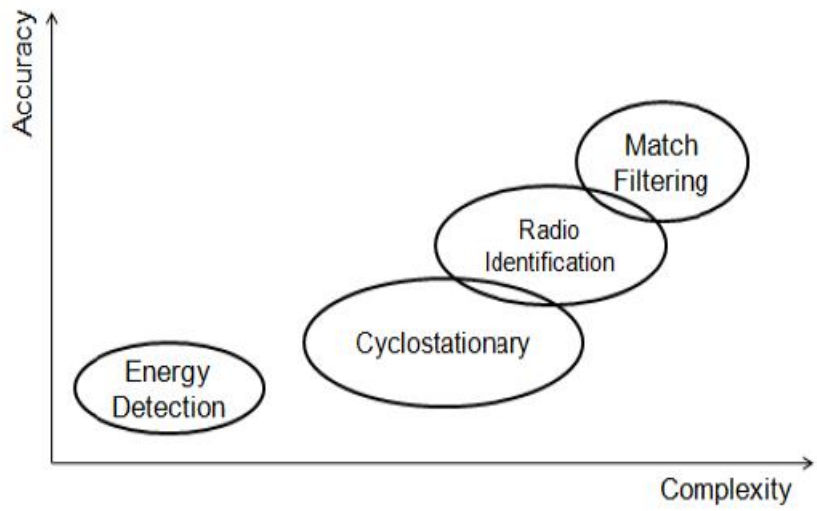

Figure 2.3: Comparison of various sensing methods.

low detection time and its regarded as the optimum PU detection method when the signal to be received is known [14]. Unfortunately, the CR may seldom have knowledge of the expected primary signal characteristics and as a result may perform poorly [3, 35]. Furthermore, it may be too cumbersome to deploy a receiver for every signal type the CR node is expected to detect [14].

The MFD is the linear filter whose impulse response $h(t) = s(T - t)$ matches the desired signal $s(t)$, where $0 \leq t \leq T$. Hence, the output is [42]

$$y(t) = \int_0^t s(\tau)\, s(T - t + \tau)\, d\tau.$$

In essence, this is the auto-correlation function of the desired signal and is maximised at time $t = T$. Also, the maximum obtainable SNR for a matched filter is [42]

$$SNR_{\max} = \frac{2S}{N_0}$$

where S is the energy of $s(t)$ and N_0 is the single sided noise power spectral density. Another interesting property of the MFD is that the output SNR depends on the energy of the waveform $s(t)$ but not on the detailed characteristics of $s(t)$. [42, pp. 241]

2.2.2.2 Cyclostationary Feature Detection

The term *cyclostationary* is used to characterise modulated signals whose statistics, mean and autocorrelation exhibit periodicity. Its main advantage is that it is implemented by analysing the spectral correlation function at the sensor which is capable of differentiating between noise energy and modulated signal energy. This is because modulated signals are cyclostationary with spectral correlation due to signal periodicity while noise is a wide-sense stationary signal with no correlation [3]. Moreover, this detector has a relatively good performance in low SNR environments. However, this technique is computationally complex, requires relatively longer observation times and a prior knowledge of the signal to be detected [35].

2.2.2.3 Energy Detection

Energy detection also known as *radiometry* is the simplest and commonest method of spectrum sensing for cognitive radio [35]. It operates by simply measuring the signal energy within the band of interest and comparing it to a given threshold to determine the presence or absence of a primary signal. In addition, it requires no prior knowledge of the signal to be detected other than the rough spectral location. Conversely, it performs poorly in low SNR levels and cannot differentiate between signal types and noise; i.e., it cannot differentiate between modulated signals, noise and interference. Hence this detector cannot profit from interference cancellation techniques. This also implies the CR sensing node would not have the ability of treating primary and secondary signals differently [27]. Notwithstanding these shortcomings, energy detection was chosen as a starting point for the spectrum sensing analysis in this thesis. This is because practically, the CR may not always have a prior knowledge of the PU signal. Therefore, a more detailed literature review of the energy detector (ED) would be presented in the following section.

2.3 The Energy Detector

There are various types of energy detectors (ED)/radiometers in use for a wide range of applications. Some of these include the wideband radiometer,

channelised radiometer, total power radiometer and correlation radiometer.[2] For example, the most common intercept receiver is the wideband radiometer, which was extensively discussed in [44] and proposed for detection of DSSS signals [31, 32], though its robustness is compromised in the narrowband. The channelised radiometer comprises of parallel channels each with a radiometer and a procedure for its implementation for detection of FH signals was demonstrated in [29, 32, 45]. Prior to the recent cognitive radio drive, EDs have extensively been used in military electronic support systems, pulse radars and radio astronomy [46].

The ED was studied by Urkowitz [47] for detection of unknown deterministic signals in a bandlimited Gaussian noise channel. Expressions for false alarm and detection probabilities were derived and relationships between the ED performance, the time-bandwidth product, number of samples and sensing duration were established. It was also alluded that the results obtained would hold for all signal types either deterministic or random. In [48], the ED was studied in the presence of non-Gaussian noise while in [49], the performance of the ED in a fading channel was discussed and expressions for the detection probability derived. This analysis was further extended in [50, 51], where alternative closed-form expressions were obtained for the probability of detection in AWGN, Rayleigh and Nakagami fading channels. Additionally, square-law selection and square-law combination (SLC) diversity schemes were analysed for both independent and identically distributed signals (i.i.d) and correlated signal inputs to the ED. Likewise, the authors of [52] investigated the effect of fading and/or diversity schemes on the probability of a missed detection. It was shown that the sensing gain is not in anyway affected by the false alarm probability but rather by the fading and/or diversity scheme. Furthermore, equal gain combination (EGC) diversity rule was applied over a Nakagami channel in [53], for analysis of an energy detection spectrum sensor of a CR.

In particular, the time-domain ED has been discussed for use in spectrum sensing in [3, 14, 26, 27, 35, 54–58], the frequency-domain ED in [59–61] and further techniques for employing EDs to implement cooperative spectrum sensing algorithms were investigated in [62–70].

[2] An extensive reference studying energy detector variations was compiled by [43].

2.3.1 The Energy Detector Model

The standard energy detector has a simple design starting with prefiltering the received signal with a bandpass filter. Next, the output of this filter is squared and integrated over an interval T (or squared and summed over N samples for a discrete signal) to produce a measure of the energy of the received waveform. The collected energy is the decision variable y of the detector. The decision variable is then compared against a threshold to make a final decision on the presence or absence of the desired primary signal. Based on this, the received signal at the receiver at time t is

$$x(t) = hs(t) + w(t), \tag{2.1}$$

where h is the channel gain between the transmitter and receiver, $s(t)$ is the transmitted signal and $w(t)$ is the AWGN at the receiver end. The task of the ED is a simple hypothesis testing problem to determine the presence or absence of $s(t)$. The two hypotheses are

$$x(t) = \begin{cases} w(t) & H_0 \\ hs(t) + w(t) & H_1. \end{cases} \tag{2.2}$$

The hypotheses H_0 and H_1 represent the signal $s(t)$ is absent or present respectively. If N_0 is the single sided noise power spectral density and W is the signal bandwidth, then the noise power is N_0W. Thus, the decision variable y for a continuous or discrete signal respectively are

$$y = \frac{1}{N_0W} \int^{T} \mid x(t) \mid^2 dt \tag{2.3a}$$

$$y = \frac{1}{N} \sum_{n=1}^{N} \mid x(n) \mid^2 \tag{2.3b}$$

where the number of samples $N = TW$ (the time-bandwidth product)

2.3.2 Performance Evaluation of the ED

The binary hypothesis test compares the decision variable y against a predetermined threshold ξ to determine the presence or absence of a primary

signal. There are mainly three probabilities that could be inferred from this technique. The first is the probability of detection P_{d} and the other two are error probabilities known as the false alarm P_{f} and missed detection P_{m} probabilities. P_{f} is the probability that the ED incorrectly decides the presence of a primary signal when it is absent. This is termed a type I error [71]. Conversely, P_{m} is a type II error defined as the probability that the ED wrongly decides the absence of a primary signal rather than its presence [71]. For a given sensing threshold ξ these probabilities can be computed as [50]

$$P_{\mathrm{f}} = \Pr\left(y > \xi \mid H_0\right) = \frac{\Gamma\left(N, \frac{\xi}{2}\right)}{\Gamma\left(N\right)} \tag{2.4}$$

$$P_{\mathrm{m}} = \Pr\left(y < \xi \mid H_1\right) = 1 - P_{\mathrm{d}} \tag{2.5}$$

where $\Gamma\left(.\right)$ and $\Gamma\left(.,.\right)$ represent the gamma function and the upper incomplete gamma functions respectively [72] and P_{d} is defined later on (see Eq. (2.6)). The ED should seek to minimise both error probabilities because, high missed detections increases the interference to the PU, while false alarms seek to increase missed opportunities thereby resulting in poor spectrum utilisation. However, it is not feasible to eliminate these error probabilities completely [71], so the two errors need to be traded against each other by changing the threshold level. The normal approach is to hold one value constant, while adjusting for the desired value of the other since it is impractical to simultaneously reduce both errors [71].

In Eq. (2.5), P_{d} is the probability of correctly detecting the presence of a signal within the band of interest and hence, the ED should seek to keep this as high as possible. Given an SNR γ, the P_{d} for an AWGN channel is [50, 51]

$$P_{\mathrm{d}} = \Pr\left(y > \xi \mid H_1\right) = Q_N\left(\sqrt{2\gamma}, \sqrt{\xi}\right) \tag{2.6}$$

where $Q_N\left(.,.\right)$ is the generalised Marcum Q-function.

As for the Rayleigh faded channel, several expressions have been expounded in the literature. The expression of the average P_{d} obtained in [50] is presented here

$$P_{\mathrm{d,Ray}} = e^{-\frac{\xi}{2}} \sum_{i=0}^{N-2} \frac{1}{i!} \left(\frac{\xi}{2}\right)^{i} + \left(\frac{1+\overline{\gamma}}{\overline{\gamma}}\right)^{N-1} \left[e^{-\frac{\xi}{2(1+\overline{\gamma})}} - e^{-\frac{\xi}{2}} \sum_{i=0}^{N-2} \frac{1}{i!} \left(\frac{\xi\overline{\gamma}}{2\left(1+\overline{\gamma}\right)}\right)^{i} \right] \tag{2.7}$$

where $\overline{\gamma}$ is the average SNR and $P_{\mathrm{d,Ray}}$ the P_{d} over the Rayleigh fading channel. The performance of the ED can be fully characterised using the receiver operating characteristic (ROC) curve or the complementary ROC curves [73], which is a plot of P_{f} against P_{d} or P_{f} against P_{m} respectively.

2.4 Interference in DSA Networks

Interference denotes the undesired received signals transmitted by devices in the vicinity of a receiver but intended for other receivers [74]. If not managed properly, interference can be disruptive to the desired operation of the network. The cornerstone of DSA/OSA existence is a guarantee of non-harmful interference for the licensed user of the spectrum. Interference analysis and characterisation is therefore important in order to achieve this objective. In spectrum sensing, there are a variety of techniques for detecting the presence and/or location of a PU transmitter, but detecting the PU receiver is much more difficult because most of the PU receivers are passive[3]. Since interference normally takes place at the receiver, this becomes a problem for the CR. The factors that contribute to the aggregate interference to a receiver in a CR network could include the distance between the source of the interfering transmission and the victim receiver, the power of transmission from the interfering source and the sensitivity of the victim receiver. Other factors are the user density, cooperation range and nature/topology of the network.

Another source of uncertainty in the network is noise. In general, several sources could account for noise accumulation such as thermal noise, receiver noise and man-made noise such as spurious emissions from electric appliances, leakage of signals from other bands due to receiver non-linearity and transmissions from other licensed and unlicensed devices within the region [76]. While thermal noise is generally assumed to be Gaussian, this may not necessarily be the case for man-made noise [76]. It is also worth noting

[3] A method of detecting the presence of passive TV receivers by measuring the local oscillator (LO) leakage power was proposed in [75].

an important difference between noise and interference, which lies in the fact that the noise power is typically constant when averaged over a short time interval, while the interference suffers from fading.

Lastly, uncertainty arises due to intentional under-modelling of system parameters. For instance, the primary signal can be modelled by imposing a cap on its power spectral density, instead of actually modelling its specific signal constellation, waveform, etc. However, under-modelling has benefits as it leads to less complexity and more flexibility in the model. [33]. Much research has been conducted on interference affecting the different users of a DSA network. In what follows, some of the above issues will be discussed.

2.4.1 Interference to the Primary Network

As mentioned earlier, the aim of spectrum sensing is to prevent harmful interference to the primary network. The IEEE 802.22 WRAN standard provides coexistence regulations for the spectrum presently licensed to TV and wireless microphones, for which extensive interference analysis has been conducted. However, while TV broadcasts high-power long range signals, the wireless microphones are low-powered devices and as such require a different interference characterisation. In [77], models for carrying out interference analysis of single and multiple CR interferers on wireless microphones were presented. The analysis demonstrated that although it is possible to minimise interference to the wireless microphone by optimising parameters, some form of interference would always exist when current spectrum sensing techniques are used regardless of the detection range. This means that there has to be a trade-off between spectral efficiency, cost and interference reduction. To further aid the CR in detection, the wireless microphones are required to transmit an inhibitory beacon [17], which alters the method of spectrum sensing involved and subsequently the probability of interference. The authors in [78] investigate the aggregate interference in such a beacon-based primary receiver network where active primary receivers indicate their presence. The aggregate interference is important because a primary user/system may be out of a single CR node's interference range, but the aggregate interference may still turn out harmful. Furthermore, because a weak detected signal could occur when the primary signal is experiencing a deep fade or heavy shadowing, the model was extended to account for the effect of cooperative spectrum sensing

on the aggregate interference distribution. It was shown that the aggregate interference is affected by the detection sensitivity, user density and cooperation range. Particularly, the aggregate interference at the primary receiver is dominated by the nearby interferers, while increasing the sensitivity would permit a higher density of users.

The authors of [79] established how cooperation could be used to improve network detection sensitivity (to reduce interference) with the aid of energy detectors and further characterised and studied the tradeoff between processing and cooperation. In [80], an outage probability analysis was conducted for a PU receiver protected by an interference radius, when the CR nodes are distributed in a Poisson field of interferers. The protective interference region, shadowing and small scale fading were all found to be beneficial in reducing the effect of interference to the PU receiver. The aggregate interference analysis in [80] was extended in [81], taking into consideration Poisson distributed interfering CR nodes shielded by an interference region radius in a Nakagami faded channel to obtain closed-form expressions for the outage probability and average fade duration.

2.4.2 Interference to the CR Network

In an opportunistic sharing scenario, the PU would not normally be bothered about the interference it inflicts on the CR because the PU is licensed. Moreover, the CR is expected to "opportunistically" access the network in the PU's absence and vacate the spectrum when the PU is present. However, it may be possible for a few CRs to be in operation while licensed users are present. Such a scenario could occur in a cooperative sharing environment or where the CRs are operating outside a certain PU protected zone. Also, when a CR misses the detection of the PU or the PU resumes while the CR network was active. In such cases, the PU may degrade the performance of the CR network. In [82], the outage probability parameter was utilised to determine the effect of the PU network on the CR network performance. The distribution and density of the primary network as well as the relative distance of both CR and primary networks were taken into consideration. It was observed that the relative distances between the networks and the interference threshold (and interference rejection capacity) of the cognitive network

were key factors affecting the outage probability. Because inter-network interference occurs when both networks are active, the authors in [83] classified the various scenarios when both networks could be active before proposing a closed-form expression for the outage probability.

Generally in a wireless network, outage occurs as a result of noise or strong interference. The probability of this occurring is measured with respect to the SNR, or the signal-to-interference-and-noise ratio (SINR), falling below a certain predetermined threshold ξ and may basically be expressed as [83]

$$P_{\text{out,N}} = \Pr\left(\text{SNR} < \xi\right)$$

for a noise only network or

$$P_{\text{out,I}} = \Pr\left(\text{SINR} < \xi\right)$$

for an interference plus noise network. The terms $P_{\text{out,N}}$ and $P_{\text{out,I}}$ represent outage probabilities for AWGN channel and an interference plus noise channel respectively. The outage and other error probabilities must be minimised especially in a cooperative CR network, as this could seriously affect the reliability of sensing information shared between the CR nodes.

2.4.3 Interference Mitigation

Based on the aforementioned factors, various methods of interference mitigation have been proposed. A technique of interference mitigation through antenna choice was specified in the IEEE 802.22 WRAN standard, where an omnidirectional antenna could be used for spectrum sensing and a directional antenna for transmission [17]. The modulation scheme (in this case OFDM), could also be exploited to avoid interference in a CR network with SUs by suppressing a certain set of subcarriers [65]. On the other hand, the nature/type of interfering signal was the focus in [30], where three interfering signal types were considered; namely, impulses, sinusoids and chirp signals. Because the interferer may be easier detected in the time or frequency domain depending on its characteristics, an algorithm was proposed to automatically select the appropriate domain for interference excision. Impulses were preferred for time domain excision while chirp and sinusoidal signals were selected for frequency domain excision.

In [84] and [85], the fact that interference occurs at the receiver was exploited to propose algorithms for interference reduction through topology control, The authors in [85] further studied the effect of an addition or removal of a single network node to the aggregate interference of a given topology. Additionally, in [86] the layout of the nodes in a network was shown to be closely related to the distance between the interfering source and the victim receiver. Hence, the authors studied the effect of the aggregate interference from a CR network given that the primary network is protected by a disc. This disc is known as the primary exclusive region (PER), where the PU transmitter and all the PU receivers are located. A wider protecting radius is then declared, within which a CR is not allowed to operate, in order to give extra protection to the PU receivers. This model was used to study the relationship and trade-offs between the PER radius, the primary transmit power and other system parameters. They further analysed a scenario of distance-dependent power scaling for the CRs, where the CR could scale their power according to their distance to further reduce harmful interference. It was observed that both the protective radius and power-scaling technique for the CRs would have a positive effect in reducing the interference measured in the network.

2.5 Multiple Access and Coexistence Techniques

In order to allow multiple users to coexist and simultaneously share a spectrum, multiple access techniques are required. An overview of some of the more common access schemes is presented at Fig. 2.4. The term multiple access is often referred to the case when dedicated channels are allocated to users [87], for example frequency division multiple access, time division multiple access or code division multiple access (see Sec. 2.5.1). The choice of using multiple access or random access or the particular multiple or random access technique to employ depends on the specific application type. For instance, applications such as video and audio that have delay constraints and require continuous transmission, generally need dedicated channels to ensure high quality of service performance. As will be seen later in Sec. 2.5.2, random access techniques are not suited for such applications.

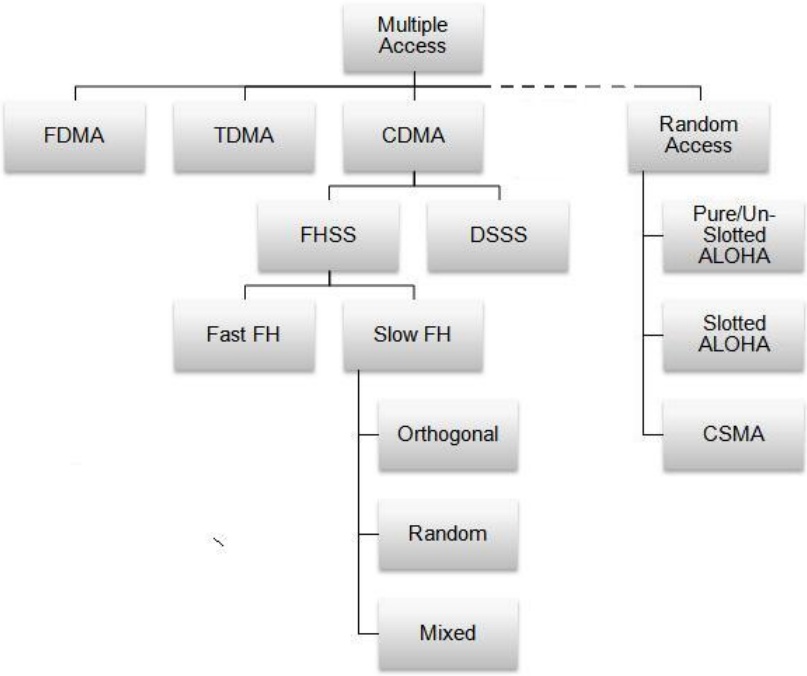

Figure 2.4: Overview of multiple access techniques.

2.5.1 Code Division Multiple Access

Code Division Multiple Access (CDMA) is a multiple access technique that allows multiple users to simultaneously occupy the same bandwidth at the same time by using *spreading codes*. The most common forms of CDMA are thus referred to as spread-spectrum, namely; direct sequence (DS) and frequency hopping (FH) [87]. These techniques possess the benefit of increasing the signal bandwidth beyond the minimum necessary for data communication and can also hide a signal below the noise floor, making it difficult to detect [87]. Among other properties, spread spectrum techniques defer from other signaling techniques that increase the transmit bandwidth by at least the following [88].

- The signal occupies a bandwidth much larger than is needed for the information signal.
- The spread-spectrum modulation is done using a spreading code, which is independent of the data in the signal.

2.5.1.1 Frequency Hopping Spread Spectrum

The type of CDMA relevant to this study is the FH spread spectrum. The basic assumption of FH is to hop the modulated data signal over a wideband by changing its carrier frequency according to the value of a pseudo random spreading code. There are two types of FH techniques, slow and fast. Let T_{h} and T_s be the hop duration and the symbol time respectively; then if the hop time exceeds the symbol time such that $T_{\mathrm{h}} = kT_{\mathrm{s}}$ for some integer k, this is referred to as slow FH. On the other hand, if there are multiple hops per symbol, such that $T_{\mathrm{h}} = T_{\mathrm{s}}/k$ then it is referred to as fast FH. In Chapter 5, a DSA primary network employing slow FH multiple access is examined.

There are three techniques of employing slow FH as defined in [89]. These include *orthogonal*, *random* and *mixed*. In the orthogonal scheme, orthogonal pseudo-random hop sequences of fixed length are assigned to different users to ensure that during any hop only one user transmits within the subband, while orthogonality is maintained by allocating distinct sets to subbands. Thus, providing frequency diversity. The protocol also assumes complete synchronisation such that two users with similar sequences will encounter continuous co-channel interference. In the random protocol, the users are assigned a unique hop sequence that may not necessarily be orthogonal to all other sequences. This protocol also exhibits interferer diversity because although cochannel interference may occur, it only occurs through a different subset of the other active users on each hop.

2.5.2 Random Multiple Access

Random multiple access also known simply as *random access* [87] or *packet radio* [76] is premised on packetized data. Random access protocols are efficient with bursty traffic, where there are many more users than available channels, yet they rarely transmit. The operation of packet radio is such that user data is collected into packets consisting of control and error detection bits. The analysis of these techniques normally assumes that, collectively, the users generate packets according to a Poisson process at a rate of λ packets per unit time. Because Poisson processes are memoryless, the number of packet arrivals during any given time period does not affect the distribution of packet arrivals in any other time period [87]. Furthermore, because network data is

generated at random time instances, assignment of dedicated channels could be severely inefficient.

The most common random access techniques are pure (or unslotted) ALOHA, slotted ALOHA, carrier sense multiple access (CSMA) and packet reservation multiple access (PRMA). In the subsequent subsection the CSMA protocol will be further discussed.

2.5.2.1 CSMA

CSMA was first proposed by Kleinrock and Tobagi [90] and is a highly researched protocol [91–97], which is now adopted in several wireless systems due to its high efficiency (compared to ALOHA protocols [74]) especially in dense networks. CSMA forms an integral part of the media access control (MAC) protocols of several communication systems[4]. For example, the primary MAC protocol under the 802.11 standard is a form of CSMA known as the distributed coordination function (DCF)[5], which can support peer-to-peer communication without centralised control of the channel access [98]. In order to avoid interference and identify channel availability for transmission, two methods of carrier sensing are defined under the 802.11 DCF protocol viz. the physical carrier sensing (PCS) and virtual carrier sensing (VCS).

The PCS is a mandatory mechanism performed at the physical layer that monitors the RF energy level in the medium directly and determines the channel availability based on the level of interference and noise around the user [97]. On the other hand, the VCS is an optional or alternative mechanism to the PCS that performs at the MAC sublayer [97]. The VCS is implemented via a two-way handshake in the form of the request-to-send (RTS) and clear-to-send (CTS) control frames, which function to reserve the channel before data transmission [99].

There are two important problems identified with CSMA protocols. The *exposed node* and the *hidden node* problems [100]. An exposed node is a node within the range of the transmitter but out of the range of the receiver. This means the intended transmitter will withhold its transmission because it can

[4]A MAC protocol is a set of rules or procedures that allow the efficient use of a shared medium

[5]With an optional protocol known as the point coordination function (PCF), where the coordination function logic is active in only one station in a service set at any given time while the network is operational [98].

hear the ongoing transmissions, while in actual fact interference occurs at the receiver and thus would have been safe to transmit. Thus resulting in underutilisation of the spectrum. On the other hand, two nodes are hidden from each other when both nodes attempt to transmit information to the same node because they are out of signal range, which results in data collision and interference.

An important reason for defining the aforementioned VCS handshake under the DCF protocol is in order to curb the *hidden node* problem. The VCS mechanism is explained thus [98]. A node intending to transmit (TX) sends out an RTS frame to the intended receiver node (RX). Node RX responds with a CTS frame granting transmission permission to TX, which also includes channel usage duration. Importantly, neighbouring nodes overhearing the RTS/CTS handshake will abide by the channel reservation by node TX. However, a neighbouring node may potentially fail to receive the RTS/CTS because a node must be located within the transmission range of TX or RX (for RTS or CTS respectively) in order to receive the channel reservation information. Although the RTS/CTS handshake is designed to further provide robustness against hidden terminal interference, unfortunately, a key assumption of the VCS mechanism is that all hidden nodes are within the receiving range of the victim receiver, which may not entirely be true in the presence of large interference ranges or when the transmitter-receiver distance grows so that some stations are outside this range [92, 97]. Hence, it was shown that the VCS has limitations in combatting the hidden node problem [92]. Nevertheless, improving the efficiency of CSMA networks could be achieved through tuning and optimising the sensing threshold [93] and other sensing parameters or by adopting other protocols like multiple access with collision avoidance (MACA) or CSMA with collision detection (CSMA/CD).

2.6 Chapter Summary

In this chapter, current spectrum sensing techniques were outlined, highlighting the pros and cons associated with each method. The ED was discussed in more detail because its performance would be further analysed in this study.

It is important to note that, no single technique or model can be applied for spectrum sensing in all situations, but the right balance should be emphasised

in order to maximise spectrum opportunities and prevent interference in the prevailing circumstance.

The various challenges affecting spectrum sensing were also discussed and an overview of the existing literature on interference analysis in DSA networks was presented. Finally, a synopsis on multiple access and coexistence techniques was given.

Chapter 3

Alternate Detection Techniques

AS the focus of the subsequent chapters in this study is mainly on the energy detector, in this chapter, two classes of alternate detector types will be analysed; namely, the power law detector and Kay's detector for unknown deterministic signals. For the former, simple but highly accurate novel approximations to the PDF and CDF of the decision variable's statistics are presented, while in the case of the latter, the decision variable is derived and its performance in both AWGN and fading channels examined. The new results are compared to the classic energy detector and validated with Monte Carlo simulations in both cases.

3.1 Background

Spectrum sensing is a crucial task in several wireless communication applications such as cognitive radios (CR), WLANs and bluetooth devices. A wide range of detector types exist to choose from, out of which a few are outlined in Sec. 2.2, while a more comprehensive survey can be found in [14]. The performance analysis of the most common types (such as energy detection (ED), matched filter detection (MFD) and cyclostationary feature detection) are widely available in the literature. However, in this chapter two alternate detector types will be further investigated.

In [23], the analysis of an improved ED was presented, subsequently referred to as the power law detector (PLD) in this study. Obtaining the statistics for the decision variable of this detector requires computation of sums of arbitrarily powered independent and identically distributed (i.i.d) Gaussian

random variables (RVs). However, at the time of presenting these results, no known closed-form expressions exist for the exact distributions of this class of RVs. Notwithstanding, approximations have been presented in [22,23,101]. Chen [23] showed that the gamma distribution provides a close fit when the summands approach 20 variates, with reduced accuracy when the summands decrease or when either the variance or exponent of the underlying Gaussian variates increase. On the other hand, in [22] it was shown that by taking advantage of the central limit theorem (CLT), a relatively close fit could be achieved using the Gaussian PDF when the summands approach 50 variates. In fact, although sums of RVs play a significant role in wireless communication applications, such as signal detection and diversity systems, the exact statistics of several of such sums are not known in closed-form. This is because the exact sum statistics of most RVs are analytically intricate and mostly require cumbersome techniques [102–109]. Within the last decade, the $\alpha-\mu$ distribution (generalised gamma) has been proposed for practical fading channels [110]. This distribution includes as special cases, the Nakagami-m, Weibull, one-sided Gaussian, Rayleigh and negative exponential distributions. As shall be shown later (see Eq. (3.4)), the PDF of an arbitrarily powered Gaussian RV is also a special case of the $\alpha-\mu$ distribution. Hence, the motivation for the approximations presented in this chapter comes from the fact that, under certain conditions, the sum of $\alpha-\mu$ powers is also $\alpha-\mu$ distributed. In Sec. 3.2.1.1, the proposed closed-form approximations are presented and the simplicity and accuracy of the approach is demonstrated in Sec. 3.2.2.

Additionally, in Sec. 3.3 the performance of a different class of detectors for unknown deterministic signals is studied. Analysis of detectors for unknown deterministic signals in AWGN have been studied by Urkowitz [47] and Kay [71]. Furthermore, the detector in [47], which is in fact the ED has been widely studied under fading channels, for example in [49,51]. However, no such analysis has been conducted for Kay's detector [71]. Hence, novel results for the analysis under AWGN and fading channels are presented in this study. Importantly, the expressions to the detection probabilities under the fading channels were derived in closed-form. To obtain this, novel alternate expressions for the complementary error function Erfc(.) and the Marcum $Q-$function $Q_m(.,.)$ of order $m = 1/2$ were first derived. In particular, the complementary error function is expressed such that the limits of integration

are finite and independent of the integrand and the random fading variable is only present in an exponent, which greatly facilitates the tractability of the analysis.

3.2 The Power Law Detector

Consider a CR network, within which a CR node employing a PLD [23] aims to detect the presence or absence of a primary user (PU) in the network. The task of the CR node can be represented as a binary hypothesis testing problem given by

$$x(n) = \begin{cases} w(n) & H_0 \\ s(n) + w(n) & H_1 \end{cases} \tag{3.1}$$

where H_0 and H_1 represent the hypotheses that the PU signal is absent or present respectively. The term $s(n) \sim \mathcal{N}(0, \sigma_s^2)$ denotes the sampled equivalent of the transmitted PU signal, $w(n) \sim \mathcal{N}(0, \sigma_w^2)$ denotes the sampled equivalent of the additive white Gaussian noise (AWGN) and $x(n)$ is the nth received sample of the sensing CR node. Both $s(n)$ and $w(n)$, $n = 1, 2, \cdots, N$ are independent. The output of the PLD is the decision variable y_{pld} which is compared against a threshold ξ to make a final decision on the presence or absence of the PU signal. If N independent samples are received during the sensing time, the decision variable for the CR node is given by

$$y_{\text{pld}} = \sum_{n=1}^{N} \left(\frac{|\, x(n) \,|}{\sigma} \right)^p \underset{H_0}{\overset{H_1}{\gtrless}} \xi \tag{3.2}$$

where p is an arbitrary positive constant and σ is the standard deviation. It could be observed that when $p = 2$, Eq. (3.2) reduces to the conventional ED [51], which presents y_{pld} as a sum of the squares of standard Gaussian RVs and therefore follows a central chi-square distribution. However, in the case of (3.2) with arbitrary $p > 0$, no known distribution exists for the statistics of y_{pld}. Hence, the need for the approximations presented in Sec. 3.2.1.1.

3.2.1 Approximations

3.2.1.1 The New Approximation

Consider the RV defined as $X = |Y|^p$, where $Y \sim \mathcal{N}(0, \sigma^2)$ and p is an arbitrary positive constant. Then the CDF is

$$\begin{aligned} F_X(x) &= \Pr(X < x) = \Pr\left(|Y| < x^{\frac{1}{p}}\right) \\ &= F_Y\left(x^{\frac{1}{p}}\right) - F_Y\left(-x^{\frac{1}{p}}\right) \\ &= 2F_Y\left(x^{\frac{1}{p}}\right) - 1. \end{aligned} \tag{3.3}$$

By differentiating (3.3), the PDF is obtained as

$$\begin{aligned} f_X(x) &= \frac{2dF_Y\left(x^{\frac{1}{p}}\right)}{dx} \\ &= \sqrt{\frac{2}{\pi}}\frac{x^{\frac{1}{p}-1}}{p\sigma}\exp\left(-\frac{x^{\frac{2}{p}}}{2\sigma^2}\right). \end{aligned} \tag{3.4}$$

In order to compute the sum of N i.i.d pth powered Gaussian variates, let

$$Z = \sum_{i=1}^{N} X_i \tag{3.5}$$

where the PDF of each X_i is given in (3.4). Note that when $\sigma^2 = 1$ and $p = 2$ in (3.4), the PDF of Z in (3.5) is straightforwardly chi-squared. However, obtaining the exact PDF for an arbitrary positive value of p is at the least a severely formidable task, if not impossible. Hence, an approximation for the PDF and CDF of Z is proposed using the envelope of the $\alpha - \mu$ distribution presented in [110] as

$$f_Z(z) = \left(\frac{\mu}{\Omega}\right)^{\mu}\frac{\alpha z^{\alpha\mu-1}}{\Gamma(\mu)}\exp\left(-\frac{\mu z^{\alpha}}{\Omega}\right) \tag{3.6}$$

$$F_Z(z) = 1 - \frac{\Gamma\left(\mu, \frac{\mu z^{\alpha}}{\Omega}\right)}{\Gamma(\mu)} \tag{3.7}$$

where $\Gamma(.)$ and $\Gamma(.,.)$ represent the gamma function and the upper incomplete gamma functions respectively [72]. The shape and scale parameters are denoted by $\alpha > 0$ and $\Omega = \mathbb{E}[Z^{\alpha}]$ respectively, while μ is the inverse

normalised variance of Z^{α}. It is worth noting that, the decision for the approximations stem from the observation that the RV with PDF as in (3.4) is in fact exactly an $\alpha - \mu$ RV with $\alpha = \frac{2}{p}$, $\mu = \frac{1}{2}$ and $\Omega = \sigma^2$, coupled with the knowledge that the sum of $\alpha - \mu$ powers is also $\alpha - \mu$ distributed [105]. As shall be demonstrated later, the suggested technique produces highly precise results for practical purposes.

Therefore, from the exact moments of Z in (3.6) and (3.7), the parameters α, μ and Ω can be computed using moment-based estimators. The procedure is outlined as follows [105].

Step 1

Firstly, by employing the multinomial expansion, the moments from (3.5) are obtained in terms of the moments of the individual pth powered Gaussian summands using the formula

$$\mathbb{E}\left[Z^n\right] = \sum_{n_1=0}^{n} \sum_{n_2=0}^{n_1} \cdots \sum_{n_{N-1}=0}^{n_{N-2}} \binom{n}{n_1}\binom{n_1}{n_2}\cdots\binom{n_{N-2}}{n_{N-1}} \times \mathbb{E}\left[X_1^{n-n_1}\right]\mathbb{E}\left[X_2^{n_1-n_2}\right]\cdots\mathbb{E}\left[X_N^{n_{N-1}}\right] \quad (3.8)$$

where $\mathbb{E}[.]$ denotes the expectation operator. The nth moment $\mathbb{E}\left[X_i^n\right]$ of the summand can be obtained using (3.4) as

$$\mathbb{E}\left[X_i^n\right] = \frac{\left(2\sigma_i^2\right)^{\frac{np}{2}}}{\sqrt{\pi}}\Gamma\left(\frac{1+np}{2}\right). \quad (3.9)$$

Step 2

Next, the moment-based estimators for μ, α and Ω can be calculated from the expressions given in [110] as

$$\frac{\mathbb{E}^2\left[Z\right]}{\mathbb{E}\left[Z^2\right] - \mathbb{E}^2\left[Z\right]} = \frac{\Gamma^2\left(\mu + \frac{1}{\alpha}\right)}{\Gamma\left(\mu\right)\Gamma\left(\mu + \frac{2}{\alpha}\right) - \Gamma^2\left(\mu + \frac{1}{\alpha}\right)} \quad (3.10a)$$

$$\frac{E^2\left[Z^2\right]}{\mathbb{E}\left[Z^4\right] - \mathbb{E}^2\left[Z^2\right]} = \frac{\Gamma^2\left(\mu + \frac{2}{\alpha}\right)}{\Gamma\left(\mu\right)\Gamma\left(\mu + \frac{4}{\alpha}\right) - \Gamma^2\left(\mu + \frac{2}{\alpha}\right)} \quad (3.10b)$$

$$\Omega = \left[\frac{\mu^{\frac{1}{\alpha}} \Gamma(\mu) \mathbb{E}[Z]}{\Gamma\left(\mu + \frac{1}{\alpha}\right)} \right]^{\alpha}. \tag{3.10c}$$

This step involves first obtaining α and μ by numerically solving (3.10a) and (3.10b) simultaneously and directly substituting the results in (3.10c) to obtain the value of Ω. Note that the numerical computation of (3.10a) and (3.10b) can be efficiently achieved using most modern software packages, such as `FindRoot` in Mathematica. Finally, by substituting the values acquired from steps 1 and 2 into (3.6) and (3.7), the required approximations are obtained.

Figs. 3.1 and 3.2 illustrate the accuracy of the new results. The approximate analytical PDFs and CDFs for the sum of four and eight i.i.d pth powered Gaussian variates are presented and compared against the exact results from simulations. In particular, values at $\sigma^2 = 1$, $p = 1, 3$ and 4.5 are shown. Note that the curves indicate agreement with the simulations for both integer and non-integer exponents, p. Furthermore, the exact results are obtained from Monte Carlo simulations in MATLAB using at least 10^5 realisations for the CDF and 10^6 sets with 20 bins for the PDF histograms (the `hist` command was used). Moreover, the results obtained here are an improvement from those obtained with the Gaussian PDF approximation in [22] or the gamma PDF approximation approach in [23]. In particular, the results are useful for very low summands, since the approach in [22] depends on the CLT for large summands and using similar parameters, the results in [23] required approximately 20 summands. The practical application of these results are presented in Sec. 3.2.2.

3.2.1.2 Gamma Approximation

For completeness, the gamma approximation employed in [23] is briefly outlined here and compared against the novel approximations in Sec. 3.2.2.

Recall the gamma PDF and CDF given by

$$f(y) = \frac{1}{\theta^{\varphi} \Gamma(\varphi)} y^{\varphi - 1} e^{-\frac{y}{\theta}} \tag{3.11}$$

$$F(y) = 1 - \frac{\Gamma\left(\varphi, \frac{y}{\theta}\right)}{\Gamma(\varphi)} \tag{3.12}$$

where φ and θ are the shape and scale parameters respectively. The statistics

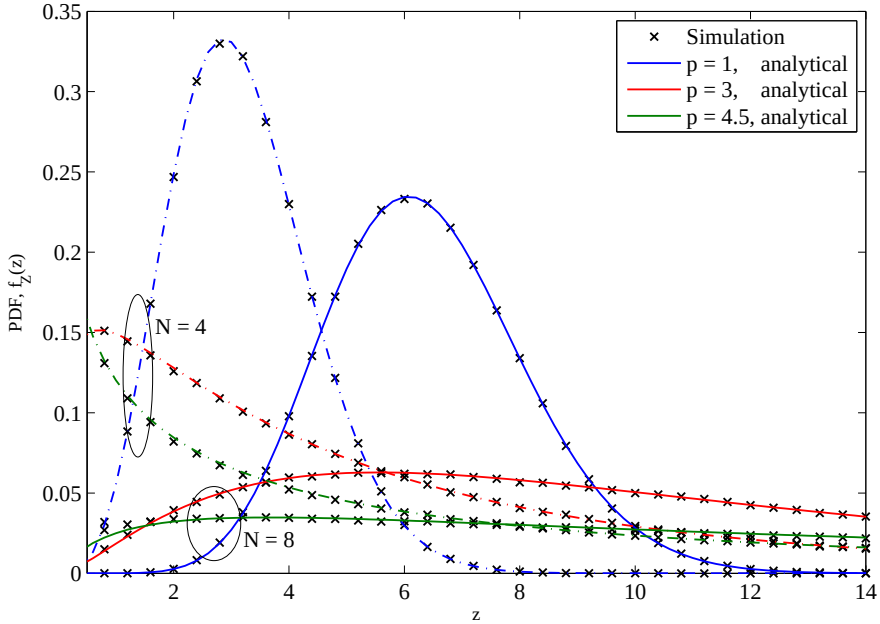

Figure 3.1: PDFs for the sum of i.i.d pth powered Gaussian RVs. $N = 4$ (dashed curves) and $N = 8$ (solid curves).

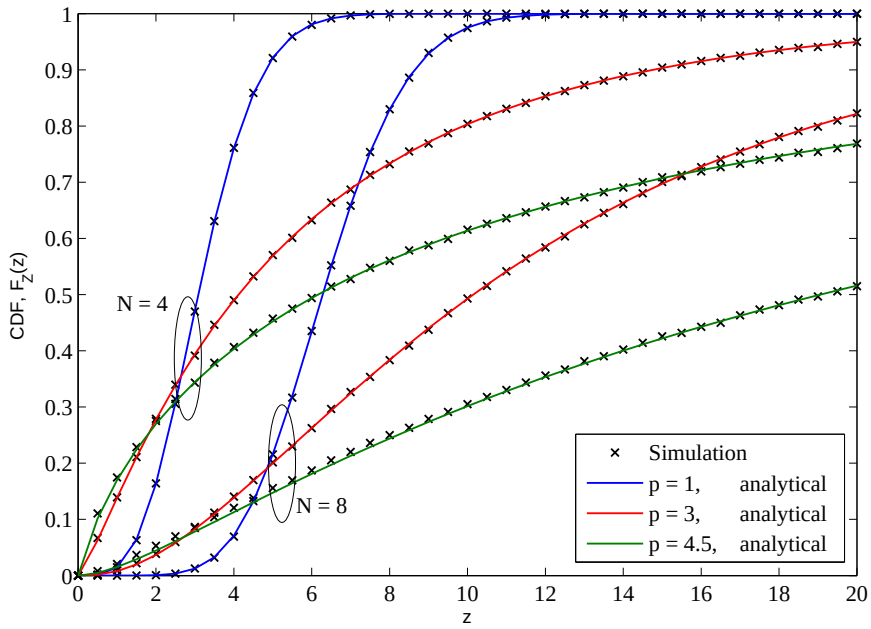

Figure 3.2: CDFs for the sum of i.i.d pth powered Gaussian RVs. $N = 4$ and $N = 8$. Exponent $p = 1, 3$ and 4.5

of y_{pld} is approximated as a gamma RV by matching its mean and variance. The shape parameter is defined as

$$\varphi = \frac{\mathbb{E}^2\left[y_{\text{pld}}\right]}{\text{var}\left[y_{\text{pld}}\right]} \tag{3.13}$$

while the scale parameter is defined as

$$\theta = \frac{\text{var}\left[y_{\text{pld}}\right]}{\mathbb{E}\left[y_{\text{pld}}\right]} \tag{3.14}$$

where $\mathbb{E}\left[x\right]$ and $\text{var}\left[x\right]$ are the expectation and variance of the RV x. Obviously the mean and variance required to compute (3.13) and (3.14) depend on the hypotheses H_0 and H_1 in (3.2). However, in general for a variance σ^2,

$$\mathbb{E}\left[y_{\text{pld}}\right] = N\frac{2^{\frac{p}{2}}\sigma^p}{\Gamma\left(\frac{1}{2}\right)}\Gamma\left(\frac{p+1}{2}\right) \tag{3.15}$$

$$\text{var}\left[y_{\text{pld}}\right] = N\frac{(2\sigma^2)^p}{\Gamma\left(\frac{1}{2}\right)}\left\{\Gamma\left(\frac{2p+1}{2}\right) - \frac{\Gamma^2\left(\frac{p+1}{2}\right)}{\Gamma\left(\frac{1}{2}\right)}\right\}. \tag{3.16}$$

A comparison of this approximation technique is presented in the subsequent subsection.

3.2.2 Results and Analysis

The analysis for the performance of the PLD is presented in this section. The detector performance is quantified by evaluating the receiver operating characteristic (ROC) curves [71], which characterises the relationship between the probability of false alarm P_{f} and the probability of detection P_{d}. The P_{f} and P_{d} are defined as

$$P_{\text{f}} = \Pr\left(y_{\text{pld}} > \xi \mid H_0\right) \tag{3.17}$$

$$P_{\text{d}} = \Pr\left(y_{\text{pld}} > \xi \mid H_1\right) \tag{3.18}$$

where ξ is the detection threshold of the detector. From (3.6) and (3.7), P_{f} and P_{d} in (3.17) and (3.18) can be computed as

$$P_{\mathrm{f}}^{\mathrm{pld}} = \frac{\Gamma\left(\mu, \frac{\mu\xi^{\alpha}}{\Omega_0}\right)}{\Gamma\left(\mu\right)} \tag{3.19}$$

and

$$P_{\mathrm{d}}^{\mathrm{pld}} = \frac{\Gamma\left(\mu, \frac{\mu\xi^{\alpha}}{\Omega_1}\right)}{\Gamma\left(\mu\right)} \tag{3.20}$$

where Ω_0 and Ω_1 in (3.19) and (3.20) are the respective scale parameters under H_0 and H_1. The scale parameters under each probability is obtained by replacing the variance σ_i^2 within the nth moment of the summand in (3.9), such that

$$\mathbb{E}\left[X_i^n\right] = \begin{cases} \frac{\left(2\sigma_{w,i}^2\right)^{\frac{np}{2}}}{\sqrt{\pi}}\Gamma\left(\frac{1+np}{2}\right), & H_0 \\ \frac{2^{\frac{np}{2}}\sigma_{w,i}^{np}(1+\gamma_i)^{\frac{np}{2}}}{\sqrt{\pi}}\Gamma\left(\frac{1+np}{2}\right) & H_1 \end{cases} \tag{3.21}$$

where $\sigma_{w,i}^2$ is the noise variance of the ith received sample and γ_i is the signal-to-noise ratio (SNR).

On the other hand, for the gamma approximation, the P_{f} and P_{d} are given by [23] as

$$P_{\mathrm{f}}^{\mathrm{gam}} = \frac{\Gamma\left(\varphi_0, \frac{\xi}{\theta_0}\right)}{\Gamma\left(\varphi_0\right)} \tag{3.22}$$

and

$$P_{\mathrm{d}}^{\mathrm{gam}} = \frac{\Gamma\left(\varphi_1, \frac{\xi}{\theta_1}\right)}{\Gamma\left(\varphi_1\right)} \tag{3.23}$$

where $\theta_0 = \theta|H_0$, $\theta_1 = \theta|H_1$, $\varphi_0 = \varphi|H_0$ and $\varphi_1 = \varphi|H_1$. Using (3.15) and (3.16) in (3.13) and (3.14) for the correct hypothesis and substituting in (3.22) and (3.23) the required probabilities are obtained as

$$P_{\mathrm{f}}^{\mathrm{gam}} = \frac{\Gamma\left(N\frac{\Gamma^2\left(\frac{p+1}{2}\right)}{\Gamma\left(\frac{2p+1}{2}\right)\Gamma\left(\frac{1}{2}\right)-\Gamma^2\left(\frac{p+1}{2}\right)}, \xi\cdot\left[2^{\frac{p}{2}}\left\{\frac{\Gamma\left(p+\frac{1}{2}\right)}{\Gamma\left(\frac{p+1}{2}\right)} - \frac{\Gamma\left(\frac{p+1}{2}\right)}{\Gamma\left(\frac{1}{2}\right)}\right\}\right]^{-1}\right)}{\Gamma\left(N\frac{\Gamma^2\left(\frac{p+1}{2}\right)}{\Gamma\left(\frac{2p+1}{2}\right)\Gamma\left(\frac{1}{2}\right)-\Gamma^2\left(\frac{p+1}{2}\right)}\right)} \tag{3.24}$$

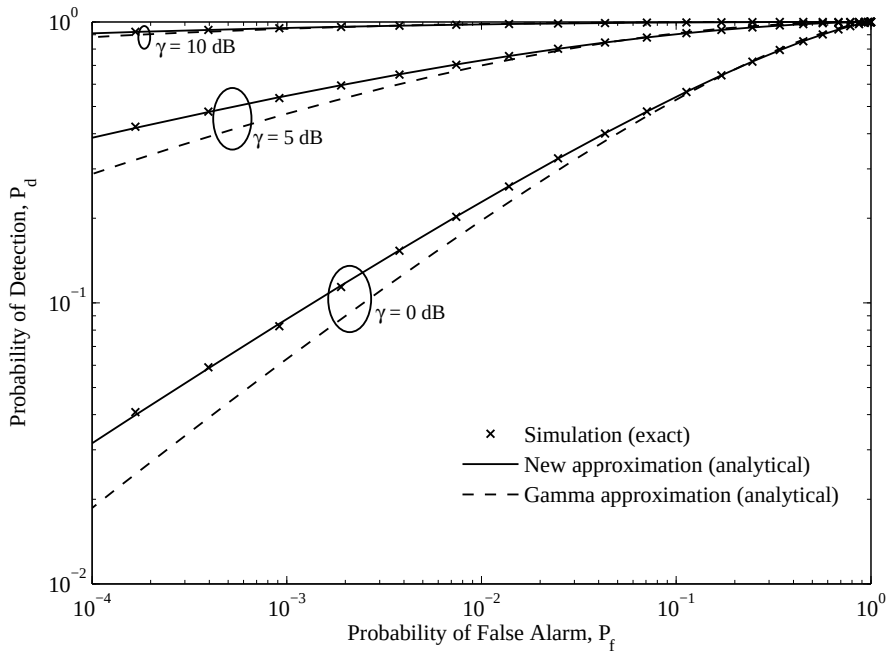

Figure 3.3: ROC for $p = 1$, $N = 8$. The $P_{\mathrm{f}}^{\mathrm{pld}}$ and $P_{\mathrm{d}}^{\mathrm{pld}}$ are plotted from (3.19) and (3.20), while the gamma approximations are from (3.24) and (3.25).

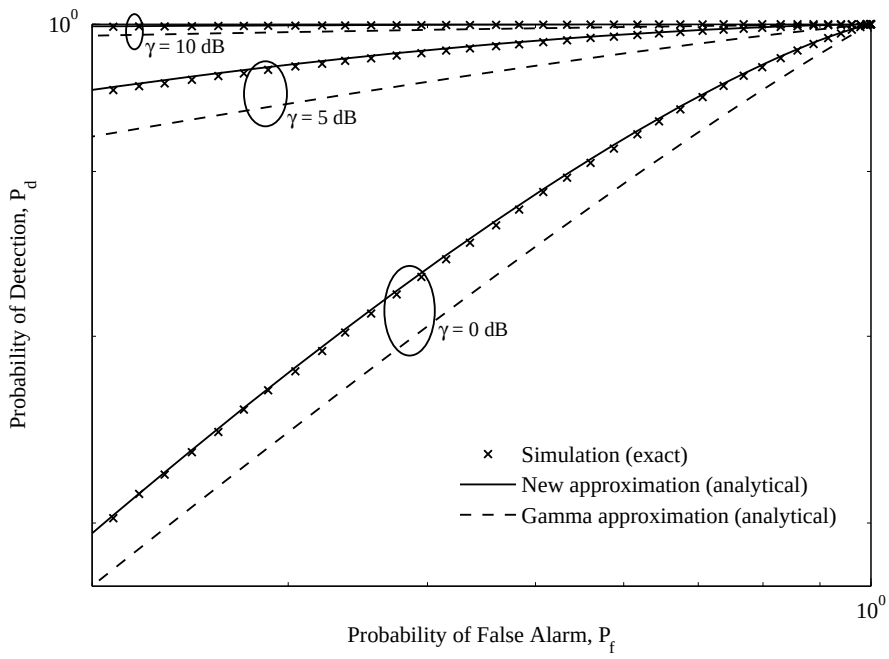

Figure 3.4: ROC for $p = 3$, $N = 8$. The $P_{\mathrm{f}}^{\mathrm{pld}}$ and $P_{\mathrm{d}}^{\mathrm{pld}}$ are plotted from (3.19) and (3.20), while the gamma approximations are from (3.24) and (3.25).

and

$$P_{\mathrm{d}}^{\mathrm{gam}} = \frac{\Gamma\left(N\frac{\Gamma^2\left(\frac{p+1}{2}\right)}{\Gamma\left(\frac{2p+1}{2}\right)\Gamma\left(\frac{1}{2}\right)-\Gamma^2\left(\frac{p+1}{2}\right)}, \xi \cdot \left[\frac{(2(1+\gamma))^{\frac{p}{2}}}{\Gamma\left(\frac{p+1}{2}\right)\Gamma\left(\frac{1}{2}\right)}\left\{\Gamma\left(\frac{2p+1}{2}\right)\Gamma\left(\frac{1}{2}\right)-\Gamma^2\left(\frac{p+1}{2}\right)\right\}\right]^{-1}\right)}{\Gamma\left(N\frac{\Gamma^2\left(\frac{p+1}{2}\right)}{\Gamma\left(\frac{2p+1}{2}\right)\Gamma\left(\frac{1}{2}\right)-\Gamma^2\left(\frac{p+1}{2}\right)}\right)}. \tag{3.25}$$

Figs. 3.3 and 3.4 display the ROC curves when SNR $\gamma = 0, 5$ and 10dB, for $N = 8$ received samples. The results are compared against the exact results obtained from Monte Carlo simulations. The $\alpha - \mu$ approximations were plotted from (3.19) and (3.20) using the technique described in Sec. 3.2.1.1, while the gamma approximations were plotted from (3.24) and (3.25). In all cases, it can be observed that the novel $\alpha - \mu$ approximations present excellent agreement with the exact results, and importantly, the curves are indistinguishable for practical purposes.

3.3 Kay's Detector

Consider the detector proposed by Kay [71, Ch. 7] for unknown deterministic signals. The detector is particularly useful when the amplitude of the signal is unknown. For the received signal $x(t)$ the binary hypothesis problem is

$$x(t) = \begin{cases} w(t) & H_0 \\ s(t) + w(t) & H_1 \end{cases} \tag{3.26}$$

where H_0 and H_1 represent the hypotheses that the desired signal is absent or present respectively. $w(t)$ is the zero mean additive white Gaussian noise while $s(t)$ is the desired signal and both $w(t)$ and $s(t)$ are independent. At the detector, N independent samples of $x(t)$ are received. The samples are then summed and finally squared. The resultant output is the decision variable y_{kay} given by

$$y_{\mathrm{kay}} = \left(\sum_{n=1}^{N} x(n)\right)^2. \tag{3.27}$$

The PDF of the decision variable Y can be shown to follow a central chi-square RV with one degree of freedom (DoF) under H_0 and a non-central chi-square RV with one DoF under H_1. Hence

$$f(y) = \begin{cases} \frac{y^{\frac{1}{2}-1} e^{-\frac{y}{2N\sigma^2}}}{\sqrt{2N\pi\sigma^2}} & H_0 \\ \frac{1}{2N\sigma^2} \left(\frac{y}{2\gamma}\right)^{-\frac{1}{4}} e^{-\frac{(y+2\gamma)}{2N\sigma^2}} I_{\frac{1}{2}-1}\left(\frac{\sqrt{2\gamma y}}{N\sigma^2}\right) & H_1 \end{cases} \tag{3.28}$$

where $I_v(.)$ is the vth order modified Bessel function of the first kind [72, Sec. 8.43] and γ is the signal-to-noise ratio (SNR).

Analogous to (3.17) and (3.18), the P_{f} and P_{d} are defined as

$$P_{\mathrm{f}} = \Pr\left(y_{\mathrm{kay}} > \xi \mid H_0\right) \tag{3.29}$$

$$P_{\mathrm{d}} = \Pr\left(y_{\mathrm{kay}} > \xi \mid H_1\right) \tag{3.30}$$

where ξ is the detection threshold of the detector. In the following subsections, (3.29) and (3.30) are employed to compute the false alarm and detection probabilities.

3.3.1 Probability of False Alarm over AWGN Channels

By applying (3.28) to compute (3.29), the false alarm probability can straightforwardly be obtained as

$$P_{\mathrm{f}}^{\mathrm{kay}} = \mathrm{Erfc}\left(\sqrt{\frac{\xi}{2N\sigma^2}}\right) \tag{3.31}$$

where $\mathrm{Erfc}(x) = \frac{2}{\sqrt{\pi}} \int_x^{\infty} \exp\left(-t^2\right) dt$ is the complementary error function [72, Sec. 8.25].

3.3.2 Probability of Detection over AWGN Channels

The detection probability can be computed by employing (3.28) under H_1 to compute (3.30). Utilising [42, Eq. (2-1-124)] yields

$$P_{\mathrm{d}}^{\mathrm{kay}} = Q_{\frac{1}{2}}\left(\sqrt{\frac{2\gamma}{\sigma^2}}, \sqrt{\frac{\xi}{N\sigma^2}}\right) \tag{3.32}$$

where $Q_m(.,.)$ is the generalised mth order Marcum Q-function [111].

3.3.3 Detection Probability under Fading Channels

In this section the detection probabilities over fading channels are derived. It is worth noting that since $P_{\mathrm{f}}^{\mathrm{kay}}$ is independent of the SNR term, it remains the same under both AWGN and fading channels.

The average $P_{\mathrm{d}}^{\mathrm{kay}}$ is obtained by averaging (3.32) over the PDF of the fading channel $f(\gamma)$. Hence

$$P_{\mathrm{d}}^{\mathrm{kay}}(\gamma) = \int_0^\infty Q_{\frac{1}{2}}\left(\sqrt{\frac{2\gamma}{\sigma^2}}, \sqrt{\frac{\xi}{N\sigma^2}}\right) f(\gamma)\, d\gamma. \tag{3.33}$$

Note that the direct computation of the integral whose integrand consists of the product of (3.32) and $f(\gamma)$ is in general a very tedious task. However, by expressing (3.32) in an alternate form that has the desired property that the RV γ appears only in the exponent, averaging out the RV using its MGF will be greatly facilitated.

To proceed further, the following Lemma is proposed.

Lemma 1. *It can be shown that (3.32) is equivalent to*[1]

$$Q_{\frac{1}{2}}\left(\sqrt{2\gamma}, \sqrt{\frac{\xi}{N}}\right) = \frac{1}{2}\left\{\mathrm{Erfc}\left(\frac{\sqrt{\xi}-\sqrt{2N\gamma}}{\sqrt{2N}}\right) + \mathrm{Erfc}\left(\frac{\sqrt{\xi}-\sqrt{2N\gamma}}{\sqrt{2N}}\right)\right\}. \tag{3.34}$$

Proof: Recall, the mth order generalised Marcum Q-function is given by [111, Eq. (4.33)]

$$Q_m(\alpha, \beta) = \frac{1}{\alpha^{m-1}} \int_\beta^\infty x^m \exp\left(-\frac{x^2+\alpha^2}{2}\right) I_{m-1}(\alpha x)\, dx \tag{3.35}$$

where $I_v(z)$ is the vth order modified Bessel function of the first kind. When $m = 1/2$, then

$$Q_{\frac{1}{2}}(\alpha, \beta) = \frac{1}{\alpha^{-\frac{1}{2}}} \int_\beta^\infty x^{\frac{1}{2}} \exp\left(-\frac{x^2+\alpha^2}{2}\right) I_{-\frac{1}{2}}(\alpha x)\, dx. \tag{3.36}$$

From the identity [72, Eq. (1.311.4)], $\cosh(x) = \frac{1}{2}(e^x + e^{-x})$ and the fact

[1] where the variance is assumed to be $\sigma^2 = 1$.

that $I_{-\frac{1}{2}}(\alpha x) = \sqrt{\frac{2}{\pi}}\frac{\cosh(\alpha x)}{\sqrt{\alpha x}}$, Eq. (3.36) can be expressed as

$$\begin{aligned} Q_{\frac{1}{2}}(\alpha,\beta) &= \sqrt{\frac{2}{\pi}}\int_{\beta}^{\infty} e^{-\frac{x^2+\alpha^2}{2}}\left\{\frac{1}{2}\left(e^{\alpha x}+e^{-\alpha x}\right)\right\}dx \\ &= \sqrt{\frac{2}{\pi}}\int_{\beta}^{\infty}\frac{1}{2}\left\{e^{-\frac{1}{2}(x+\alpha)^2}+e^{-\frac{1}{2}(x-\alpha)^2}\right\}dx \\ &= \frac{1}{2}\left\{\text{Erfc}\left(\frac{\beta-\alpha}{\sqrt{2}}\right)+\text{Erfc}\left(\frac{\beta+\alpha}{\sqrt{2}}\right)\right\}. \end{aligned} \tag{3.37}$$

■

Furthermore, the following Lemma is proposed.

Lemma 2. *For any $y > 0$, then*

$$\text{Erf}(y \pm b) = \frac{2}{\sqrt{\pi}}\int_0^y \exp\left(-\left(x^2 \pm 2bx + b^2\right)\right)dx \pm \text{Erf}(b) \tag{3.38}$$

where $\text{Erf}(x) = \frac{2}{\sqrt{\pi}}\int_0^x \exp(-t^2)\,dt$ is the error function [72, Eq. (8.250.1)] .

Proof: Invoking the identity [112, Eq. (7.4.32)]

$$\int e^{-\left(ax^2+2bx+c\right)}dx = \frac{1}{2}\sqrt{\frac{\pi}{a}}\exp\left(\frac{b^2-ac}{a}\right)\text{Erf}\left(\sqrt{a}x+\frac{b}{\sqrt{a}}\right)+C \tag{3.39}$$

where $a \neq 0$. Then by selecting an arbitrary upper limit $y > 0$, it is possible to obtain a value for the constant of integration C in (3.39). Thus

$$\int_0^y e^{-\left(ax^2+2bx+c\right)}dx = \frac{1}{2}e^{\frac{b^2}{a}-c}\sqrt{\frac{\pi}{a}}\left[\text{Erf}\left(\frac{b+a\sqrt{y}}{\sqrt{a}}\right)-\text{Erf}\left(\frac{b}{\sqrt{a}}\right)\right]. \tag{3.40}$$

By inspection of (3.40), it can be observed that C in (3.39) is $\text{Erf}\left(\frac{b}{\sqrt{a}}\right)$. Hence, substituting this value into (3.39) and rearranging yields

$$\text{Erf}\left(\sqrt{a}y+\frac{b}{\sqrt{a}}\right) = \text{Erf}\left(\frac{b}{\sqrt{a}}\right)+2\sqrt{\frac{a}{\pi}}e^{\frac{ac-b^2}{a}}\int_0^y e^{-\left(ax^2+2bx+c\right)}dx \qquad a \neq 0. \tag{3.41}$$

For values $a = 1$ and $c = 0$ in (3.41), the following transformation can be obtained

$$\text{Erf}(y \pm b) = \frac{2}{\sqrt{\pi}}\int_0^y \exp\left(-\left(x^2 \pm 2bx + b^2\right)\right)dx \pm \text{Erf}(b) \tag{3.42}$$

which is the desired proof.

■

Thus with the aid of (3.34) and (3.38), while using the fact that $\text{Erf}(x) = 1 - \text{Erfc}(x)$, Eq. (3.33) can be expressed in an alternate form

$$P_{\text{d}}^{\text{kay}}(\gamma) = \int_0^{\infty} \left\{ 1 - \frac{1}{\sqrt{\pi}} \int_0^{u} \left\{ e^{-\left(x-\sqrt{\gamma}\right)^2} + e^{-\left(x+\sqrt{\gamma}\right)^2} \right\} dx \right\} f(\gamma)\, d\gamma \tag{3.43}$$

where $u = \sqrt{\frac{\xi}{2N}}$. The form of the equation in (3.43) has the desired form that the RV γ appears only in the exponent, which greatly facilitates averaging out the RVs using their MGFs.

3.3.3.1 Rayleigh Fading

To compute the average detection probability over the Rayleigh fading channel, the PDF of the Rayleigh channel [111, Eq. (2.7)] is required. This is given by

$$f_{\text{Ray}}(\gamma) = \frac{1}{\bar{\gamma}} \exp\left(-\frac{\gamma}{\bar{\gamma}}\right), \qquad \gamma \geq 0 \tag{3.44}$$

where $\bar{\gamma}$ is the average SNR. Using (3.44) in (3.43), the average probability of detection over the Rayleigh channel is

$$P_{\text{d,Ray}}^{\text{kay}} = \text{Erfc}\left(\sqrt{\frac{\xi}{2N}}\right) + \left\{ \text{Erf}\left(\sqrt{\frac{\xi\bar{\gamma}}{2N(1+\bar{\gamma})}}\right) \exp\left(-\frac{\xi}{2N(1+\bar{\gamma})}\right) \left(\frac{\bar{\gamma}}{1+\bar{\gamma}}\right)^{\frac{1}{2}} \right\} \tag{3.45}$$

3.3.3.2 Nakagami-m Fading

As far as the Nakagami-m channel is concerned, the PDF of the SNR γ is a gamma RV given by [111, Eq. (2.21)]

$$f_{\text{Nak}}(\gamma) = \frac{m^m \gamma^{m-1}}{\bar{\gamma}^m \Gamma(m)} \exp\left(-\frac{m\gamma}{\bar{\gamma}}\right), \qquad \gamma \geq 0 \tag{3.46}$$

where $\Gamma(.)$ represents the gamma function [72] and m is the Nakagami parameter. By employing (3.46) to compute (3.43), it could be shown that the

average P_{d} over the Nakagami channel is

$$P_{\mathrm{d,Nak}}^{\mathrm{kay}} = 1 - \frac{2}{\sqrt{\pi}} \left(\frac{m}{m+\bar{\gamma}} \right)^{m} \int_{0}^{\sqrt{\frac{\xi}{2N}}} e^{-x^2} {}_1F_1 \left(m; \frac{1}{2}; \frac{x^2\bar{\gamma}}{m+\bar{\gamma}} \right) dx \tag{3.47}$$

where ${}_1F_1(.;.;.)$ is the confluent hypergeometric function [72, Sec. 9.2]. Upon further manipulations, (3.47) can be reduced to

$$P_{\mathrm{d,Nak}}^{\mathrm{kay}} = 1 - \sqrt{\frac{2\xi}{N\pi}} \left(\frac{m}{m+\bar{\gamma}} \right)^{m} \Phi_2 \left(\frac{1}{2} - m, m, \frac{3}{2}; -\frac{\xi}{2N}, -\frac{\xi}{2N} \left(\frac{m}{m+\bar{\gamma}} \right) \right) \tag{3.48}$$

where $\Phi_2(.,.,.;.,.)$ is the Humbert series of the second type [113, Sec. 7.2.4]. The proof of (3.48) from (3.47) is presented in what follows.

Proof: The inner integral of (3.47) is

$$\int_{0}^{u} e^{-x^2} {}_1F_1 \left(m; \frac{1}{2}; \frac{x^2\bar{\gamma}}{m+\bar{\gamma}} \right) dx \tag{3.49}$$

where $u = \sqrt{\frac{\xi}{2N}}$. By expanding and expressing the exponential and confluent hypergeometric terms in their infinite series forms, (3.49) becomes

$$\int_{0}^{u} \sum_{n}^{\infty} \sum_{r}^{\infty} \frac{(-x^2)^n}{n!r!} \left(\frac{x^2\bar{\gamma}}{m+\bar{\gamma}} \right)^{r} \frac{(m)_r}{\left(\frac{1}{2}\right)_r} dx \tag{3.50}$$

where the notation $(.)_n$ in (3.50) denotes the Pochhammer symbol. Interchanging the summation and integral operations, then integrating yields

$$\sum_{n}^{\infty} \sum_{r}^{\infty} \frac{(-1)^n u^{1+2r+2n}}{2n!r!\left(\frac{1}{2}+r+n\right)} \left(\frac{\bar{\gamma}}{m+\bar{\gamma}} \right)^{r} \frac{(m)_r}{\left(\frac{1}{2}\right)_r}. \tag{3.51}$$

Eq. (3.51) can be represented as $\Phi_2\left(\frac{1}{2} - m, m, \frac{3}{2}; -u^2, -\frac{u^2 m}{m+\bar{\gamma}}\right)$ after several manipulations, which is in the form of the third term in (3.48). ■

3.3.4 Results

In this section, results are presented to illustrate the performance of the detector. Receiver operating characteristic (ROC) curves are plotted for the various expressions derived in Sec. 3.3 and Monte Carlo simulations are performed

and presented alongside, which indicate perfect agreement with the numerical results. In all figures, Monte Carlo simulations are for at least 10^5 trials and are denoted by symbols in the curves. Other parameters include $\sigma^2 = 1$ and $N = 10$ unless otherwise mentioned.

Figs. 3.5 and 3.6 present results for both detectors. In both cases a better performance is observed in the ROC curves of the Kay's detector. Particularly, in Fig. 3.6 where the effect of altering the received samples is compared. It is known from [47,51] that the ROC performance of the ED drops with increased samples. However, it is observed that for the Kay's detector, the performance is constant along the same ROC curves even if the samples are increased. This could be explained from the fact that the detector has only one DoF.

Figs. 3.7 and 3.8 illustrate the effect of the detection threshold on $P_{\mathrm{d,Nak}}^{\mathrm{kay}}$ under Nakagami fading for $m = 1, 2$ and 3. Note that for $m = 1$, the Nakagami channel reduces to a Rayleigh faded channel. Again it is observed from both figures that the simulations are in agreement with the derived numerical results. Furthermore, it is observed that an improved average SNR and increased received samples (Figs. 3.7 and 3.8 respectively) both improve the detection probability as expected.

3.4 Chapter Summary

Two detectors were analysed under this chapter. The first, which is the power law detector was revisited. The statistics of the decision variable for this detector type involves the need to compute the sum of arbitrarily powered Gaussian random variables, for which simple but highly precise approximations for the PDF and CDF were presented. The technique proposed was illustrated to be more accurate than a currently existing techniques for the range of values examined. Furthermore, it is worth noting that the approximation of these sums are also useful in other areas of wireless communication not mentioned here. For instance in p-Law combining (pLC), where the receiver combines all diversity branches before making a decision. As for the second detector type, the current analysis in the literature was extended from the AWGN channel to Rayleigh and Nakagami fading channels for which the relevant analytical expressions were derived and the results contrasted against that of the classic energy detector. For both detector types, Monte

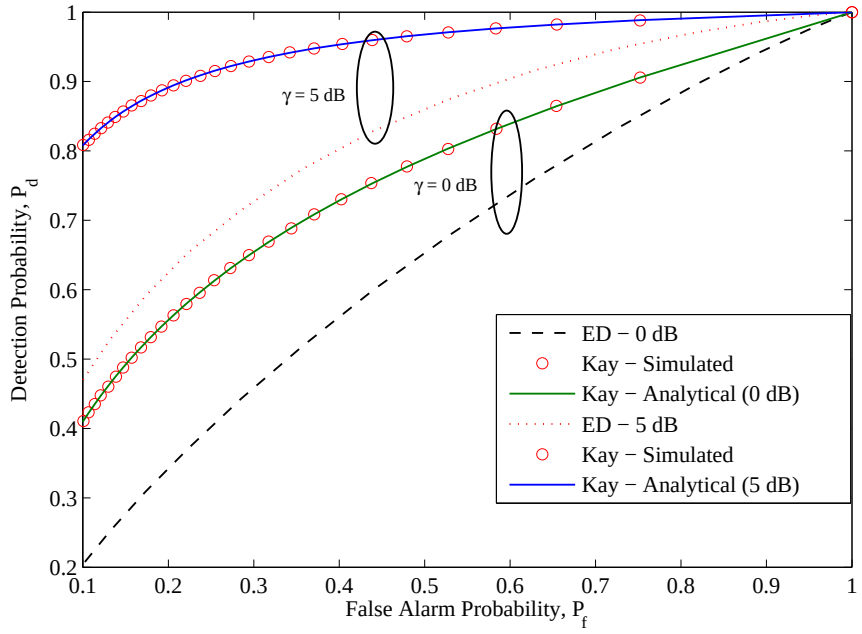

Figure 3.5: ROC curves for an AWGN channel. Both detectors compared. Analytical curves for Kay's detector from (3.31) and (3.32), while ED curves using (2.4) and (2.6).

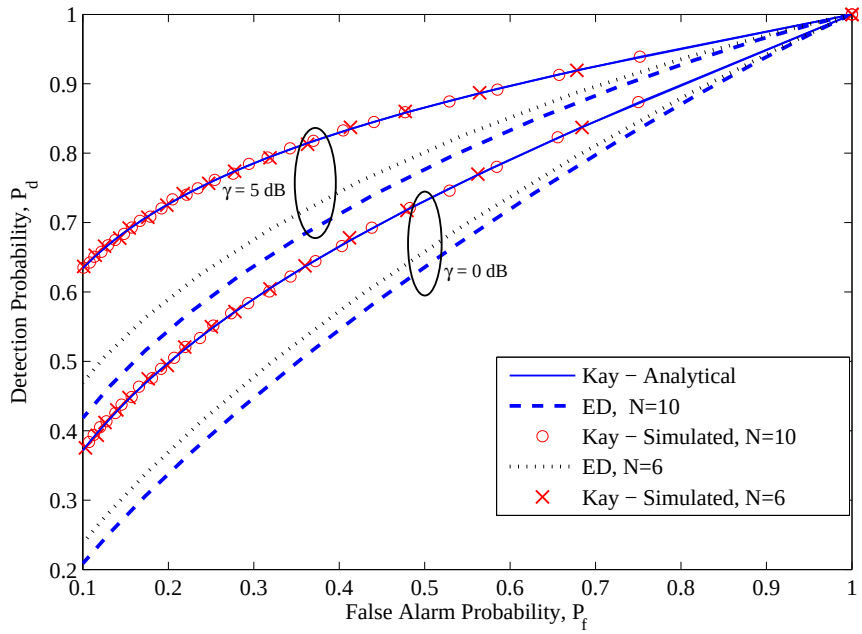

Figure 3.6: ROC curves for a Rayleigh faded channel. Both detectors compared. Analytical curves for Kay's detector using (3.31) and (3.45), while ED curves using (2.4) and (2.7).

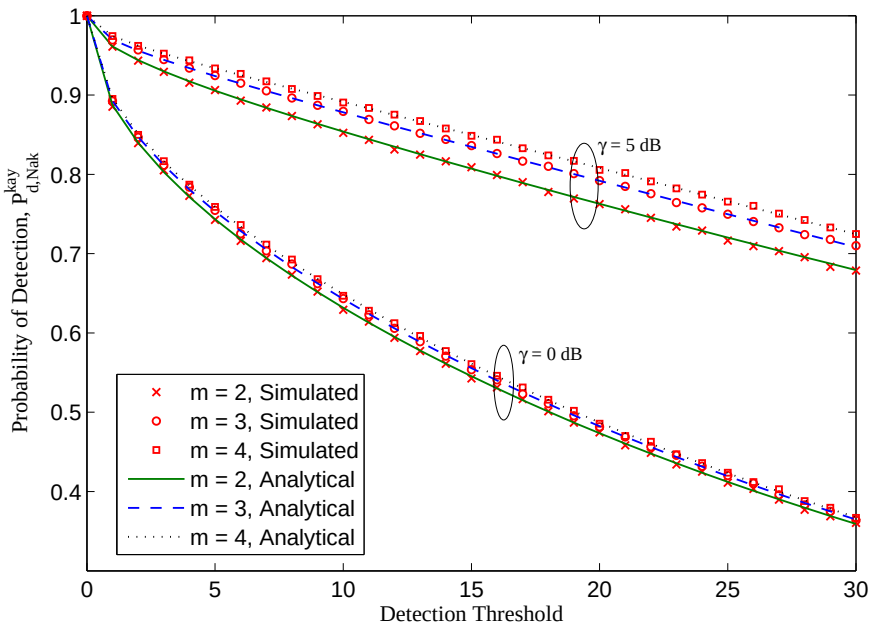

Figure 3.7: Probability of detection curves for a Nakagami-m faded channel comparing effect of varying the detection threshold against the parameter m and SNR. Analytical curves for Kay's detector from (3.48).

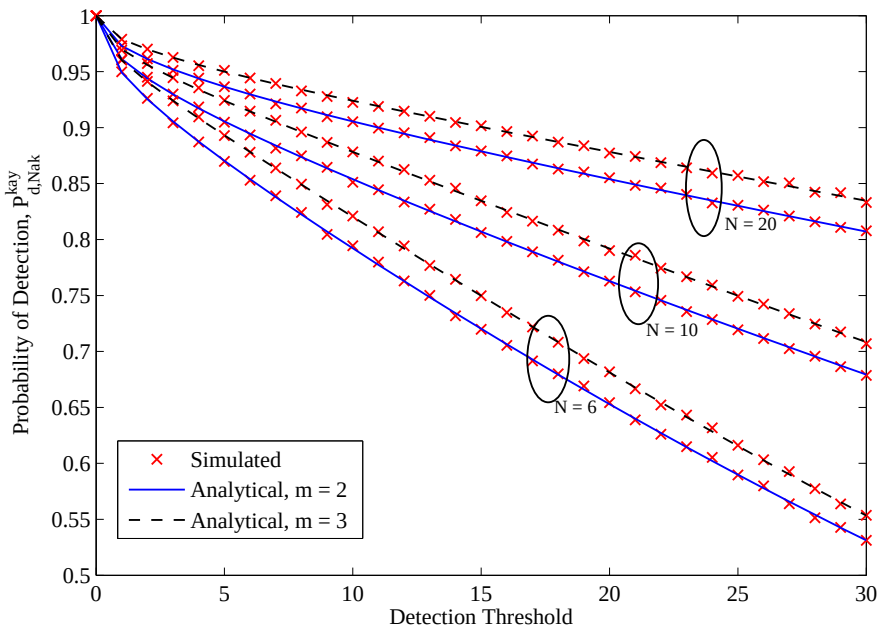

Figure 3.8: Probability of detection curves for a Nakagami-m faded channel comparing effect of varying the detection threshold against the parameter m and number of samples N. Analytical curves for Kay's detector from (3.48).

Carlo simulation results were presented alongside to show the validity of the mathematical analysis.

Chapter 4

Efficiency of Detectors in the Presence of Co-Channel Interference

THIS chapter introduces the key interference models used to analyse the performance of the energy detector for spectrum sensing. The relevant performance metrics based on these models are also derived. Most results in this chapter have been published in [114–116].

4.1 Background

As previously discussed in Sec. 2.3, the energy detector (ED) by definition measures the energy present in a received signal sample and can be classified as a *blind-detector* [117] since it requires no further information on the properties of the desired signal. Therefore it has no means of differentiating between noise, interference or different signal types [3, 27]. This means that when the ED is used for spectrum sensing, it would be limited in its capability to differentiate between the primary user (PU) and another secondary user (SU). Such "blind-detectors" are good choices for the CR, since the CR would not always have the luxury of having *a priori* knowledge of the desired signal to be detected. As a result, it is pertinent to analyse the performance of the ED in the presence of interfering signals.

The performance of EDs have been extensively studied in various literature including [26, 27, 47–49, 51–53, 55–57, 69]. In the classic paper by Urkowitz [47],

energy detection of unknown deterministic signals in a bandlimited Gaussian noise channel was studied, while [48] investigates the performance of an ED in the presence of non-Gaussian noise. Further studies were conducted in [49, 51–53, 55], for ED performance over various fading channels and performance based on false alarm and detection probabilities obtained. In particular, ED performance for specific use in CR spectrum sensing have been discussed in [26, 27, 52, 53, 55–57, 69]. In the aforementioned literature, the ED performance is analysed in either Gaussian/non-Gaussian noise channels or over fading channels [48, 50–52]. This indicates that the other secondary users (SU) are either assumed to be silent during the sensing period or their presence is disregarded.

Regarding interference modelling in CR applications, analysis of interference to the primary network [77, 78, 80, 118–121] has received considerably much more attention than analysis conducted on the interference to the CR network. The reason for this interest could probably be due to the expectation of CR nodes avoiding harmful interference to the primary user (PU) network and not vice versa. In the few cases where interference analysis is conducted with respect to the CR network, the interference at the spectrum sensing node or the specific case of the ED have received less attention. In fact, [82] considers the aggregate interference generated by multiple primary user presence on the entire CR network as against a single CR node. In which case, the intra-network interference of the secondary CR network is still not accounted for. More recently, [122] and [123] have examined the effect of interference on ED performance with the latter employing moment bound techniques for interferers with unknown distributions, while Nieminen et al. [124] investigated the performance of CR nodes interfering with each other due to timing inaccuracies. Furthermore, [125] proposed a feature detection based pre-sensing scheme to be conducted during the CR active periods, due to the limited sample size of the quiet periods. The scheme required taking into account the CR intra-network interference during sensing. The issues raised in [124, 125] are realistic, since the complete eradication of harmful interference is unavoidable due to sensing errors from the SUs in a multi-user environment. Moreover, the performance of certain detector types such as energy detectors, could be seriously reduced at very low SNR levels and noise uncertainty [33].

Hence, the contribution in this chapter is that the performance of a single

spectrum sensing node is analysed by taking into account the intra-network interference generated by the secondary network. For the purpose of this study, such interference is justified because other secondary users are not assumed to be silent when the reference CR node is conducting spectrum sensing. This situation may arise when the secondary network is non-cooperating and active SUs[1] either missed detecting the presence of the PU and/or the sensing node or were already in operation when the sensing node commenced spectrum sensing. This means all CR nodes do not commence and terminate sensing and transmission simultaneously.

It should be emphasised that accurately obtaining the statistics of the random interference generated by such a secondary network is a very difficult task. This is because conventional direct methods involve averaging out the aggregate random interference by computing several integral operations which also requires a knowledge of the distribution of the variance. Alternatively, one has to resort to the Gaussian approximation (GA) [19], commonly used in the performance analysis of wireless communications in the presence of interference, where the sum of the accumulated interference is approximated by a pure Gaussian random variable (RV) with a (non-random) variance. Though the accuracy of this approximation is justified by the central limit theorem (CLT), its validity under certain conditions is questionable [20], which further underpins the need to investigate its accuracy in ED applications. A performance comparison between the technique proposed in this thesis and the GA approach is presented in the results (Sec. 4.6). Furthermore, when using direct methods (including the GA method), significant deviations from practical performances may occur when using the general path loss model $r^{-\beta}$ [21], where r is the distance between transmitter and receiver while β is the path loss exponent. This occurs because the model manifests a singularity at $r = 0$ and considerably amplifies the transmitted signal in the region $r < 1$. Alternative models that provide relevant bounds to the path loss function have been studied in [21, 126, 127]. Hence, to overcome these shortcomings, new expressions in terms of the moment generating functions (MGF) of the random interference power are derived to aid the analysis. Thereafter, closed-form expressions for the MGFs in various interference scenarios are computed. A key benefit of the MGF approach is that it simplifies

[1]The terms SU and CR may be used interchangeably.

the arduous task of computing several integral operations when obtaining the statistics of the aggregate random interference, as shall be seen. Direct methods will require at least $(K+1)$-fold numerical integrations to average out the $K+1$ random variables. Finally, unlike the analysis in [122], fewer observation samples for the sensing node is maintained. By so doing, the ED analysis presented will be suited for applications in which the ED decision statistics does not approach the Gaussian distribution. Moreover, the uncertainty which may occur due to SU or PU traffic during prolonged sensing is reduced.

Finally, the analysis is completed by contrasting the performance of the ED with the MFD in the presence of co-channel interference. A similar technique to that used with the ED is employed and the required MFD expressions are expressed in an alternate form that lends itself to analysis based on the MGF of the random interferer variance.

The outline for the rest of the chapter is as follows. In Sec. 4.2, the simplest case for the interference model is presented. The main expressions for the false alarm and detection probabilities are presented. In Sec. 4.3, an interference model for correlated active users is presented, where the CR nodes undergo a contention protocol and the decision of each CR node to transmit is dependent on the status of other CR nodes in the network. To this end, two solutions to the MGF of the interferer powers are presented. Additionally, a more realistic model is introduced, within which the separation between a reference sensing node and the PU transmitter during sensing becomes random. Sec. 4.4 presents a model that describes the reference sensing node within a Poisson field of SU interferers. The thinning property of the Poisson process is employed to determine the density of active interferers under each hypothesis. To complete the analysis, in Sec. 4.5, expressions that aid the analysis of the MFD are derived and lastly in Sec. 4.6, the analytical and simulations results are presented.

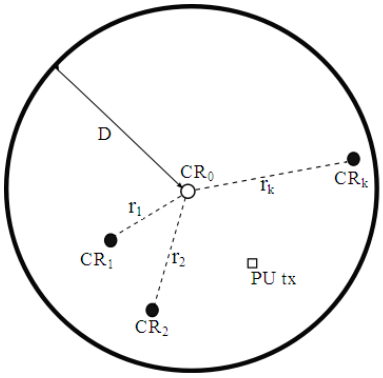

Figure 4.1: Spectrum sensing node in the presence of multiple secondary user interferers

4.2 Basic Interference Model

4.2.1 The System Model

Consider an ad-hoc CR network with several CR nodes competing to opportunistically access a licensed network within the same spatial region (see Fig. 4.1). Each CR node has the capability to sense the spectrum, transmit and receive. Without any loss of generality, consider an arbitrary node CR_0 to be the reference node. The distance from the kth CR node to CR_0 is denoted r_k, while distances between the jth node and the kth node is r_{jk} $j = 1, 2 \ldots K$; $k = 1, 2, \ldots K$ and $j \neq k$. The primary user transmitter (PU tx) is assumed to be at a relatively fixed distance from CR_0. The PU has priority of transmission, while network policy allows CR nodes to access the channel only when the PU is idle. The network policy is enforced by tasking each CR node to look-up the availability of the channel from a database. If the channel is registered as busy, the CR node defers its transmission to a later cycle.

Here the focus is on the performance of non-cooperating CR networks, such that CR quiet periods are neither synchronised nor coordinated. In this case, CR nodes may be unaware of the location and status of each other and may become active prior to the reference CR node's transmission, which may result in possible interference to CR_0.

Note that under H_1 i.e. when the PU is present, no secondary transmissions occur. This is because CR nodes can verify the presence of the PU from a database or errors due to missed detections are considered negligible. However, under H_0 i.e. when the PU is absent other SUs can become active and

constitute interference.

Let K_0 represents the number of active CR nodes under H_0. Then the aggregate interference at the reference node is given by the sum of the instantaneous active interfering signals. If $x(t)$ represents the composite received signal at CR_0, the binary hypothesis for the final decision is

$$x(t) = \begin{cases} w(t) + \sum_{k=1}^{K_0} i_k(t) & H_0 \\ s(t) + w(t) & H_1 \end{cases} \tag{4.1}$$

where H_0 and H_1 are the hypotheses representing the absence or presence of the PU signal $s(t)$ respectively, and $w(t)$ is the additive white Gaussian noise (AWGN) at CR_0.

In (4.1), $i_k(t)$ is the complex envelope of the signal transmitted by the kth interfering CR node which can be written as

$$i_k(t) = \sqrt{p_k A(r_k)} g_k(t) \tag{4.2}$$

where $g_k(t)$ is a low-pass zero-mean complex Gaussian random process. Consider also that $i_k(t)$ has an arbitrary autocorrelation function $\mathcal{R}(\tau) = \mathbb{E}[i_k^*(t) i_k(t+\tau)]$, which is normalised such that $\mathcal{R}(0) = 1$. The transmission power of the kth interferer is p_k at a distance r_k from the reference node. $A(r_k)$ is the distant dependent path loss function for the kth interferer. To circumvent the problem of singularity at the origin when using the classic path loss function, other modified path loss models could be used, such as $(c+r)^{-\beta}$ in [127] and $\left(1+r^{\beta}\right)^{-1}$ or $\min\left\{1, r^{-\beta}\right\}$ in [21, 126]. Here the following path loss model is adopted

$$A(r) = (c+r)^{-\beta} \tag{4.3}$$

where β is the path loss exponent and c is a constant which provides a bound for the function by improving the model such that the singularity at 0 is avoided. Note that when $c = 0$, then $A(r) = r^{-\beta}$. On the other hand, when $c = 1$, then for a co-located transmitter-receiver pair, it is observed that $A(0) = 1$, which reflects no power loss between the nodes. It is also worth noting that when r_k is random, then the signal $i_k(t)$ in (4.2) becomes a conditionally Gaussian random process (conditioned on the distance r_k).

The output of the ED is the decision variable y which is compared against a threshold ξ to make a final decision on the presence or absence of the desired primary signal. If N independent samples of the equivalent sampled signal $x(n)$, $n = 1, 2, \ldots, N$ are received during the sensing time, the decision variable is given by

$$y = \frac{1}{N} \sum_{n=1}^{N} \mid x(n) \mid^2 \tag{4.4}$$

such that when B is the ED filter bandwidth, then $\mathcal{R}(\frac{n}{B}) = 0, \quad n = 1, 2, \cdots, N$.

As far as the statistics of the decision variable y under H_0 is concerned, note that the samples $x\left(\frac{n}{B}\right) = w(\frac{n}{B}) + \sum_{k=1}^{K_0} i_k(\frac{n}{B})$ are conditionally independent and identically distributed (i.i.d.) RVs (conditioned on the number of active CR nodes' positions, K_0 and their positions $r_1, r_2, \ldots, r_k$), each of them is a complex Gaussian RV with zero-mean and conditional variance

$$\begin{aligned} \vartheta_0 &= \text{var}\left(x(n) \mid H_0, r_1, \ldots, r_k, K_0\right) \\ &= p_{\text{w}} + \sum_{k=1}^{K_0} p_k A(r_k) \end{aligned} \tag{4.5}$$

where p_{w} is the noise power. Accordingly, when ϑ_0 is given, y in (4.4) becomes a sum of squares of zero-mean complex Gaussian RVs. Therefore under H_0, y follows a conditional central chi-square distribution represented as

$$f_Y(y \mid \vartheta_0) = \frac{1}{y\Gamma(N/2)} \left(\frac{y}{\vartheta_0}\right)^{\frac{N}{2}} e^{-\frac{y}{\vartheta_0}} \tag{4.6}$$

where $\Gamma(.)$ represents the gamma function [72] and ϑ_0 is the variance of y under H_0.

4.2.2 False Alarm and Detection Probabilities

The performance of an ED is mainly measured in terms of the probability of detection P_{d} and false alarm P_{f}. For an AWGN channel and in the absence of interference, the detection probability has been computed in [50, 51] as

$$P_{\text{d}} = \Pr\left(y > \xi | H_1\right) = Q_{\frac{N}{2}}\left(\sqrt{2\gamma}, \sqrt{\xi}\right) \tag{4.7}$$

where $Q_{\frac{N}{2}}(.,.)$ is the Marcum Q-function with order $N/2$ [128], while ξ is the detection threshold of the ED and γ is the signal-to-noise ratio (SNR) at the sensing node. On the other hand, the probability of false alarm is defined as

$$P_{\mathrm{f}} = \Pr\left(y > \xi \mid H_0\right). \tag{4.8}$$

The conditional P_{f} (conditioned on the random variance ϑ_0 given in (4.5) can be computed from (4.6) and (4.8) as [49, 51]

$$P_{\mathrm{f}}\left(\vartheta_0\right) = \Pr\left(y > \xi \mid H_0, \vartheta_0\right) = \frac{\Gamma\left(\frac{N}{2}, \frac{\xi}{\vartheta_0}\right)}{\Gamma\left(\frac{N}{2}\right)} \tag{4.9}$$

where $\Gamma(a,b) = \int_b^\infty t^{a-1}e^{-t}dt$ is the upper incomplete gamma function [72]. The average false alarm is thus

$$P_{\mathrm{f}} = \mathbb{E}\left[\frac{\Gamma\left(N/2, \xi/\vartheta_0\right)}{\Gamma\left(N/2\right)}\right] \tag{4.10}$$

where the average is with respect to the random variance ϑ_0, defined in (4.5). However, deriving a closed-form expression for the PDF of the random variance ϑ_0 is difficult (if not impossible) when $K > 2$ (where K is the number of RVs). Therefore, direct methods to calculate the average false alarm probability (4.10) would require at least $(K+1)$-fold numerical integrations to average out the $K+1$ variables $(r_1, r_2, \ldots, r_k, K_0)$ which represents CR node locations and their number. Hence, an approach for the efficient computation of (4.10) directly in terms of the MGF of the random variance is proposed.

Lemma 3. *The probability of false alarm is given by*

$$P_{\mathrm{f}} = 1 - \frac{1}{\Gamma\left(\frac{N}{2}\right)} \int_0^\infty z^{\frac{N}{4}-1} J_{\frac{N}{2}}\left(2\sqrt{z}\right) \mathcal{M}\left(\frac{z}{\xi}\right) e^{-\left(\frac{z}{\xi}\right)p_{\mathrm{w}}} dz \tag{4.11}$$

where

$$\mathcal{M}(z) = \mathbb{E}\left[e^{-z\sum_{k=1}^{K_0} p_k A(r_k)}\right] \tag{4.12}$$

is the MGF of the aggregate interferer powers under H_0 and $J_v(.)$ is the vth order Bessel function of the first kind.

Proof: Recall the identity [72, Eq. (8.356.3)]

$$\Gamma(s,a)+\gamma(s,a)=\Gamma(s) \tag{4.13}$$

where $\gamma(.,.)$ is the lower incomplete gamma function, also given as [72, Eq. (8.354.1)]

$$\gamma(s,a)=\sum_{q=0}^{\infty}\frac{(-1)^q}{q!}\frac{a^{s+q}}{s+q}. \tag{4.14}$$

Using (4.13) and (4.14), then (4.9) can be expressed in the form

$$\begin{aligned}P_{\mathrm{f}}(\vartheta_0)&=1-\frac{\gamma\left(\frac{N}{2},\frac{\xi}{\vartheta_0}\right)}{\Gamma\left(\frac{N}{2}\right)}\\&=1-\frac{1}{\Gamma\left(\frac{N}{2}\right)}\sum_{q=0}^{\infty}\frac{(-1)^q}{\left(\frac{N}{2}+q\right)q!}\left(\frac{\xi}{\vartheta_0}\right)^{\frac{N}{2}+q}.\end{aligned} \tag{4.15}$$

Invoking the identities [72, Eq. (8.312.2)]

$$\frac{1}{x^n}=\int_0^{\infty}\frac{z^{n-1}}{\Gamma(n)}e^{-zx}dz \tag{4.16}$$

and [72, Eq. (8.402)]

$$J_\alpha(z)=\sum_{m=0}^{\infty}\frac{(-1)^m}{m!\Gamma(m+\alpha+1)}\left(\frac{z}{2}\right)^{2m+\alpha}$$

then (4.17) can be directly obtained from (4.15). Hence

$$\begin{aligned}P_{\mathrm{f}}(\vartheta_0)&=1-\frac{1}{\Gamma\left(\frac{N}{2}\right)}\sum_{q=0}^{\infty}\left\{\frac{(-1)^q}{\left(\frac{N}{2}+q\right)q!}\xi^{\frac{N}{2}+q}\int_0^{\infty}\frac{z^{\frac{N}{2}+q-1}}{\Gamma\left(\frac{N}{2}+q\right)}e^{-z\vartheta_0}dz\right\}\\&=1-\int_0^{\infty}\left\{\frac{1}{\Gamma\left(\frac{N}{2}\right)}\sum_{q=0}^{\infty}\frac{(-1)^q}{\left(\frac{N}{2}+q\right)q!}\xi^{\frac{N}{2}+q}\frac{z^{\frac{N}{2}+q-1}}{\Gamma\left(\frac{N}{2}+q\right)}\right\}e^{-z\vartheta_0}dz\\&=1-\int_0^{\infty}\left\{\frac{\Gamma\left(\frac{N}{2}+1\right)}{\frac{N}{2}\Gamma^2\left(\frac{N}{2}\right)}\xi^{\frac{N}{2}}z^{\frac{N}{2}-1}J_{\frac{N}{2}}\left(2\sqrt{z\xi}\right)(z\xi)^{-\frac{N}{4}}\right\}e^{-z\vartheta_0}dz.\end{aligned} \tag{4.17}$$

Substituting $\Gamma(s+1)=s\Gamma(s)$ [72, Eq. (8.331.1)], it is possible to simplify (4.17) to arrive at the following expression for the conditional probability of

false alarm

$$P_{\mathrm{f}}\left(\vartheta_0\right) = 1 - \frac{1}{\Gamma(\frac{N}{2})} \int_0^{\infty} \xi^{\frac{N}{4}} z^{\frac{N}{4}-1} J_{\frac{N}{2}}\left(2\sqrt{z\xi}\right) e^{-z\vartheta_0} dz. \tag{4.18}$$

Recall the random variance, $\vartheta_0 = p_{\mathrm{w}} + \sum_{k=1}^{K_0} p_k A\left(r_k\right)$. Then after some manipulations and simplifications, (4.18) can be expressed as (4.11).

■

4.2.2.1 Detection Probability under Non-Negligible Missed Detections

When the assumption of a PU database is relaxed, the interference under H_1 can no longer be considered as negligible. Hence, the received signal under Eq. (4.1) for H_1 is modified to

$$x(t) = s\left(t\right) + w(t) + \sum_{k=1}^{K_1} i_k(t) \tag{4.19}$$

where K_1 represents the number of active CR nodes under H_1 and $i_k(t)$ is defined in (4.2). The PU transmitted signal $s(t) = \sqrt{p_{\mathrm{p}} r_0^{-\beta}} g_0\left(t\right) \exp\left(j\phi_0\right)$ transmitting with power p_{p} and phase ϕ_0. Without any loss of generality the phase is subsequently set as $\phi_0 = 0$. The term $g_0\left(t\right)$ is a lowpass complex Gaussian random process while the PU is assumed to be at a relatively fixed and unit distance from the reference sensing node, such that $r_0 = 1$.

Based on these new assumptions, the statistics of y under H_1 becomes a sum of squares of zero-mean complex Gaussian RVs, where the conditional variance is $\mathrm{var}\left(x\left(n\right) \mid H_1, r_1, \ldots, r_k, K_1\right)$. Given that $P_{\mathrm{d}} = \Pr\left(y > \xi | H_1\right)$, while invoking (4.11) of Lemma 3, the unconditional P_{d} can be expressed as

$$P_{\mathrm{d}} = 1 - \frac{1}{\Gamma\left(\frac{N}{2}\right)} \int_0^{\infty} z^{\frac{N}{4}-1} J_{\frac{N}{2}}\left(2\sqrt{z}\right) \mathcal{M}_1\left(\frac{z}{\xi}\right) e^{-\frac{z}{\xi}\left(p_{\mathrm{w}}+p_{\mathrm{p}}\right)} dz \tag{4.20}$$

where $\mathcal{M}_1\left(z\right) = \mathbb{E}\left[e^{-z\sum_{k=1}^{K_1} p_k A(r_k)}\right]$ is the MGF of the aggregate interferer powers under H_1. Consequently, the task in the following section is to compute the MGFs $\mathcal{M}\left(z\right)$ and $\mathcal{M}_1\left(z\right)$ in (4.11) and (4.20).

4.2.3 Computation of the MGF

In this section, the MGFs required for the computation of P_{f} and P_{d} in (4.11) and (4.20) are derived. it is worth noting that (4.12) depends on the joint distribution of the distances $\{r_1, r_2, ..., r_{K_0}\}$ of active nodes. When the active users are equally likely to be anywhere within a disk of radius D around CR_0, the PDF of the distance r_k (the distance from CR_k to CR_0) is given by [129,130]

$$f(r) = \begin{cases} \frac{2r}{D^2}, & 0 < r_k \leq D \\ 0, & \text{otherwise.} \end{cases} \tag{4.21}$$

Therefore, in this case the conditional MGF (conditioned on the number of active users K_0)

$$\begin{aligned} \mathcal{M}(z|K_0) &= \mathbb{E}\left[e^{-z\sum_{k=1}^{K_0} p_k (c+r_k)^{-\beta}} | K_0\right] \\ &= \prod_{k=1}^{K_0} \mathbb{E}\left[e^{-z p_k (c+r_k)^{-\beta}}\right] \\ &= \prod_{k=1}^{K_0} \Lambda_c(p_k z) \end{aligned} \tag{4.22}$$

where $\Lambda_c(z) = \mathbb{E}\left[e^{-z(c+r)^{-\beta}}\right]$, and the expectation was taken with respect to the users' locations.

Using (4.21), it can be shown that when $\beta > 2$

$$\begin{aligned} \Lambda_c(z) = \mathbb{E}\left[e^{-z(c+r_k)^{-\beta}}\right] &= \int_0^D e^{-z(c+r)^{-\beta}} \frac{2r}{D^2} dr \\ &= \frac{2z^{\frac{2}{\beta}}\left\{\Gamma\left(-\frac{2}{\beta}, z(c+D)^{-\beta}\right) - \Gamma\left(-\frac{2}{\beta}, zc^{-\beta}\right)\right\}}{\beta D^2} \\ &+ \frac{2z^{\frac{1}{\beta}} c\left\{\Gamma\left(-\frac{1}{\beta}, zc^{-\beta}\right) - \Gamma\left(-\frac{1}{\beta}, z(c+D)^{-\beta}\right)\right\}}{\beta D^2}. \end{aligned} \tag{4.23}$$

When $c = 0$ then (4.23) can be further reduced into the simpler expression

$$\Lambda_0(z) = \frac{D^2 e^{-zD^{-\beta}} - z^{\frac{2}{\beta}}\Gamma\left(1 - \frac{2}{\beta}, zD^{-\beta}\right)}{D^2}. \tag{4.24}$$

Replacing the terms (4.23) or (4.24) in (4.22) and substituting into (4.11) gives the expression for the false alarm probability conditioned on the number of active interferers K_0.

When all CR's have identical transmit powers[2], $p_1 = p_2 = \cdots = p_K = p_s$, then (4.22) becomes

$$\mathcal{M}\left(z|K_0\right) = \left\{\Lambda_c\left(p_s z\right)\right\}^{K_0} \tag{4.25}$$

and in the limit as $K_0 \to \infty, D \to \infty$ such that $0 < \frac{K_0}{\pi D^2} = \lambda < \infty$, then it can be shown that (4.25) reduces to (4.26)

$$\begin{aligned}\lim_{\substack{K_0\to\infty, D\to\infty \\ K_0/\pi D^2=\lambda}} \mathcal{M}\left(z\right) &= \lim_{\substack{K_0\to\infty, D\to\infty \\ K_0/\pi D^2=\lambda}} \left[\frac{D^2 e^{-zp_s D^{-\beta}} - \left(zp_s\right)^{\frac{2}{\beta}} \Gamma\left(1-\frac{2}{\beta}, zp_s D^{-\beta}\right)}{D^2}\right]^{K_0} \\ &= \lim_{K_0\to\infty} \left[1 - \frac{\lambda\pi}{K_0}\left(zp_s\right)^{\frac{2}{\beta}} \Gamma\left(1-\frac{2}{\beta}, 0\right)\right]^{K_0} \\ &= \exp\left(-\lambda\pi\left(zp_s\right)^{\frac{2}{\beta}} \Gamma\left(1-\frac{2}{\beta}\right)\right)\end{aligned} \tag{4.26}$$

which corresponds to the MGF of a Poisson field of interferers with λ being the interferers density (average number of interferers per unit area), as would be demonstrated later in Sec. 4.4.

Using similar analysis to the derivation of (4.25), the MGF under H_1 could straightforwardly be obtained as

$$\mathcal{M}\left(z|K_1\right) = \left\{\Lambda_c\left(p_s z\right)\right\}^{K_1}. \tag{4.27}$$

4.3 Correlated Active CR Nodes

In this section, the analysis of Sec. 4.2 is extended to include a more realistic scenario whereby active CR locations are no longer independent. Note that for the analysis of Sec. 4.2, the locations of the strictly non-cooperating SUs were assumed independent and uniformly distributed over the service area. However, this can not be assumed when a practical contention based protocol (such as a CSMA-like protocol) is employed to control random access of

[2]It is plausible to assume that transmit powers of all nodes are equal when interferers are homogenous or if implementing power control is too complex e.g. ad hoc networks [131].

the channel among the SUs. Indeed, the CR nodes become in this case "locally cooperating" and as a consequence the active CR users become highly correlated.

4.3.1 The System Model

Consider a network with a PU and several CR nodes dispersed within a given geographical region as illustrated in Fig. 4.1. The PU has priority of transmission while network policy allows CR nodes to randomly access the channel only when the PU is idle. A non-cooperating CR network is assumed, such that CR quiet periods are not synchronised and CR nodes may be unaware of the location and status of each other. The output of the ED at each CR node is used to make a local decision to either transmit or defer during each transmission cycle. Each CR node senses the channel on its arrival and makes a local decision as to the state of the channel by comparing its received energy with a pre-determined detection threshold, such that when the received energy is less than this threshold, the CR node commences transmission otherwise it defers transmission until the next transmission cycle. The received energy will generally be based on its relative distances to the other CR nodes and particularly its distance to the PU transmitter. The CR node then becomes active when it accurately decides the absence of the PU (even though other SUs may be present) or when it misses the detection of the PU. This will constitute a form of intra-network interference and affect the performance of the sensing node.

The PU transmitter (PU tx) is also assumed to be randomly located at a distance d_0 from CR_0 and d_k from the kth CR node. The distance from the kth interfering CR node to the sensing node is denoted r_k, while the distance between any other two CR nodes is denoted r_{jk} $j = 1, 2 \ldots K$; $k = 1, 2, \ldots K$ and $j \neq k$. and $j \neq k$.

Accordingly, $\delta_{\epsilon,k} \in \{0, 1\}$ denotes the status of the kth CR node, where $\epsilon \in \{0, 1\}$ represents the status under H_0 and H_1 respectively, such that

$$\delta_{\epsilon,k} = \begin{cases} 1, & \text{when the } k\text{th CR transmits during the cycle} \\ 0, & \text{otherwise.} \end{cases} \tag{4.28}$$

The probability of each state occurring is defined as

$$\Pr\left(\delta_{\epsilon,k}=0\right)=\begin{cases}P_{\mathrm{f}}, & H_0\\ P_{\mathrm{d}}, & H_1\end{cases} \tag{4.29}$$

and

$$\Pr\left(\delta_{\epsilon,k}=1\right)=\begin{cases}1-P_{\mathrm{f}}, & H_0\\ 1-P_{\mathrm{d}}, & H_1.\end{cases} \tag{4.30}$$

Therefore, it follows from (4.30) that $i_k(t)$ becomes active under H_0 when it correctly decides the absence of the PU with probability $(1-P_{\mathrm{f}})$ and under H_1 it becomes active when it fails to detect the presence of the PU or miss-detects the PU with probability $(1-P_{\mathrm{d}})$. In this way it is possible to account for the imperfect sensing results obtained by other CR nodes within the region.

To proceed, let K denote the total number of CR nodes in the network, then the binary hypothesis in (4.1) is modified as follows

$$x(t)=\begin{cases}w(t)+\sum_{k=1}^{K}\delta_{0,k}i_k(t) & H_0\\ s(t)+w(t)+\sum_{k=1}^{K}\delta_{1,k}i_k(t) & H_1\end{cases} \tag{4.31}$$

where the actual number of active users (K_0 and K_1 in Sec. 4.2) becomes a random variable given by $K_0=\sum_{k=0}^{K}\delta_{0,k}\leq K$ under H_0 and $K_1=\sum_{k=0}^{K}\delta_{1,k}\leq K$ under H_1.

4.3.2 False Alarm and Detection Probabilities

The definition of P_{f} and P_{d} conditioned on the variances can be given as

$$P_{\mathrm{f}}\left(H_0,\vartheta_0\right) = \Pr\left(y>\xi \mid H_0,\vartheta_0\right) \tag{4.32}$$

$$P_{\mathrm{d}}\left(H_1,\vartheta_1\right) = \Pr\left(y>\xi \mid H_1,\vartheta_1\right) \tag{4.33}$$

where ξ is the detection threshold of the ED and the respective conditional variances under H_0 and H_1 are

$$\begin{aligned}\vartheta_0 &= \text{var}\left(x\left(n\right) \mid H_0, r_1, \ldots, r_K, \delta_{0,1}, \delta_{0,2}, \ldots \delta_{0,K}\right) \\ &= p_{\text{w}} + \sum_{k=1}^{K} \delta_{0,k} p_k A\left(r_k\right)\end{aligned} \tag{4.34}$$

and

$$\begin{aligned}\vartheta_1 &= \text{var}\left(x\left(n\right) \mid H_1, d_0, r_1, \ldots, r_k, \delta_{1,1}, \delta_{1,2}, \ldots \delta_{1,K}, K\right) \\ &= p_{\text{w}} + \sum_{k=1}^{K} \delta_{1,k} p_k A\left(r_k\right) + p_{\text{p}} A\left(d_0\right)\end{aligned} \tag{4.35}$$

where p_{w} is the noise power while p_k and p_{p} are the SU and PU transmit powers respectively.

As discussed earlier in Sec. 4.2.1, the samples of the received signal $x\left(n\right)$ $\{n = 1, 2, \ldots N\}$ are conditionally i.i.d. complex Gaussian RV with zero-mean and conditional variance (conditioned on the interfering CR node positions $r_1, r_2, \ldots, r_K$ in addition to their status $\delta_{\epsilon,1}, \delta_{\epsilon,2}, \ldots \delta_{\epsilon,K}$). Hence, following similar analysis to Sec. 4.2.1, the expression for the probability of false alarm can still be computed by using the general expression (4.11). However, the MGF $\mathcal{M}\left(z\right)$ in this case is modified to include the statstics of the status variables $\delta_{0,1}, \delta_{0,2}, \ldots \delta_{0,K}$. Thus, invoking Lemma 3, the false alarm probability is

$$P_{\text{f}} = 1 - \frac{1}{\Gamma\left(\frac{N}{2}\right)} \int_0^\infty z^{\frac{N}{4}-1} J_{\frac{N}{2}}\left(2\sqrt{z}\right) \mathcal{M}\left(\frac{z}{\xi}\right) e^{-\left(\frac{z}{\xi}\right)p_{\text{w}}} dz \tag{4.36}$$

where $\mathcal{M}\left(z\right) = \mathbb{E}\left[e^{-z\sum_{k=1}^{K}\delta_{0,k}p_k A(r_k)}\right]$. Using (4.33) and employing similar analysis, the detection probability can be expressed as

$$P_{\text{d}} = 1 - \frac{1}{\Gamma\left(\frac{N}{2}\right)} \int_0^\infty z^{\frac{N}{4}-1} J_{\frac{N}{2}}\left(2\sqrt{z}\right) \mathcal{N}\left(\frac{z}{\xi}\right) \Phi\left(\frac{z}{\xi}\right) e^{-\frac{zp_{\text{w}}}{\xi}} dz \tag{4.37}$$

where $\mathcal{N}\left(z\right) = \mathbb{E}\left[e^{-z\sum_{k=1}^{K}\delta_{1,k}p_k A(r_k)}\right]$ is the MGF of the aggregate interferer powers under H_1 and the MGF of the PU random signal is $\Phi\left(z\right) =$

$\mathbb{E}\left[e^{-zp_{\mathrm{p}}A(d_0)}\right]$. Consequently, the task in the following subsection is to compute the MGFs $\mathcal{M}(z)$, $\mathcal{N}(z)$ and $\Phi(z)$ in (4.36) and (4.37).

4.3.3 Computation of the MGFs

Regarding the analysis in this section, it is worth mentioning that although the distances $r_1, r_2, \ldots, r_K$ are independent and distributed as in (4.21), it is not plausible to also assume that the interferer states $\delta_{\epsilon,1}, \delta_{\epsilon,2}, \ldots \delta_{\epsilon,K}$ are also independent. Firstly, the distances $r_1, r_2, \ldots, r_K$ are now representing the locations of arbitrary users (regardless of being transmitting or deferring), while the locations of transmitting nodes are not independent. Their correlation is taken into account through the set of correlated binary RVs $\delta_{\epsilon,1}, \delta_{\epsilon,2}, \ldots \delta_{\epsilon,K}$. Moreover, the decision of each interferer depends on the status of other CR nodes in the region (based on the aggregate interference already present), which in turn depends on the relative distances to the other CR nodes and the PU. Thus, the problem of evaluating expressions for the exact joint statistics is a very arduous task, if not impossible. Using direct methods, this solution would require at least $(2K+1)$-fold numerical integrations to average out the $2K+1$ variables $(\delta_{\epsilon,1}, \delta_{\epsilon,2}, \ldots \delta_{\epsilon,K}, r_1, r_2, \ldots, r_K, K)$ which represents CR's status, locations and their number.

Owing to the difficulty of evaluating the joint statistics of $\delta_{\epsilon,1}, \delta_{\epsilon,2}, \ldots \delta_{\epsilon,K}$, two possible approaches to the problem are proposed. In the subsequent subsections, it is shown that despite this difficulty it is possible to derive approximations and accurate bounds for the MGFs required.

4.3.3.1 Approximation

The first method involves approximating all interfering CR states $\delta_{0,1}, \delta_{0,2}, \ldots \delta_{0,K}$ as independent RVs. Assuming identical transmit powers, $p_1 = p_2 = \cdots = p_K = p_{\mathrm{s}}$, the approximate MGF under (4.36) is

$$\begin{aligned}\mathcal{M}^{\mathrm{aprx}}(z) &\approx \mathbb{E}\left[e^{-z\sum_{k=1}^{K}\delta_{0,k}p_{\mathrm{s}}(c+r_k)^{-\beta}}\right] \\ &\approx \prod_{k=1}^{K}\mathbb{E}\left[e^{-z\delta_{0,k}p_{\mathrm{s}}(c+r_k)^{-\beta}}\right] \\ &\approx \left\{P_{\mathrm{f}} + (1-P_{\mathrm{f}})\,\Lambda_c(p_{\mathrm{s}}z)\right\}^K \end{aligned} \tag{4.38}$$

where $\Lambda_c(z)$ is given in (4.23), while $\Pr(\delta_{0,k}=1|H_0)=\Pr(y_k<\xi|H_0)=1-P_{\mathrm{f}}$ and $\Pr(\delta_{0,k}=0|H_0)=1-\Pr(a_k=1|H_0)=P_{\mathrm{f}},\ \ k=1,2,\ldots K$ as shown in (4.29) and (4.30).

Following similar analysis for obtaining (4.38), $\mathcal{N}(z)$ can be approximated as

$$\mathcal{N}(z)\simeq\left\{P_{\mathrm{d}}+(1-P_{\mathrm{d}})\,\Lambda_c(p_{\mathrm{s}}z)\right\}^K \tag{4.39}$$

where $\Pr(\delta_{1,k}=1|H_1)=\Pr(y_k<\xi|H_1)=1-P_{\mathrm{d}}$ and $\Pr(\delta_{1,k}=0|H_1)=1-\Pr(a_k=1|H_1)=P_{\mathrm{d}}\ ,\ \ k=1,2,\ldots K$ as shown in (4.29) and (4.30). $\Lambda_c(z)$ is given in (4.23) and y_k is the decision variable of the kth node.

The expectation of the PU random signal as a result of the random location of the PU, relative to a reference sensing node is given by $\Phi(z)=\mathbb{E}\left[e^{-zp_{\mathrm{p}}d_0^{-\beta}}\right]$ where $0<d_0<D$ with distribution $2d_0/D^2$. From the derivation of (4.24), then

$$\Phi(z)=\Lambda(p_{\mathrm{p}}z)\,. \tag{4.40}$$

To summarise, the false-alarm probability in this case is obtained by substituting (4.38) in (4.36). The following non-linear equation is arrived at

$$P_{\mathrm{f}}^{\mathrm{aprx}}\approx 1-\frac{1}{\Gamma\left(\frac{N}{2}\right)}\int_0^\infty z^{\frac{N}{4}-1}J_{\frac{N}{2}}\left(2\sqrt{z}\right)e^{-\left(\frac{z}{\xi}\right)p_{\mathrm{w}}}\left\{P_{\mathrm{f}}+(1-P_{\mathrm{f}})\,\Lambda_c\left(\frac{p_{\mathrm{s}}z}{\xi}\right)\right\}^K dz. \tag{4.41}$$

On the other hand, the detection probability can be computed by combining (4.39) and (4.40) into (4.37). Thus

$$P_{\mathrm{d}}^{\mathrm{aprx}}\approx 1-\frac{1}{\Gamma\left(\frac{N}{2}\right)}\int_0^\infty z^{\frac{N}{4}-1}J_{\frac{N}{2}}\left(2\sqrt{z}\right)\left\{P_{\mathrm{d}}+(1-P_{\mathrm{d}})\,\Lambda_c\left(\frac{p_{\mathrm{s}}z}{\xi}\right)\right\}^K \times e^{-\left(\frac{z}{\xi}\right)p_{\mathrm{w}}}\Lambda\left(\frac{p_p z}{\xi}\right)dz. \tag{4.42}$$

Both (4.41) and (4.42) can be solved by using an iterative method similar to that shown in Algorithm 4.1. The term τ in the algorithm is a chosen small constant, depicting the required tolerance of the subroutine.

4.3.3.2 Upper Bound

In this approach the interfering CR states $\delta_{\epsilon,1}, \delta_{\epsilon,2}, \ldots \delta_{\epsilon,K}$ are not independent. A lower bound to the MGF $\mathcal{M}(z)$ is set by invoking Jensen's inequality [132, pp. 265], which asserts that

$$\mathbb{E}[e^{-zp_{\mathrm{s}}\sum_{k=1}^{K}\delta_{\epsilon,K}}] \geq e^{-zp_{\mathrm{s}}\sum_{k=1}^{K}\mathbb{E}[\delta_{\epsilon,K}]} \tag{4.43}$$

then the bounded MGF required to compute P_{f} in (4.36) is

$$\mathcal{M}^{\mathrm{bd}}(z) \geq e^{-zp_{\mathrm{s}}\sum_{k=1}^{K}\mathbb{E}[\delta_{0,K}]}. \tag{4.44}$$

where the average is with respect to the set of random variables $\delta_{0,1}, \delta_{0,2}, \ldots \delta_{0,K}$. Using (4.44), the required bound on the MGF can be obtained by noting firstly that, when the average is computed with respect to the status variables only, then

$$\begin{aligned}\mathbb{E}\left[e^{-zp_{\mathrm{s}}\sum_{k=1}^{K}a_k(c+r_1)^{-\beta}}|r_1, r_2, \ldots, r_K\right] &\geq e^{-zp_{\mathrm{s}}\sum_{k=1}^{K}\mathbb{E}[\delta_{0,1}](c+r_1)^{-\beta}} \\ &\geq e^{-zp_{\mathrm{s}}\sum_{k=1}^{K}(1-P_{\mathrm{f}})(c+r_1)^{-\beta}}\end{aligned} \tag{4.45}$$

where the term $\mathbb{E}[\delta_{0,k}] = \Pr(\delta_{0,k} = 1) = 1 - P_{\mathrm{f}}\ \forall k = 1, 2, \ldots K$.

Now from (4.45), then averaging out $r_1, r_2, \ldots r_K$ gives

$$\begin{aligned}\mathcal{M}^{\mathrm{bd}}(z) &\geq \mathbb{E}\left[e^{-zp_{\mathrm{s}}\sum_{k=1}^{K}(1-P_{\mathrm{f}})(c+r_1)^{-\beta}}\right] \\ &\geq \prod_{k=1}^{K}\mathbb{E}\left[e^{-zp_{\mathrm{s}}(1-P_{\mathrm{f}})(c+r_1)^{-\beta}}\right] \\ &\geq \left\{\mathbb{E}\left[e^{-zp_{\mathrm{s}}(1-P_{\mathrm{f}})(c+r_1)^{-\beta}}\right]\right\}^{K} \\ &\geq \{\Lambda_c(zp_{\mathrm{s}}(1-P_{\mathrm{f}}))\}^{K}.\end{aligned} \tag{4.46}$$

where the function $\Lambda_c(z)$ is defined in (4.23). Similarly, for the bounded P_{d} the MGF term $\mathcal{N}(z)$ is modified to

$$\mathcal{N}^{\mathrm{bd}}(z) = \{\Lambda_c(zp_{\mathrm{s}}(1-P_{\mathrm{d}}))\}^{K} \tag{4.47}$$

while the PU signal expectation remains unchanged such that $\Phi(z) = \Lambda(p_{\mathrm{p}} z)$ as defined in (4.40).

In summary, when the lower-bound on $\mathcal{M}(z)$ from (4.46) is substituted into the general expression for the false-alarm probability (4.36), the following upper bound on false alarm probability is obtained

$$P_{\mathrm{f}}^{\mathrm{bd}} \leq 1 - \frac{1}{\Gamma\left(\frac{N}{2}\right)} \int_0^\infty z^{\frac{N}{4}-1} J_{\frac{N}{2}}\left(2\sqrt{z}\right) e^{-\left(\frac{z}{\xi}\right)p_{\mathrm{w}}} \left\{\Lambda_c\left(\frac{z p_{\mathrm{s}}}{\xi}\left(1 - P_{\mathrm{f}}\right)\right)\right\}^K dz. \quad (4.48)$$

Likewise, when (4.40) and (4.47) are substituted into (4.37), the upper bound to the detection probability is

$$P_{\mathrm{d}}^{\mathrm{bd}} \leq 1 - \frac{1}{\Gamma\left(\frac{N}{2}\right)} \int_0^\infty z^{\frac{N}{4}-1} J_{\frac{N}{2}}\left(2\sqrt{z}\right) e^{-\left(\frac{z}{\xi}\right)p_{\mathrm{w}}} \left\{\Lambda_c\left(\frac{z p_{\mathrm{s}}}{\xi}\left(1 - P_{\mathrm{d}}\right)\right)\right\}^K \Lambda\left(\frac{p_{\mathrm{p}} z}{\xi}\right) dz. \quad (4.49)$$

Hence, the recurrence equations in (4.48) and (4.49) can be solved recursively by employing Algorithm 4.1 and the tidiness of the bounds are discussed in Sec. 4.6.

4.3.4 Recursive Algorithm

This section provides an algorithm to compute the probabilities derived in Sec. 4.3.3. In particular, the approximate expressions in (4.41) and (4.42) and the bounded expressions in (4.48) and (4.49) are recurrence equations. Hence, an iterative approach is proposed in order to find the exact solutions of $P_{\mathrm{f}}^{\mathrm{aprx}}$, $P_{\mathrm{d}}^{\mathrm{aprx}}$, $P_{\mathrm{f}}^{\mathrm{bd}}$ and $P_{\mathrm{d}}^{\mathrm{bd}}$. Algorithm 4.1 presents the procedure employed, where τ_{d} and τ_{f} in the algorithm are arbitrary small constants that depict the desired tolerance of the subroutine, based on the required precision for $P_{\mathrm{d}}^{\mathrm{bd}}$ and $P_{\mathrm{f}}^{\mathrm{bd}}$. Note also that Algorithm 4.1 depicts the syntax for $P_{\mathrm{f}}^{\mathrm{bd}}$ and $P_{\mathrm{d}}^{\mathrm{bd}}$ but could be easily adapted for $P_{\mathrm{f}}^{\mathrm{aprx}}$ and $P_{\mathrm{d}}^{\mathrm{aprx}}$.

Algorithm 4.1 Iterative algorithm for computing $P_{\mathrm{f}}^{\mathrm{bd}}$ or $P_{\mathrm{d}}^{\mathrm{bd}}$.

Input: $P_{\mathrm{d}}^{\mathrm{bd}\{0\}}$, $P_{\mathrm{f}}^{\mathrm{bd}\{0\}}$ {Any value of $P_{\mathrm{d}}^{\mathrm{bd}}$ and $P_{\mathrm{f}}^{\mathrm{bd}}$ between 0 and 1}
Initialisation: $j \Leftarrow 0$
repeat

1. Given $P_{\mathrm{d}}^{\mathrm{bd}\{j\}}$, find $P_{\mathrm{d}}^{\mathrm{bd}\{j+1\}}$ that solves Eq. (4.49)
2. Given $P_{\mathrm{f}}^{\mathrm{bd}\{j\}}$, find $P_{\mathrm{f}}^{\mathrm{bd}\{j+1\}}$ that solves Eq. (4.48)
3. $P_{\mathrm{d}}^{\mathrm{bd}\{j\}} \Leftarrow P_{\mathrm{d}}^{\mathrm{bd}\{j+1\}}$
4. $P_{\mathrm{f}}^{\mathrm{bd}\{j\}} \Leftarrow P_{\mathrm{f}}^{\mathrm{bd}\{j+1\}}$
5. $j \Leftarrow j+1$

until $|P_{\mathrm{d}}^{\mathrm{bd}\{j-1\}} - P_{\mathrm{d}}^{\mathrm{bd}\{j\}}| < \tau_{\mathrm{d}}$ and $|P_{\mathrm{f}}^{\mathrm{bd}\{j-1\}} - P_{\mathrm{f}}^{\mathrm{bd}\{j\}}| < \tau_{\mathrm{f}}$
output $P_{\mathrm{d}}^{\mathrm{bd}\{j\}}$, $P_{\mathrm{f}}^{\mathrm{bd}\{j\}}$

4.4 Poisson Field of SU Interferers

In this section, the system model presented in Sec. 4.3 is modified. To facilitate the statistical analysis of the network interference, the Poisson model is adopted. This enables extensive characterisation of network interference including spatial distribution of nodes and node densities. The Poisson model was extensively described for cellular networks in [133], for unlicensed frequency bands in [129] and for CR networks in [78]. Furthermore, to account for the density of interferers under each hypothesis, the thinning property of the Poisson process [134] is employed to split each process with respect to its probability of occurrence. Closed-form expressions are then derived for the MGF required in studying the performance of a sensing node in the given interference scenario.

4.4.1 The System Model

Consider the communication network with a PU and several CR nodes dispersed within a given geographical region as described in Sec. 4.3 and illsutrated in Fig. 4.1. Again a non-cooperating CR network is assumed, which may become active when SU nodes miss the detection of the PU or accurately sense the absence of the PU prior to the arrival of a reference sensing node.

This will constitute a form of intra-network interference. Here the PU transmitter (PU tx) is assumed to be at a relatively fixed distance from CR_0. If $x(t)$ represents the received signal and $i_k(t)$ the kth interfering CR signal, then analogous to (4.31), the binary hypothesis for the final decision is

$$x(t) = \begin{cases} w(t) + \sum_{k=1}^{K} \delta_{0,k} i_k(t) & H_0 \\ s(t) + w(t) + \sum_{k=1}^{K} \delta_{1,k} i_k(t) & H_1 \end{cases} \tag{4.50}$$

where the hypotheses H_0 and H_1 represent the absence or presence of $s(t)$ respectively. The signal from the kth interfering CR node $i_k(t)$ has a status under H_0 and H_1 defined as $\delta_{0,k} \in \{0,1\}$ and $\delta_{1,k} \in \{0,1\}$ respectively. The probabilities of each state occurring are defined in (4.29) and (4.30). Therefore, when kth CR node miss-detects the PU under H_1 it becomes active with probability $\Pr(\delta_{1,k} = 1) = 1 - P_{\mathrm{d}}$. On the other hand, when a correct decision on the PU absence is made under H_0, CR_k becomes active with probability $\Pr(\delta_{0,k} = 1) = 1 - P_{\mathrm{f}}$. The statistics of the signals $s(t)$, $i_k(t)$ and $w(t)$ remain unchanged from Sec. 4.3. The number of nodes in the network is K. The probability of K interfering nodes within the circular area πD^2 with average density λ, is given as

$$\Pr[K = k] = \frac{e^{-\lambda \pi D^2} (\lambda \pi D^2)^k}{k!} \tag{4.51}$$

whereas the distribution of node distances r for Poisson distributed nodes within a disc is given in [130] similar to (4.21) as

$$f(r) = \begin{cases} \frac{2r}{D^2} & 0 < r < D \\ 0, & \text{otherwise.} \end{cases} \tag{4.52}$$

The false alarm and detection probabilities are discussed next.

4.4.2 False Alarm and Detection Probabilities

Recall the form of the expressions for P_{f} and P_{d} based on Lemma 3

$$P_{\mathrm{f}} = 1 - \frac{1}{\Gamma(N/2)} \int_0^\infty z^{\frac{N}{4}-1} J_{\frac{N}{2}}\left(2\sqrt{z}\right) \mathcal{M}_{\mathrm{psn}}\left(\frac{z}{\xi}\right) e^{-\left(\frac{z}{\xi}\right)p_{\mathrm{w}}} dz \tag{4.53}$$

and

$$P_{\mathrm{d}} = 1 - \frac{1}{\Gamma(N/2)} \int_0^\infty z^{\frac{N}{4}-1} J_{\frac{N}{2}}\left(2\sqrt{z}\right) \mathcal{N}_{\mathrm{psn}}\left(\frac{z}{\xi}\right) e^{-\frac{z}{\xi}(p_{\mathrm{w}}+p_{\mathrm{p}})} dz \tag{4.54}$$

where $\mathcal{M}_{\mathrm{psn}}(z) = \mathbb{E}\left[e^{-z\sum_{k=1}^{K}\delta_{0,k}p_k A(r_k)}\right]$, $\mathcal{N}_{\mathrm{psn}}\left(\frac{z}{\xi}\right) = \mathbb{E}\left[e^{-z\sum_{k=1}^{K}\delta_{1,k}p_k A(r_k)}\right]$ and $J_v(.)$ is the vth order Bessel function of the first kind [72]. The path loss function $A(r_k)$ is defined in (4.3). For simplicity, the analysis in this section assumes $c = 0$ such that $A(r_k) = r_k^{-\beta}$.

4.4.2.1 Computation of the MGF

The spatial distribution of the interfering nodes are modelled as a Poisson process. For the total interference $\sum_{k=1}^{K}\delta_{0,k}p_k r_k^{-\beta}$ the MGF in (4.53) is represented accordingly as $\mathbb{E}\left[e^{-z\sum_{k=1}^{K}\delta_{0,k}p_k r_k^{-\beta}}\right] = \prod_{k=1}^{K}\mathbb{E}\left[e^{-z\delta_{0,k}p_k r_k^{-\beta}}\right]$ and conditioned on r, δ and K. Hence

$$\mathcal{M}_{\mathrm{psn}}(z \mid K, \delta_{0,k}, r_k) = \lim_{D\to\infty}\left\{E\left[e^{-z\delta_{0,k}p_k r_k^{-\beta}}\right]\right\}^K \tag{4.55}$$

Using (4.51) and removing the condition on K in (4.55) leaves

$$\mathcal{M}_{\mathrm{psn}}(z \mid \delta_{0,k}, r_k) = \lim_{D\to\infty}\sum_{k=0}^{\infty}\frac{e^{-\lambda\pi D^2}\left(\lambda\pi D^2\right)^k}{k!}\left\{\mathbb{E}\left[e^{-z\delta_{0,k}p_k r_k^{-\beta}}\right]\right\}^K. \tag{4.56}$$

Taking the MGF of the poisson function gives

$$\mathcal{M}_{\mathrm{psn}}(z \mid \delta_{0,k}, r_k) = \lim_{D\to\infty}\exp\left(-\lambda\pi D^2\left(1 - \mathbb{E}\left[e^{-z\mathbb{E}\left[\delta_{0,k}\right]p_k r_k^{-\beta}}\right]\right)\right). \tag{4.57}$$

Solving both expectations yields (4.58a). Note that the density λ is a function of the interferer presence under the hypotheses examined. Particularly,

under H_0 only the SUs which do not observe false alarms commence transmissions ($i.e.$ $\Pr(\delta_{0,k}=1)$ with density $\lambda\left(1-P_{\mathrm{f}}\right)$), while under H_1 only SUs which fail to detect the PU presence become active ($i.e.$ $\Pr(\delta_{1,k}=1)$ with density $\lambda\left(1-P_{\mathrm{d}}\right)$). As a result the MGF under each hypothesis becomes

$$\mathcal{M}_{\mathrm{psn}}\left(z\right) = e^{-\lambda\pi(1-P_{\mathrm{f}})\Gamma\left(1-\frac{2}{\beta}\right)z^{\frac{2}{\beta}}} \tag{4.58a}$$

$$\mathcal{N}_{\mathrm{psn}}\left(z\right) = e^{-\lambda\pi(1-P_{\mathrm{d}})\Gamma\left(1-\frac{2}{\beta}\right)z^{\frac{2}{\beta}}}. \tag{4.58b}$$

Therefore, the closed-form expressions of P_{f} and P_{d} for the sensing node in this scenario is obtained by substituting (4.58a) into (4.53) and (4.58b) into (4.54) respectively. Thus

$$P_{\mathrm{f}}^{\mathrm{psn}} = 1 - \int_0^\infty \frac{z^{\frac{N}{4}-1} J_{\frac{N}{2}}\left(2\sqrt{z}\right)}{\Gamma(N/2)} e^{-\pi\lambda(1-P_{\mathrm{f}})\Gamma\left(1-\frac{2}{\beta}\right)\left(\frac{z}{\xi}\right)^{\frac{2}{\beta}} - \frac{zp_{\mathrm{w}}}{\xi}} dz \tag{4.59}$$

and

$$P_{\mathrm{d}}^{\mathrm{psn}} = 1 - \int_0^\infty \frac{z^{\frac{N}{4}-1} J_{\frac{N}{2}}\left(2\sqrt{z}\right)}{\Gamma(N/2)} e^{-\pi\lambda(1-P_{\mathrm{d}})\Gamma\left(1-\frac{2}{\beta}\right)\left(\frac{z}{\xi}\right)^{\frac{2}{\beta}} - \frac{z}{\xi}(p_{\mathrm{w}}+p_{\mathrm{p}})} dz. \tag{4.60}$$

Note that this result corresponds to that obtained in (4.26). However, the density of interferers λ is scaled by the probabilities $\Pr(\delta_{0,k}=1)$ and $\Pr(\delta_{1,k}=1)$, which is inherent in the thinning property of the Poisson process.

4.4.2.2 Exact Solution of P_{f} and P_{d}

Because the closed-form expressions obtained in (4.59) and (4.60) are recursive functions, an iterative approach is proposed to find the exact solutions of the false alarm and detection probabilities. The procedure employed is analogous to that proposed in Algorithm 4.1, but reproduced below for completeness. Again τ_{d} and τ_{f} in the algorithm are arbitrary small constants that depict the desired tolerance of $P_{\mathrm{d}}^{\mathrm{psn}}$ and $P_{\mathrm{f}}^{\mathrm{psn}}$ in the subroutine.

Algorithm 4.2 Iterative algorithm for computing $P_{\mathrm{d}}^{\mathrm{psn}}$ and $P_{\mathrm{f}}^{\mathrm{psn}}$

Input: $P_{\mathrm{d}}^{\mathrm{psn}\{0\}}$, $P_{\mathrm{f}}^{\mathrm{psn}\{0\}}$ {Any value of $P_{\mathrm{d}}^{\mathrm{psn}}$ and $P_{\mathrm{f}}^{\mathrm{psn}}$ between 0 and 1}

Initialisation: $j \Leftarrow 0$

repeat

1. Given $P_{\mathrm{d}}^{\mathrm{psn}\{j\}}$, find $P_{\mathrm{d}}^{\mathrm{psn}\{j+1\}}$ that solves Eq. (4.60)
2. Given $P_{\mathrm{f}}^{\mathrm{psn}\{j\}}$, find $P_{\mathrm{f}}^{\mathrm{psn}\{j+1\}}$ that solves Eq. (4.59)
3. $P_{\mathrm{d}}^{\mathrm{psn}\{j\}} \Leftarrow P_{\mathrm{d}}^{\mathrm{psn}\{j+1\}}$
4. $P_{\mathrm{f}}^{\mathrm{psn}\{j\}} \Leftarrow P_{\mathrm{f}}^{\mathrm{psn}\{j+1\}}$
5. $j \Leftarrow j+1$

until $|P_{\mathrm{d}}^{\mathrm{psn}\{j-1\}} - P_{\mathrm{d}}^{\mathrm{psn}\{j\}}| < \tau_{\mathrm{d}}$ and $|P_{\mathrm{f}}^{\mathrm{psn}\{j-1\}} - P_{\mathrm{f}}^{\mathrm{psn}\{j\}}| < \tau_{\mathrm{f}}$

output $P_{\mathrm{d}}^{\mathrm{psn}\{j\}}$, $P_{\mathrm{f}}^{\mathrm{psn}\{j\}}$

4.5 The Matched Filter Detector

For completeness, in this section the performance of the MFD under interference is evaluated. Recall the MFD [3, 14] as a detection technique has been introduced in Sec. 2.2. The performance analysis of this detector is widely available in the literature. However, only a few studies are currently available comparing its actual performance with the ED. For example, in [135], a study was conducted comparing the performances under AWGN channels, while in [136] a similar comparative study was conducted under noise uncertainty and very low SNR environments, where it was shown that fundamental limits existed for all detector types, no matter how long the observations were conducted. In addition to noise uncertainty, a comparative analysis between EDs and MFDs under interference uncertainties was carried out in [123, 137, 138]. For instance in [123], using moment bound techniques, sharp upper and lower bounds for the false-alarm and missed detection probabilities were obtained under interference with known range and maximum powers.

In this study, a novel alternate expression for the complementary error function is derived. This makes it possible to express the false-alarm and

detection probabilities of the MFD in an alternative form, which has the desirable property that the random interferers' variance appears only within the exponent, and as linear summations. This greatly facilitates averaging out the RVs using the MGF. Moreover, the limits of integration in the new expression are independent of the integrand as well as significantly reducing the complexity of the approach in [123]. Thereafter, the performance of the MFD is contrated against that of the ED.

4.5.1 False Alarm and Detection Probabilties

In this section, for simplicity the desired signal is presumed to be known, for instance where a pilot signal is available such that coherent detection can be employed. The decision variable y_{mfd} is

$$y_{\text{mfd}} = \frac{1}{N}\sum_{n=1}^{N} x(n)\, s(n) \tag{4.61}$$

where $x(n)$ is the sampled equivalent of the received signal defined in (4.19). Note that under both H_0 and H_1 the signal term $x(n)\, s(n)$ is Gaussian. Since, y_{mfd} is a linear combination of Gaussian RVs, then

$$y_{\text{mfd}} \sim \begin{cases} \mathcal{N}\left(0, \frac{S(\sigma_I^2+\sigma_w^2)}{N}\right) & H_0 \\ \mathcal{N}\left(S, \frac{S(\sigma_I^2+\sigma_w^2)}{N}\right) & H_1 \end{cases} \tag{4.62}$$

where $S = \sum_{n=1}^{N} |s(n)|^2$ is the energy of the desired signal. The terms σ_I^2 and σ_w^2 are the interference and noise variances respectively, obtained from

$$\begin{aligned} \text{var}\left[y_{\text{mfd}}|H_0\right] &= \text{var}\left[\frac{1}{N}\sum_{n=1}^{N}\left(w(n)+i(n)\right)s(n)\right] \\ &= \frac{1}{N}\sum_{n=1}^{N}\text{var}\left[w(n)+i(n)\right]s^2(n) \\ &= \frac{S}{N}(\sigma_w^2+\sigma_I^2). \end{aligned} \tag{4.63}$$

Following similar analysis under H_1, $\text{var}\left[y_{\text{mfd}}|H_1\right] = \frac{S}{N}(\sigma_w^2 + \sigma_I^2)$. Consequently, the false alarm probability is

$$P_{\text{f}}^{\text{mf}} = \Pr\left\{y_{\text{mfd}} > \xi | H_0\right\} = \frac{1}{2}\text{Erfc}\left(\frac{\xi}{\sqrt{\frac{2S}{N}\left(\sigma_I^2 + \sigma_w^2\right)}}\right) \tag{4.64}$$

where $\text{Erfc}\left(.\right)$ is the complementary error function. The detection probability is given as

$$P_{\text{d}}^{\text{mf}} = \Pr\left\{y_{\text{mfd}} > \xi | H_1\right\} = \frac{1}{2}\text{Erfc}\left(\frac{\xi - S}{\sqrt{\frac{2S}{N}\left(\sigma_I^2 + \sigma_w^2\right)}}\right). \tag{4.65}$$

In Lemma 4, an alternative expression to (4.64) and (4.65) in which the RVs are present only in the exponent is proposed.

Lemma 4. *For any arbitrary random variable $\zeta > 0$, then*

$$\mathbb{E}\left[\frac{1}{2}\text{Erfc}\left(\left(\xi - S\right)\cdot\sqrt{\frac{N}{\zeta}}\right)\right] = \frac{1}{2} - \frac{1}{2\pi}\int_0^\infty \frac{\sin\left(2\left(\xi - S\right)\sqrt{zN}\right)}{z}\mathcal{M}\left(z\right)dz \tag{4.66}$$

where $\mathcal{M}\left(z\right) = \mathbb{E}\left[e^{-z\zeta}\right]$ is the MGF of the RV ζ.

The proof is as follows.

Proof: Recall the identities [72, Eq. (8.250.4)] and [72, Eq. (8.250.5)]

$$\text{Erfc}\left(\zeta\right) = 1 - \text{Erf}\left(\zeta\right) \tag{4.67}$$

$$\begin{aligned}\int_0^\infty \frac{e^{-\zeta(\rho+z)}}{\pi\left(\rho+z\right)}\sin\left(a\sqrt{z}\right)dz = \frac{1}{2}e^{-a\sqrt{\rho}}\text{Erf}\left(\frac{a}{2\sqrt{\zeta}} - \sqrt{\rho\zeta}\right) \\ + \frac{1}{2}e^{a\sqrt{\rho}}\text{Erf}\left(\frac{a}{2\sqrt{\zeta}} - \sqrt{\rho\zeta}\right) - \sinh\left(a\sqrt{\rho}\right)\end{aligned} \tag{4.68}$$

where $\text{Erf}\left(.\right)$ is the error function and $\sinh\left(.\right)$ is the hyperbolic sine function.

Setting $\rho = 0$ and $a = 2\xi\sqrt{N}$ while combining (4.67) with (4.68) yields

$$\text{Erfc}\left(\xi\sqrt{\frac{N}{\zeta}}\right) = 1 - \frac{1}{\pi}\int_0^\infty \frac{\sin\left(2\xi\sqrt{zN}\right)}{z} e^{-z\zeta} dz. \tag{4.69}$$

Plugging (4.69) into (4.65), the expression (4.66) is obtained. ■

4.5.2 Computation of the MGFs

Consider the case where a certain number of CR nodes are transmitting at the same time without sensing for the PU. This is the simplest case and is merely introduced mainly to compare between the performance of the ED and the MFD. Based on the model described in Sec. 4.2, the samples of the received signal $x(n)$ are conditional i.i.d. complex Gaussian RV (in this case conditioned on the interfering node positions $r_1, r_2, \ldots, r_K$), with zero-mean and conditional variance.

In the case of the ED, the MGF $\mathcal{M}(z) = \mathbb{E}\left[e^{-z\sum_{k=1}^{K} p_k r_k^{-\beta}}\right] = \prod_{k=1}^{K} \mathbb{E}\left[e^{-zp_k r_k^{-\beta}}\right]$. By averaging out the RV r_k over its PDF, for $c = 0$ in (4.3) and a path loss exponent $\beta > 2$, Eq. (4.25) is straightforwardly obtained i.e. $\mathcal{M}(z) = \{\Lambda_0(p_s z)\}^K$. However, for the MFD, the MGF $\mathcal{M}_{\text{mf}}(z)$ under P_{f}^{mf} is

$$\begin{aligned}\mathcal{M}_{\text{mf}}(z) &= \mathbb{E}\left[e^{-zS\sum_{k=1}^{K} p_s r_k^{-\beta}}\right] \\ &= \{\Lambda_0(Sp_s z)\}^{K_0}\end{aligned} \tag{4.70}$$

where $\Lambda_0(z)$ is given in (4.24), p_s is the SU transmission power, S is the energy of the PU signal and K_0 is the number of active secondary interferers under H_0. Similarly, under P_{d}^{mf} the MGf $\mathcal{M}_{\text{mf}}(z) = \{\Lambda_0(Sp_s z)\}^{K_1}$ where K_1 is number of active secondary interferers under H_1 . Hence, after substituting the MGFs, P_{f}^{mf} and P_{d}^{mf} can be computed as

$$\begin{aligned}P_{\text{f}}^{\text{mf}} = \frac{1}{2} - \frac{1}{2\pi}\int_0^\infty \frac{\sin\left(2\xi\sqrt{zN}\right)}{z} e^{-zSp_s p_w} \\ \times \left\{\frac{D^2 e^{-Sp_s z D^{-\beta}} - (Sp_s z)^{\frac{2}{\beta}}\Gamma\left(1-\frac{2}{\beta}, Sp_s z D^{-\beta}\right)}{D^2}\right\}^{K_0} dz\end{aligned} \tag{4.71}$$

and

$$P_{\mathrm{d}}^{\mathrm{mf}} = \frac{1}{2} - \frac{1}{2\pi}\int_0^{\infty} \frac{\sin\left(2\left(\xi - S\right)\sqrt{zN}\right)}{z} e^{-zSp_s p_w} \times \left\{ \frac{D^2 e^{-Sp_{\mathrm{s}} z D^{-\beta}} - \left(Sp_{\mathrm{s}} z\right)^{\frac{2}{\beta}} \Gamma\left(1 - \frac{2}{\beta}, Sp_{\mathrm{s}} z D^{-\beta}\right)}{D^2} \right\}^{K_1} dz. \quad (4.72)$$

4.6 Results

In this section, numerical results are presented in order to show the performance of the detector in the presence of SU interference. Unless otherwise stated, the path loss exponent $\beta = 3$, number of samples $N = 10$, the coverage range (see Fig. 4.1) $D = 1$ and an equal PU prior probabilities i.e. $\Pr(H_0) = \Pr(H_1) = 0.5$. Furthermore, a unit noise power is assumed i.e. $p_{\mathrm{w}} = 1$, while the constant c in (4.3) equal to zero. Numerical results were obtained by plotting the relevant expressions derived in the previous sections and the results were verified by employing Monte Carlo simulation techniques.

4.6.1 Effectiveness against the Gaussian Approximation

In Fig. 4.2 the theoretical results for P_{f} against the number of active interferers K_0 were presented. Here, the SU transmission powers have been normalised by their numbers such that $p_1 = p_2 = \ldots = p_k = \frac{p}{K_0}$, and the new expression (4.11) (with (4.25) and (4.23)) is used. Monte Carlo simulation results were included in Fig. 4.2 to validate the new theoretical results. The new exact results were then used to assess the accuracy and credibility of the GA approach in energy detection. In the case of the GA, the total interference signal is approximated by a Gaussian signal with non-random variance. The average of the random variance in (4.9) is given by

$$\mathrm{var}\left(x\left(n\right)|H_0\right) = p_{\mathrm{w}} + \mathbb{E}\left[\sum_{k=1}^{K_0} p_k \left(c + r_k\right)^{-\beta}\right]. \quad (4.73)$$

When the transmit powers $p_1 = p_2 = \ldots = p_k = {}^{p}/_{K_0}$, then this reduces into

$$\operatorname{var}\left(x\left(n\right)|H_0\right) = p_{\mathrm{w}} + \frac{p \cdot \left[2c^{2-\beta} - 2\left(c+D\right)^{-\beta}\left\{\left(c+D\right)\left(c-D+\beta D\right)\right\}\right]}{D^2\left(\beta-2\right)\left(\beta-1\right)} \tag{4.74}$$

which is independent of the total number of secondary interferers. To obtain the approximate P_{f} using the GA method, the random variance in (4.9) is replaced by the average variance computed in (4.74). Thus, the false alarm is given by

$$\begin{aligned} P_{\mathrm{f}} &= \Pr\left(y > \xi | H_0\right) \\ &= \frac{\Gamma\left(\frac{N}{2}, \frac{\xi}{p_{\mathrm{w}} + \frac{p \cdot \left[2c^{2-\beta} - 2(c+D)^{-\beta}\{(c+D)(c-D+\beta D)\}\right]}{D^2(\beta-2)(\beta-1)}}\right)}{\Gamma\left(\frac{N}{2}\right)}. \end{aligned} \tag{4.75}$$

Note that a major shortcoming of the GA method is the fact that a singularity exists at $r = 0$ when $c = 0$ in (4.73). Hence, the modified path loss model is employed for non-zero $c > 0$. Fig. 4.2 further shows that as the number of interferers K is increased, the false-alarm probability for both the new exact solution and the GA converges to the same value which can be explained by the CLT [134]. In fact, by assuming each interferer transmits with ${}^{p}/_{K}$, the total power is kept constant, such that the total power is independent of the number of users. However the curves show that the false-alarm probability does not depend just on the total power. Importantly, this highlights the fact that the GA becomes increasingly inaccurate with lower number of users.

4.6.2 Effect of Modified Path Loss Model

It is worthwhile discussing the effect of the modified path loss model adopted. Fig. 4.2 shows that for a fixed detection threshold, the margin of error between the exact solution and the GA is relatively large when interferers are few for all values of c adopted. Also, convergence occurs faster for larger values of c, e.g. $c = 0.4$ as depicted. However, the deviation is more pronounced at $c = 0.1$. This is because as $c \to 0$, the path loss model becomes less reliable for the GA. Therefore it is possible to conclude that the newly computed expressions

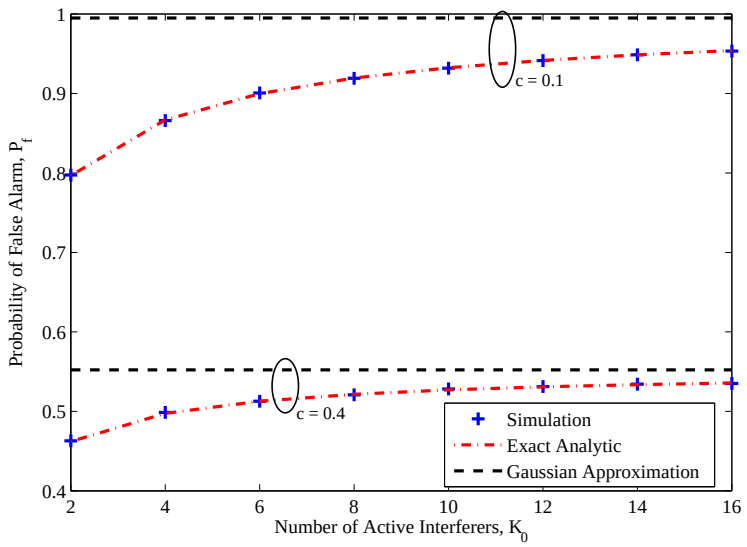

Figure 4.2: Variation of false alarm probability P_f with changing number of active interferers K_0, comparing the GA method from Eq. (4.75) with the computed exact result obtained by substituting Eqs. (4.23) and (4.22) into (4.11). Detection threshold $\xi = 10$ and SU transmit power $p_s = 1$.

provide a superior accuracy especially under low interferer presence.

4.6.3 General Detector Performance

The general performance of the detector is mainly quantified by employing two metrics. The first is the complementary receiver operating characteristic (ROC) curve obtained by plotting P_f against P_m, where $P_m = 1 - P_d$, is the probability of a missed detection (see Eq. (2.5)). Secondly, the probability of error P_e of the ED is calculated as [71]

$$P_e = P_f \Pr(H_0) + P_m \Pr(H_1) \tag{4.76}$$

where $\Pr(H_0)$ and $\Pr(H_1)$ are the respective probabilities of obtaining the hypotheses H_0 and H_1 (and $\Pr(H_0) = 1 - \Pr(H_1)$). With respect to a CR node, P_e is important because it provides a measure of the detection errors P_f and P_m. A high P_f value means poor spectral utilisation while large P_m translates into more harmful interference to the PU. For this analysis, the distance between the sensing node and the primary transmitter were fixed and normalised to unity.

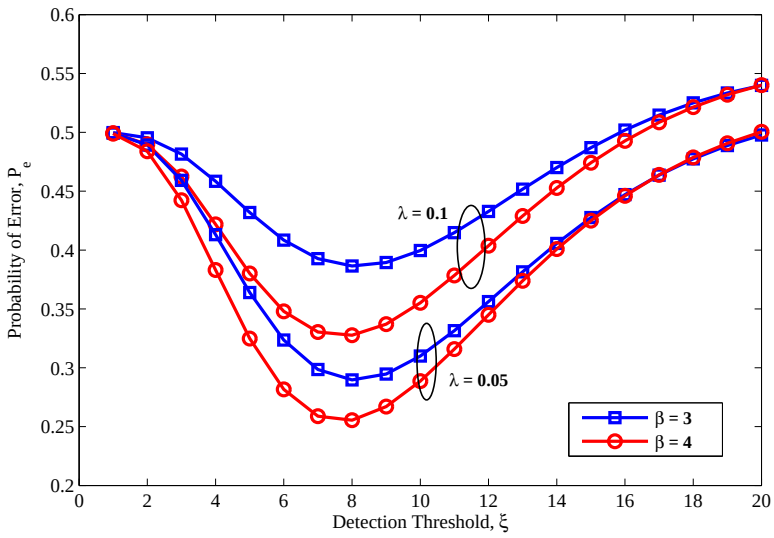

Figure 4.3: Error probability P_{e} against detection threshold ξ for Poisson interferers illustrating effect of changing interferer density λ and path loss exponent β. SU transmit power $p_s = 1$.

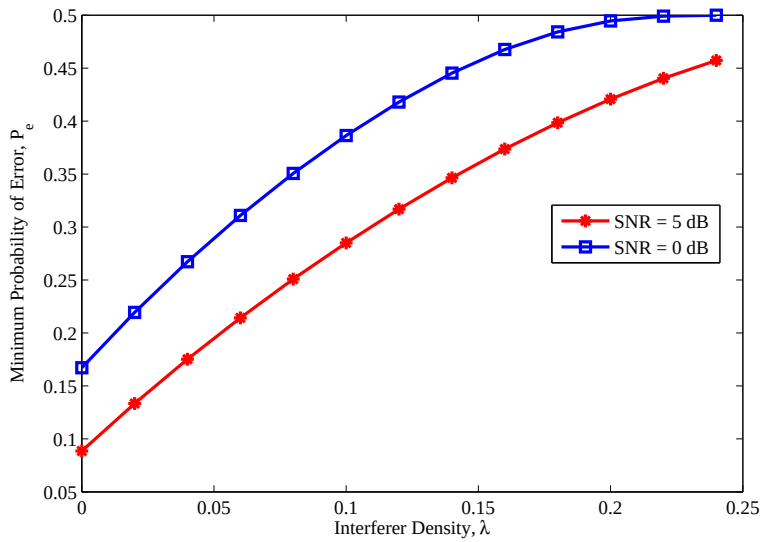

Figure 4.4: Minimised error probability P_{e} at the optimal threshold ξ_{opt} against interferer density λ [interferer/m^2] for Poisson interferers illustrating effect of different PU signal-to-noise ratio.

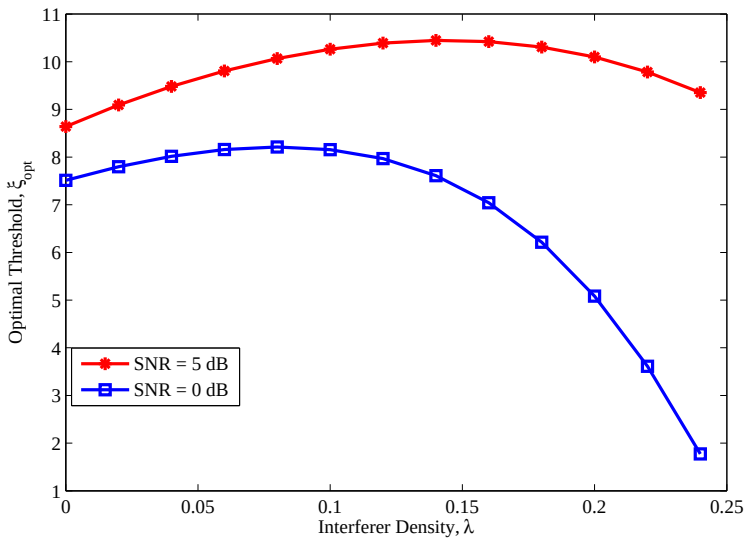

Figure 4.5: Optimal threshold ξ_{opt} for minimum error against interferer density λ [interferer/m^2] at different PU signal-to-noise ratios.

In Figs. 4.3, 4.4 and 4.5, the values of P_{f} were plotted by combining (4.26) with (4.11), while P_{d} was evaluated using (4.7). Fig. 4.3 investigates the detection error probability P_{e} in the presence of Poisson distributed interfering SU nodes. The most obvious result in Fig. 4.3 is that at a given detection threshold, P_{e} is directly proportional to the interferer density λ and inversely proportional to the path loss exponent β. Also, the effect of β is more pronounced for higher interferer densities. This confirms that the presence of interference degrades the sensing performance and the path loss reduces the effect of interference at the sensing node. A further observation is that for every curve, an optimal threshold point exists (henceforth denoted as ξ_{opt}) providing the best trade-off between P_{f} and P_{m} and consequently the least P_{e}.

Therefore the minimum probabilities of error based on the optimal values ξ_{opt} were computed in Fig. 4.4. Again P_{e} is observed to increase steadily as λ increases. Furthermore, for a fixed value of λ when the PU received SNR improves from 0dB to 5dB, the minimum error probability drops as expected, since a stronger PU signal will reduce the effect of interference at the sensing node. Next, the effect of λ on the optimal detection threshold was examined in Fig. 4.5. λ was observed to increase under both SNR regimes investigated and the value of ξ_{opt} that minimises P_{e} follows a concave curvature. This means that at a certain interferer density, the value ξ_{opt} begins to decrease.,

which occurs because P_{e} is a function of both P_{m} and P_{f} while the interferer affects only P_{f} (under H_0). Note that the increasing ξ reduces P_{f} but increases P_{m}. However, maintaining the same level of P_{f} requires a higher detection threshold under higher interference thereby also increasing P_{m}. Hence, to obtain the best P_{m} to P_{f} tradeoff, ξ_{opt} compensates to maintain a low P_{m} at higher interferer densities.

In Figs. 4.6, 4.7, 4.8 and 4.9, the values of $P_{\mathrm{f}}^{\mathrm{psn}}$ and $P_{\mathrm{d}}^{\mathrm{psn}}$ were plotted from (4.59) and (4.60). Again, the complementary ROC curves in Fig. 4.6 illustrate the degraded performance of the ED due to a higher aggregate interference accumulation at the sensing node. In Fig. 4.7, further investigations into the relationship between P_{e} and ξ were conducted and similar results to Fig. 4.11 were obtained. To obtain a suitable range for ξ in Fig. 4.8, a maximum possible spectrum utilisation of 80% (corresponding to a maximum tolerable $P_{\mathrm{f}} = 0.2$ with respect to a certain N and $\Pr(H_0)$) is assumed. It can be deduced that at each λ, the sensing node is highly sensitive to the detection threshold selected, such that the best performance at any λ value is recorded at the optimal threshold ξ_{opt}. Furthermore, the greatest error margin among different λ values is recorded at ξ_{opt}. Hence, for a fixed N, the detection threshold should be carefully decided to obtain a suitable trade-off between minimising P_{e} or making the sensor less sensitive to the interfering nodes.

Fig. 4.9 also investigates the effect of the PU presence in the spectrum of interest during sensing. Interestingly, when $\Pr(H_1)$ is higher, the error probability is greatly reduced and the sensing node is less affected by a change in interferer density. This is because a higher PU presence reduces the probability of interferer transmissions (P_{d} increases and hence P_{m} reduces).

4.6.4 Effect of Number of Observed Samples

To further investigate the performance of the sensing node, P_{e} was plotted against N in Figs. 4.8 and 4.9. Intuitively, a higher value of N is expected to translate into a better performance for the ED sensor because it gives a measure of the sensing time for the ED (although a longer sensing time ultimately reduces the transmission time for a CR node). In Fig. 4.8, two sets of curves were plotted at different threshold values, each comparing the effect of changing λ within a range of N values. The value $\xi_{\mathrm{opt}} = 7$ was acquired from the optimal threshold in Fig. 4.7, while an arbitrary reference threshold was

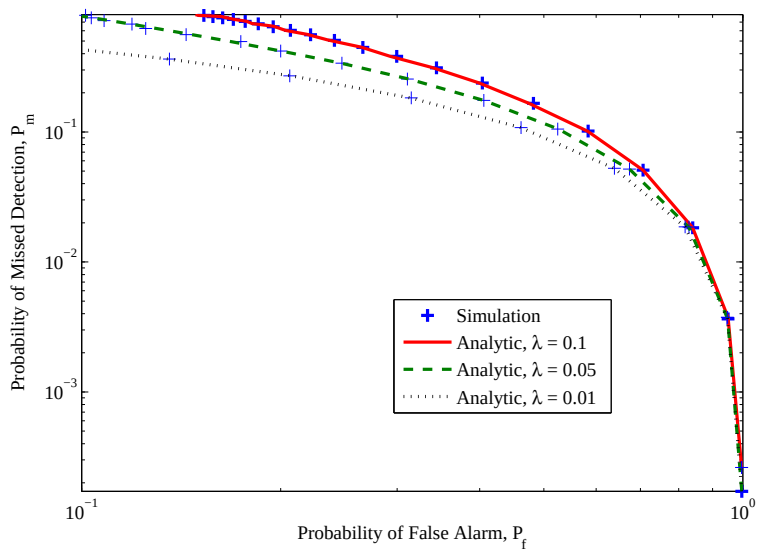

Figure 4.6: Complementary ROC curves showing performance of sensing node under different interferer densities λ [interferer/m^2].

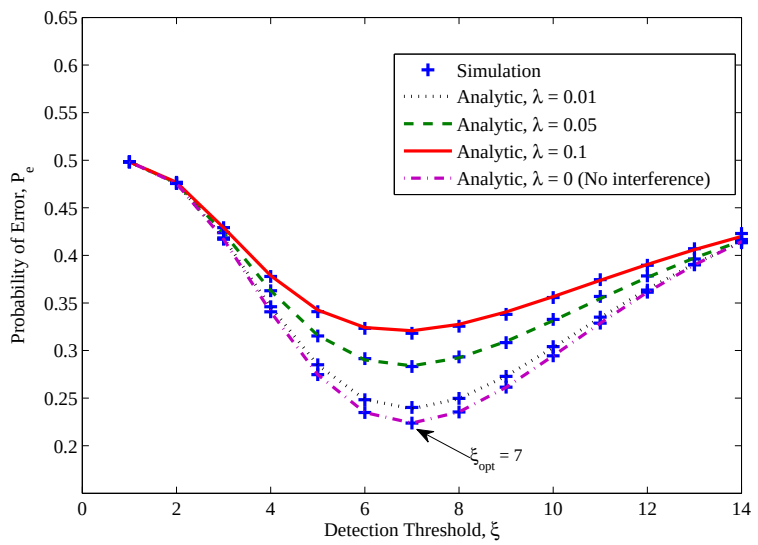

Figure 4.7: P_{e} against ξ comparing effect of interferer density λ [interferer/m^2] on sensing. $\Pr(H_0) = 0.5$ and $N = 10$.

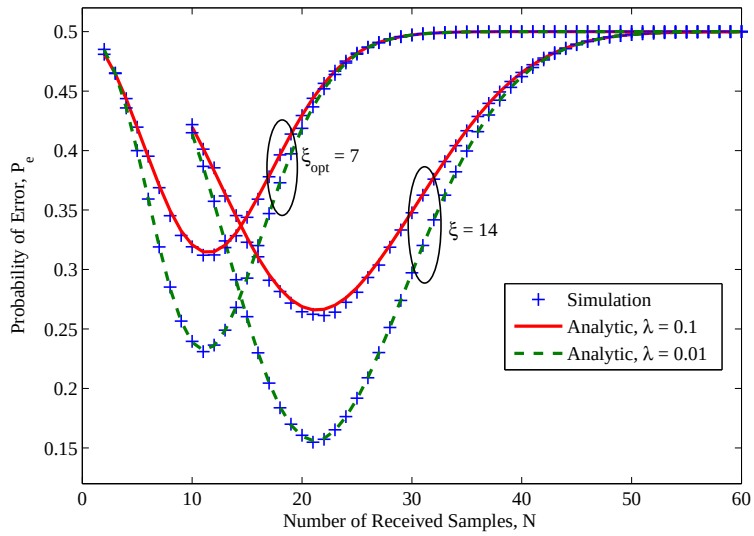

Figure 4.8: P_e against N illustrating the effect of various interferer densities λ [interferer/m^2] with respect to changing detection threshold ξ.

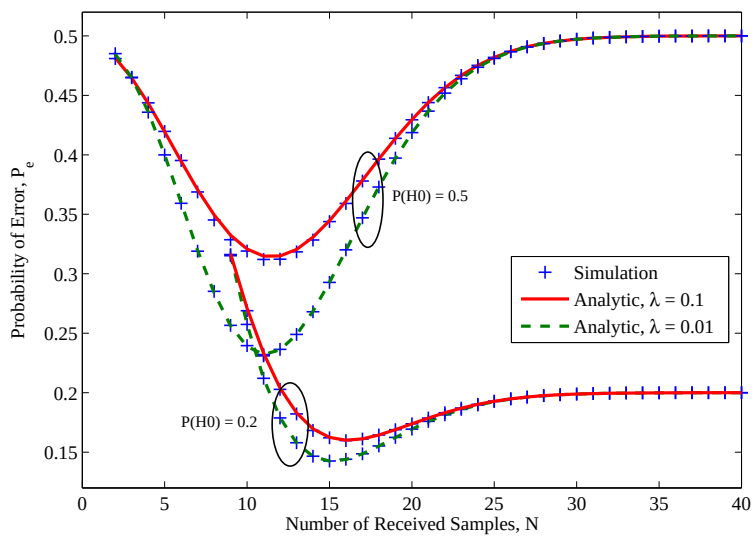

Figure 4.9: P_e against N, comparing the effect of various interferer densities λ [interferer/m^2] for different $\Pr(H_0)$.

selected for comparison. Firstly, it can be observed that for each ξ the sensing performance improves when λ decreases as expected. Secondly, the optimal number of received samples (N_{opt}) that gives the least P_{e} is highly dependent on ξ, since changing N affects the values of both P_{f} and P_{m} and ultimately P_{e}. Most importantly, at a certain high value of N, the error probability becomes insensitive to both ξ and λ and converges to $P_{\text{e}} = \Pr(H_0)$. To understand why this occurs, it should be recalled that as N is increased for a fixed detection threshold, then both P_{d} and P_{f} tend to unity, while P_{m} tends to zero. Hence, the term $P_{\text{m}} \Pr(H_1)$ in (4.76) diminishes and P_e approaches $\Pr(H_0)$.

Therefore, it can be concluded that for any given ξ, increasing the received samples only corresponds to a better performance between the region $N_{\text{min}} < N < N_{\text{opt}}$. Thereafter, when $N > N_{\text{opt}}$ any further increase in N steadily reduces performance. More so, when N becomes too high, further increase will only reduce the transmission time available to the CR without any gain in terms of improving P_{e}. Fig. 4.9 emphasises the results acquired in Fig. 4.8 indicating the performance only improves when $N_{\text{min}} < N < N_{\text{opt}}$ and reduces thereafter. Again this confirms that at high values of N, the error probability becomes insensitive to both ξ and λ and converges to $P_{\text{e}} = \Pr(H_0)$, at both $\Pr(H_0) = 0.2$ and 0.5.

4.6.5 Correlated Active CR nodes

In Fig. 4.10 the effect of the model assumptions introduced in Sec. 4.3 are analysed. In this case, (4.41) and (4.48) are recursive functions and the iterative Algorithm 4.1 was employed to obtain the exact numerical solution. From Fig. 4.10 it can be observed that for both values of detection threshold, the false alarm probability steadily increases as the number of potential interfering nodes in the network increase (This degradation can also be observed from Fig. 4.11 in the case of P_{e} against the threshold). This suggests that for denser networks, lower thresholds are required to guarantee a low level of false alarms. Furthermore, for both values of the selected threshold, the contention protocol introduced results in less false alarms with respect to the no-contention case. This result is not surprising, since contention between the nodes guarantees that not all nodes in the network become active. Moreover, the solution computed in (4.48) maintains a tight bound on the simulated value for both values of the selected threshold within the range of interfering

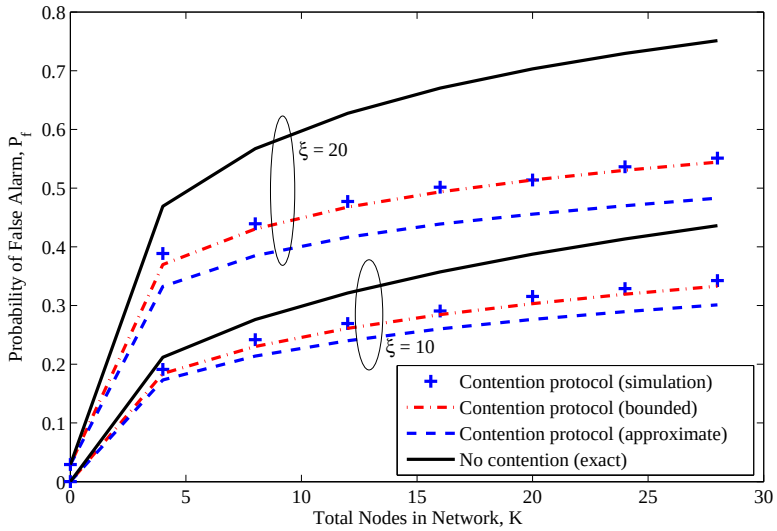

Figure 4.10: Probability of false alarm against number of secondary users at different detection thresholds ξ.

nodes, while the approximated solution in (4.38) is less accurate. Hence, approximating the CR nodes status in the network as independent variables is less credible with respect to the bounded solution.

The curves in Fig. 4.11 depict the probability of error P_e against the Detection threshold ξ. Again, it can be easily observed that the sensing error increases in the presence of SU interferers. Recall that the actual number of active nodes is less than or equal to K. It can further be observed that $P_e \approx 0.32$ even when there is no interferer. This value is quite high and results from the random relative distances between the sensing node and the PU position adopted in the approximate expressions in (4.41) and (4.42) and the bounded expressions in (4.48) and (4.49). To justify this conclusion, a third curve is plotted to account for a sensing node at a relatively fixed and normalised position of $d_0 = 1$ with no interferer presence, which shows a significant improvement in the sensing performance. Additionally, from Fig. 4.11 it can be observed that each curve indicates an optimal operating detection threshold providing the best trade-off between P_f and P_m and consequently minimum P_e, therefore the error probability at the optimal threshold was plotted to observe the effect of increasing the SU node density, in Fig. 4.12. Note that the SU transmit powers p_s have been normalised by the number of nodes such

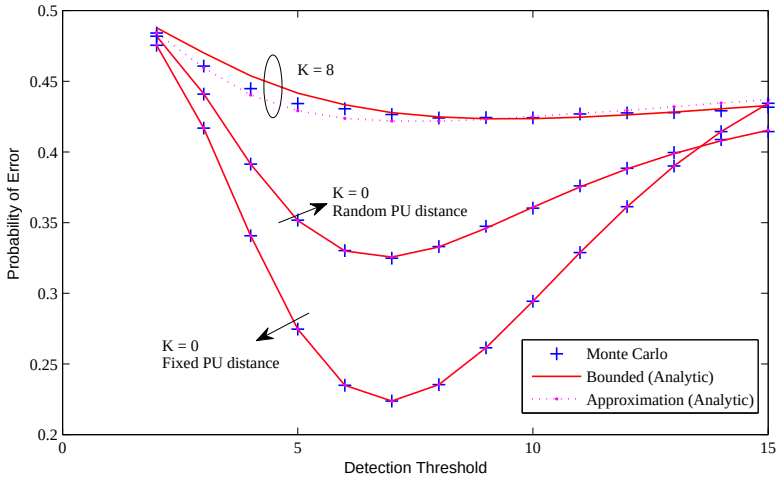

Figure 4.11: Error probability against detection threshold

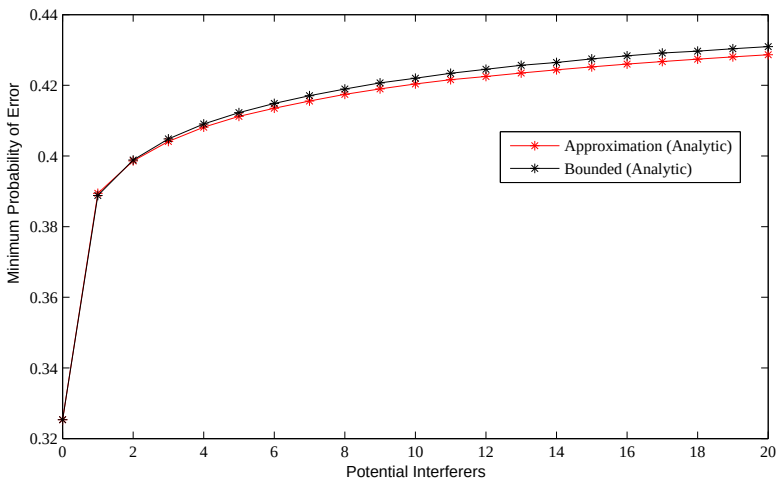

Figure 4.12: Minimum error probability against potential interferers at optimal detection threshold

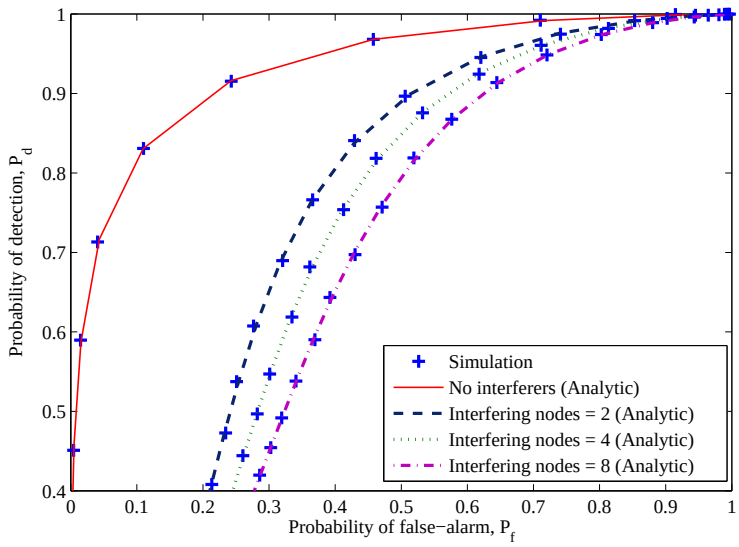

Figure 4.13: ROC curves of an energy detector for varying number of interfering nodes.

that the total power is unity, $p_s = 1/K$. This indicates the effect of the interference introduced by the SU nodes. In practice, the node transmit powers will hardly be uniform and other power control mechanisms are usually adopted with each node transmitting to optimise its parameters. Both the bounded and approximate P_e curves were found to increase when the potential SU nodes increase.

4.6.6 Comparison against the MFD

Fig. 4.13 and Fig. 4.14 present numerical results based on the analysis in Sec. 4.5, which are then validated by simulations. Studying the ROC curves would enable an objective comparison of the detectors, since the detection performance could then be observed vis-a-vis various false-alarm probabilities for each detector directly. To simplify the analysis, the distance between the sensing node and the primary transmitter is assumed to be fixed and normalised to unity. Other parameters assumed are $N = 20$, $\beta = 3$, $D = 2$ and SU node transmit powers p_k are assumed equal and normalised by the number of transmitting nodes.

Observing both figures, when no interference exists, it can be seen that both detectors are at their best performance but the MFD is at almost 100%

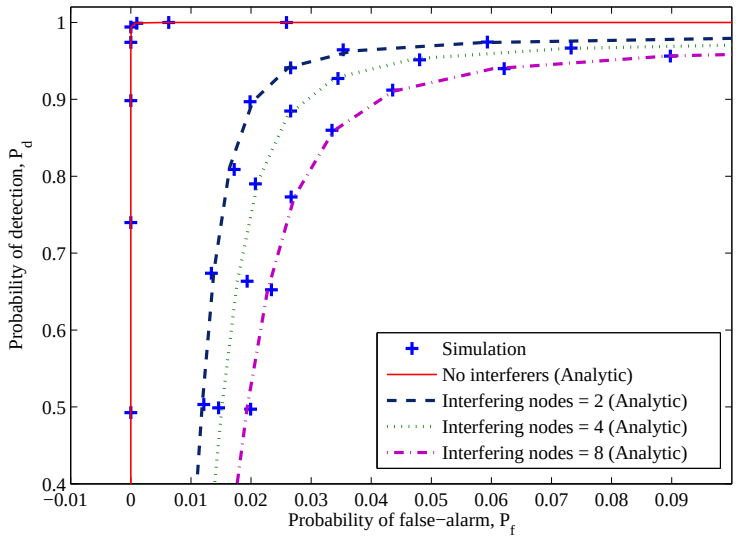

Figure 4.14: ROC curves of a matched filter detector for varying number of interfering nodes. Curves plotted with (4.71) and (4.72).

performance, since it is matched to the PU signal. It can also be observed that for all other cases with interference, when $P_{\mathrm{d}}^{\mathrm{mf}} = 0.4$, the worst MFD performance indicates a $P_{\mathrm{f}}^{\mathrm{mf}} < 0.02$ while the best ED performance indicates a $P_{\mathrm{f}} > 0.2$. This confirms the benefit derived in the MFD from the known pilot signal. Nevertheless, the MFD is also seen to be affected by the presence of the CCI.

4.7 Chapter Summary

In this chapter, the efficiency of a sensing node employing energy detection in the presence of SU generated interference was investigated. The presented approach was shown to be computationally more efficient than direct methods and provided higher accuracies over other traditional approaches such as the GA method, even at low interference levels. Novel expressions were derived to calculate the false alarm and detection probabilities while closed-form expressions were obtained for the MGFs in the various interference scenarios considered.

Generally, results confirm that the sensing node's performance is degraded with the presence of the SU interfering nodes. Observations show that both

the number of received samples N and detection threshold ξ have optimal points which correspond to minimum error probabilities for the sensor. In particular, it was noted that at a fixed N, the detection threshold should be decided to obtain a suitable trade-off between minimising P_{e} or making the sensor less sensitive to the interfering nodes. Meanwhile, increasing the received samples only guarantees an improved performance when $N < N_{\mathrm{opt}}$. However, after a certain high value of N, a change in interferer density or detection threshold has no effect on the sensing node's performance and the error converges to $P_{\mathrm{e}} = \Pr(H_0)$.

When the active SU nodes are correlated as a result of contention protocols, a tight bound to the solution was obtained. Generally, the presence of interference was observed to degrade the quality of sensing, while an increase in the received PU SNR or a change in the environment to increase the severity of the path loss exponent, resulted in an improved quality of sensing.

Chapter 5

Efficiency of Energy Detectors for Wideband Sensing of Frequency Hopping Users

IN this chapter the efficiency of the energy detector when employed for wideband spectrum sensing is investigated. The primary user of the network is assumed to be employing frequency hopping spread spectrum techniques. Several scenarios for the relative PU-SU frame lengths are examined and frameworks are proposed for computing the channel throughput and interference to the primary user. It is worth noting that the results in this chapter have mostly been presented in [139] and [140].

5.1 Background

Numerous studies have been conducted on narrowband spectrum sensing for cognitive radio (CR) in both spectrum sharing and opportunistic spectrum access applications. Other studies have investigated sensing a wideband through cooperation by several narrowband sensing nodes and taking final decisions on spectral occupancy using centralised control stations or decentralised algorithms [141, 142]. However, the authors of [143, 144] adopt a different approach to wideband sensing by jointly detecting an OFDM based primary user (PU) signal over the wideband and optimising various parameters to improve sensing performance.

In this chapter, a strategy was adopted to simultaneously sense a wideband frequency slot, which has been divided into multiple narrowband frequency slots for transmission. Particularly, the case of PUs using slow frequency hopping (FH) spread spectrum for communication was assumed. In contrast to most conventional devices that use a fixed frequency for operation, FH devices operate quite differently. The FH device dynamically changes its frequency of operation within a wideband thereby spreading its signal to occupy a wider spectrum making this form of signal type difficult to detect. The problem could be reduced if the sensing node has a knowledge of the hopping sequence, which is not likely in an opportunistic scenario. However, in [28–32], attempts have been made to show how energy detectors with no prior knowledge of the hopping sequence or spreading codes could be utilised for primary transmitter detection.

The main contribution in this chapter is that a modified concept of wideband sensing involving FH signals for CR node transmission is presented. It is worth noting that whilst most literature on FH detection are interested in the FH sequence of the desired user in the channel (for interception and/or jamming), this approach would not be of any benefit to a CR and could in fact be counterproductive. Hence, the proposed model seeks to identify the hopping period of the PU signal, such that the CR nodes can opportunistically transmit in other unoccupied subbands before the PU hop duration elapses. This assumption is possible because slow frequency hopping is assumed for the PU, such that the hop duration is long enough for a combined CR sensing and transmission time slot. It is also worth noting that this model could be adopted to suit other existing spectrum sharing networks. Examples of such applications include Wireless Local Area Networks (WLANs) and Bluetooth employing the Listen-before-Talk (LBT), Dynamic and Adaptive Frequency Hopping (AFH) techniques in the ISM unlicensed spectrum band [16, 145–147]. Particularly, [147] studies the mitigation of co-channel interference in non-collaborative Bluetooth piconets by sensing if the following subband for the FH hop is active or idle. In some cases, spectrum sensing is not enough and hence other mitigation techniques are incorporated such as AFH. However, the aforementioned models in [16, 145–147] were proposed under the assumption of synchronous frequency hopping, thus the proposed framework was extended to address and incorporate both synchronous and

asynchronous opportunistic access networks.

Another vital contribution is that the analysis assumes a model in which the secondary user (SU) frame time and PU hop duration were known and equal, for both cases when the time frames are synchronised or not. Next, this assumption is relaxed to the general case when the PU hop duration is unknown, which increases the overall complexity of the analysis. The aforementioned models are employed to characterise the hopping period of the PU signal.

The rest of this chapter is organised as follows. In Sections 5.2 and 5.3, the system performance is studied for the case where the PU-SU frame lengths are equal, but have synchronised or unsynchronised time slots respectively. On the other hand, Section 5.4 studies a system with unequal PU-SU frame lengths. In each of the aforementioned sections, the system models for the study, were described then the performance analysed for the detection and transmission phases of the SU. Furthermore, for each case the subband analysis was conducted prior to examining the joint wideband scenarios.

5.2 Equal PU-SU Frame Length, Synchronised Time Slot

5.2.1 The System Model

Consider a wideband communication channel B consisting of Q non-overlapping subbands each with bandwidth W_{r}. The wideband could be accessed by multiple PUs employing orthogonal frequency hopping to access the channel, such that interference is mitigated within the primary system [146]. Each PU has a hop bandwidth $W_{\mathrm{h}} = {}^{B}/_{Q}$ and hop duration T_{h} as illustrated in Fig. 5.1 for a two PU system. This implies a PU occupies only one subband during a single hop duration, such that spectrum holes exist within the remaining idle subbands for opportunistic access by secondary users. Furthermore, the entire PU signal energy is assumed to be contained within the hop bandwidth and evenly distributed over the hop duration [28]. On the other hand, the network policy requires that each SU should sense the channel before transmission by comparing the received energy to a threshold. If the threshold is not exceeded the transmission resumes in the subband

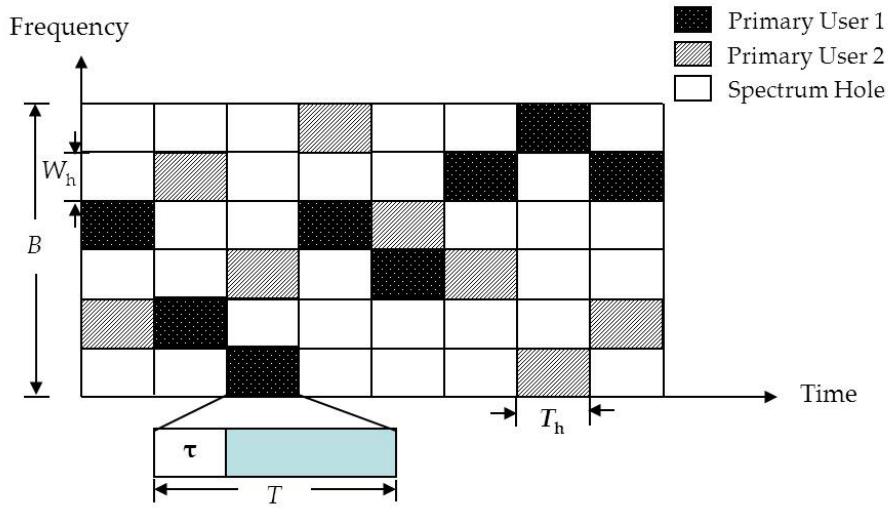

Figure 5.1: Illustration of a two primary user system employing frequency hopping to access a wideband channel. $T_h = T$, $W_h = W_r$

otherwise it is deferred. To ensure periodic sensing while allowing the CR to transmit within detected spectrum holes, a slotted time frame structure is adopted, in which each frame interval T consists of a sensing time τ followed by a transmission time $T - \tau$. For a given sampling frequency f_s the analysis is made more tractable by denoting the number of samples observed by the SU over the sensing period as $N = \tau f_s$ while $M = T f_s$ denotes the sampled equivalent of the entire SU time slot. To further simplify the analysis, it is assumed that while a CR node is sensing, only the PU transmits while other SUs remain silent. Consequently, in each subband the problem for the CR node is to determine the presence or absence of the PU signal.

In this section the time-frequency cell of the PU signal is assumed to be perfectly synchronised with the SU receiver, such that the ED sensing cycle frame is an exact integer multiple of the hop duration ($T_h = nT$) as illustrated in Fig. 5.1 (for $n = 1$) . Furthermore, both the ED and hopping bandwidth are assumed to be synchronised and equal i.e. $W_r = W_h$.

5.2.2 Detection Analysis

The received wideband signal is decomposed into narrowbands such that the SU detector bandwidth equals the hopping bandwidth. Each narrowband signal forms the single input to an ED for normal detection. The PU hop

duration is unknown while the ED integration time is τ, which commences after every SU sensing-transmission interval T. If an ED decides the absence of the PU during any sensing slot within a subband, transmission is resumed during the interval $T - \tau$ within that subband, otherwise it remains silent until the next frame. A synchronised quiet time for the SUs is enforced by the MAC protocol, such that while a CR node is sensing, only the PU transmits while other CRs remain silent.

5.2.2.1 Subband Detection

The task of each ED is to determine the presence or absence of the PU signal in a subband. All the signal energy is assumed to be contained within the hop bandwidth and the signal energy is assumed to be evenly distributed over the hop duration [28]. Here analysis is commenced with the simplest case when perfect alignment exists between the PU hopping bandwidth and each subband ED bandwidth, such that $W_{\mathrm{r}} = W_{\mathrm{h}}$. Also the hop duration and sensing-transmission frame are equal and synchronised i.e. $T = T_{\mathrm{h}}$. In subsequent sections, separate analysis will be made for unsynchronised frames. If an ED decides for the hypothesis H_0 during any sensing slot within a subband, transmission is resumed during the interval $T - \tau$ within that subband, otherwise it remains silent until the next frame.

The output of each ED is the decision variable y which is compared against a threshold ξ to make a final decision on the presence or absence of the desired primary signal within the subband. If N samples are received during the sensing time, the decision variable is given by

$$y = \sum_{n=1}^{N} \mid x\left(n\right) \mid^2 \tag{5.1}$$

where $N = \tau f_{\mathrm{s}}$, the number of samples and f_{s} is the sampling frequency. while the binary hypothesis for the final decision is;

$$x(n) = \begin{cases} w(n), & H_0 \\ s(n) + w(n), & H_1 \end{cases} \tag{5.2}$$

where $s(n)$ is the PU transmitted signal and $w\left(n\right) \sim \mathcal{N}\left(0, \sigma_w^2\right)$ is the additive white Gaussian noise (AWGN) at the sensing CR node. The hypotheses H_0

and H_1 represent the absence or presence of $s(n)$ respectively. For a large number of samples, say $N > 40$, the central limit theorem (CLT) applies and y can be approximated as a Gaussian random variable (RV) with mean

$$\mathbb{E}[y] = \begin{cases} N\sigma_w^2 & H_0 \\ N\left(\sigma_w^2 + \sigma_s^2\right) & H_1 \end{cases}$$

and variance

$$\text{var}(y) = \begin{cases} 2N\sigma_w^4 & H_0 \\ 2N\left(\sigma_w^2 + 2\sigma_s^2\right)\sigma_w^2 & H_1 \end{cases}$$

where σ_w^2 and σ_s^2 are the respective noise and signal variances.

Assuming for simplicity that $\sigma_w^2 = 1$, then the probability that the threshold is exceeded in any subband q when only noise is in the subband (false alarm) is

$$P_{\text{f},q}(\xi_q, \tau) = \Pr(y_q > \xi_q \mid H_0) = \frac{1}{2}\text{Erfc}\left(\frac{\xi_q - N}{2\sqrt{N}}\right). \tag{5.3}$$

On the other hand, when the signal is present in the subband with SNR $\gamma_q = \frac{\sigma_{s,q}^2}{\sigma_{w,q}^2}$, the probability of detection is

$$P_{\text{d},q}(\xi_q, \tau) = \Pr(y_q > \xi_q \mid H_1) = \frac{1}{2}\text{Erfc}\left(\frac{\xi_q - N(\gamma_q + 1)}{2\sqrt{N(2\gamma_q + 1)}}\right) \tag{5.4}$$

where ξ_q in (5.3) and (5.4) is the sensing threshold employed in the qth subband and $\text{Erfc}(x) = \frac{2}{\sqrt{\pi}}\int_x^\infty \exp(-t^2)\,dt$ is the complementary error function [72, Sec. 8.25].

5.2.2.2 Wideband Joint Detection

To ensure interference avoidance, a high accuracy of sensing is required. Therefore errors in correctly detecting the PU signal increases the interference to the primary network. To determine the interference on the PU system from the SU, the overall joint detection probability P_{D} for the subbands needs to be computed. Calculation of the joint detection is significant, since the subband detection probabilities are not independent. Moreover, the overall probability of missing the detection of the primary signal in the wideband is

related to P_{D} by the relation

$$P_{\mathrm{M}} = 1 - P_{\mathrm{D}}. \tag{5.5}$$

By designating a weight c as the cost incurred when the PU is interfered, then the probability of interference to the PU is quantified as

$$I_{\mathrm{p}} = cP_{\mathrm{M}} \tag{5.6}$$

where P_{M} is the probability of missing the detection of the PU in the wideband as defined in (5.5).

To determine P_{D} in (5.5), the channelised radiometer detection models for FH signals described in previous works [29] is modified. Moreover, in contrast to the normal channelised radiometer as described in [148], the particular subband within which the PU is located is of importance in this analysis to avoid interference. Hence, there is no assumption as to a decision rule to amalgamate the results from all EDs, but an alarm strategy is adopted to pinpoint the subband location of the PU signals. Also the FH signal is not observed over several hops, but each hop duration is assumed independent. Furthermore, the subband ED threshold is adjustable such that false alarms across all subbands remains fixed at the minimum desired value.

The overall detection probability given that the signal can be present in only one subband per sensing slot is

$$P_{\mathrm{D}} = 1 - \prod_{q \in \Xi} (1 - P_{\mathrm{d},q}) \prod_{i \notin \Xi} (1 - P_{\mathrm{f},i}) \tag{5.7}$$

where $q \neq i$ and Ξ denotes the set of active subbands. Note that (5.7) was arrived at, due to the fact that a PU employing FH can only occupy one subband at a time. Therefore, the detection probability of the PU occupying one subband depends on it (the same PU) not occupying other subbands.

5.2.3 Transmission Analysis

Intuitively, the SU will access a subband, either when the PU is absent or the presence of the PU was missed during sensing. The probability that the qth subband is actually idle is $1 - P_{\mathrm{f},q}(\xi, \tau)$, while the probability that the presence of the PU was missed in the subband is $1 - P_{\mathrm{d},q}(\xi, \tau)$. Thus, the subband transmission rate (in bps/Hz) when the qth subband is idle could be

given as

$$C_{0,q} = \log_2 (1 + \gamma_{\mathrm{s},q}) \tag{5.8}$$

and when the PU is active in the subband as

$$C_{1,q} = \log_2 \left(1 + \frac{\gamma_{\mathrm{s},q}}{1 + \gamma_{\mathrm{p},q}}\right) \tag{5.9}$$

where $\gamma_{\mathrm{s},q}$ and $\gamma_{\mathrm{p},q}$ are the respective signal-to-noise ratios of the SU and PU in the qth subband. Furthermore, the transmission interval is completely available to transmit the payload (i.e no preambles). The number of subbands in the set of active subbands Ξ is l, such that the total possible ways the SU can transmit within a channel consisting of Q subbands is

$$L = \sum_{l=1}^{Q} \binom{Q}{l} \tag{5.10}$$

where $\binom{n}{k}$ is the binomial operator n choose k. Thus, the average aggregate channel throughput for SU access is

$$\begin{aligned} R(\xi, \tau) &= \mathbb{E}\left[\frac{T-\tau}{T} \left(R_1 (\xi, \tau) + R_0 (\xi, \tau)\right)\right] \\ &= \frac{1}{L} \sum_{q \in \Xi, q=1}^{l} \sum_{i \neq q, i=1}^{Q-l} \frac{T-\tau}{T} \left(R_1 (\xi, \tau) + R_0 (\xi, \tau)\right) \end{aligned} \tag{5.11}$$

where the term $\frac{T-\tau}{T}$ denotes the fraction of time in which the idle subband is available for transmission and the respective throughput for the busy and idle subbands R_1 and R_0 are

$$R_1 (\xi, \tau) = C_{1,q} \left(1 - P_{\mathrm{d},q} (\xi, \tau)\right) \tag{5.12a}$$

$$R_0 (\xi, \tau) = C_{0,i} \left(1 - P_{\mathrm{f},i} (\xi, \tau)\right) \tag{5.12b}$$

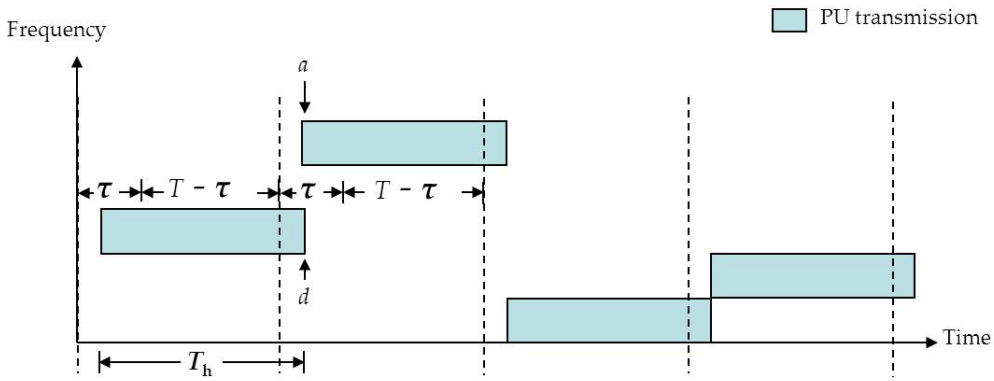

(a) Delayed ED time frame resulting in interference from SU at beginning of hop duration.

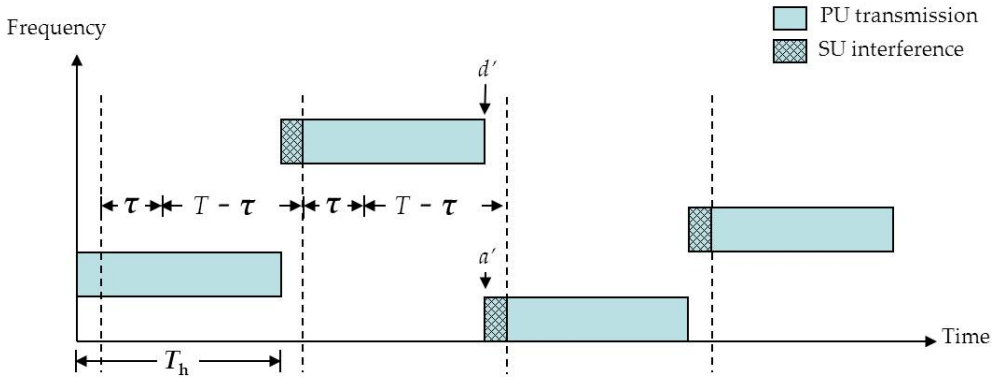

(b) Delayed FH signal cell resulting in single hop signal energy divided between two ED time intervals. a = time after which FH signal arrives into sensing slot. d = time after which FH signal departs from sensing slot.

Figure 5.2: FH misaligned Illustration. τ = sensing frame, $T - \tau$ = transmission frame and $T_h = T$ (but misaligned).

5.3 Equal PU-SU Frame Length, Unsynchronised Time Slot

5.3.1 The System Model

In this section, the frames are again adopted as $T = T_h$. However, as illustrated in Fig. 5.2 the commencement of the hop duration and the SU time frame are not synchronised. If the PU signal arrives or departs the subband during the SU transmission, the arrival and departure samples are denoted as a' and d' respectively. On the other hand, if arrival and departure occurs during the SU sensing slot, this is denoted as a and d respectively.

5.3.2 Detection Analysis

5.3.2.1 Subband Detection

Considering a single SU time frame T, then three scenarios are possible:

- **Sensing Case 1:** As illustrated in Fig. 5.2a, the PU signal hops to a new subband during the SU transmission slot such that $N < a' \leq M$, $N < d' \leq M$ and $a' = d'$. From the PU's perspective, the SU frame is slightly delayed resulting in an interference before commencement of the next sensing cycle. The interference is equivalent to the misalignment existing between the PU and SU frames. From the ED's perspective, the subband and overall detection probabilities given in (5.4) and (5.7) are not affected.

- **Sensing Case 2:** As illustrated in Fig. 5.2b, the PU signal hops during the sensing phase such that $0 < a \leq N$ and $a = d$, while the transmission phase remains uninterrupted. In this case EDs in two different subbands observe partial hop energy from the same PU, within the same secondary time slot T.

- **Sensing Case 3:** When two consecutive hops occur within the same subband, only one subband is affected and no arrival or departure of the PU signal is experienced during the sensing or transmission period. The ED observes an uninterrupted sensing duration, with detection probabilities (5.4) and (5.7). No additional interference is inflicted on the PU within other subbands and this event could occur either when $0 < a \leq N$ or $N < a' \leq M$ as observed in the first two aforementioned cases.

5.3.2.2 Wideband Joint Detection

With regards the wideband detection probability, only Cases 2 and 3 are considered, since detection is not affected in Case 1. Given the presence of K PUs in the wideband channel, the probability the PU signal remains in the same subband during the next hop (Case 3) is K/Q, while the probability the PU hops to a different band is $(Q - K)/Q$. Hence, the overall detection probability is given as

$$P_{\mathrm{D}}(a,d) = \frac{K}{Q}\left[1-(1-P_{\mathrm{d},q})^{K}(1-P_{\mathrm{f},q})^{Q-K}\right] + \frac{Q-K}{Q}\left[1-\left(1-P_{\mathrm{d},q}^{\mathrm{arr}}(a)\right)^{K}\left(1-P_{\mathrm{d},q}^{\mathrm{dep}}(d)\right)^{K}(1-P_{\mathrm{f},q})^{Q-K}\right] \quad (5.13)$$

where $P_{\mathrm{d},k}^{\mathrm{arr}}(a)$ and $P_{\mathrm{d},k}^{\mathrm{dep}}(d)$ represent the detection probabilities for the subband with the arriving and departing hop signal respectively and are conditioned on the respective arrival and departure samples of the hop signal as observed by the ED. The hypothesis, as earlier presented in (5.1) and (5.2), is modified to reflect this change. When the hop signal is absent at the beginning of the sensing period but seems to appear while sensing is ongoing, the ED obtains a subband decision variable

$$y_q = \sum_{n=1}^{a}(w(n))^2 + \sum_{n=a+1}^{N}(s(n)+w(n))^2 \quad (5.14)$$

On the other hand when the hop signal is present at the beginning of the sensing period, but departs before sensing is complete, the ED observes

$$y_q = \sum_{n=1}^{d}(s(n)+w(n))^2 + \sum_{n=d+1}^{N}(w(n))^2 \quad (5.15)$$

From (5.14) and (5.15), the corresponding detection probabilities are therefore [149]

$$P_{\mathrm{d},q}^{\mathrm{arr}}(a) = \frac{1}{2}\mathrm{Erfc}\left(\frac{\xi_q - N(\gamma_q+1)+a\gamma_q}{2\sqrt{N(2\gamma_q+1)-2a\gamma_q}}\right) \quad (5.16)$$

and

$$P_{\mathrm{d},q}^{\mathrm{dep}}(d) = \frac{1}{2}\mathrm{Erfc}\left(\frac{\xi_q - N - d\gamma_q}{2\sqrt{2}\sqrt{\frac{N}{2}+d\gamma_q}}\right) \quad (5.17)$$

From (5.15) also note that when d is sufficiently large, the ED will declare

a detection when in fact, the signal has hopped to another subband by the end of the sensing period and this results in a false alarm. Observe that whatever the degree of misalignment in Cases 1 and 2, $a = d$ (assuming the time between arrival and departure in consecutive hops is negligible), such that when $a = d = 0$ Eq. (5.16) reduces to (5.4), and Eq. (5.17) reduces to (5.3).

5.3.3 Transmission Analysis

With respect to channel capacity, the following observations can be made:

- **Transmission Case 1:** Two different subbands are affected. The PU is present throughout sensing of one subband, but hops to a different subband before transmission is complete i.e. $N < a' \leq M$. (see Fig. 5.2a). Note that the second subband occupied by the PU signal at the end of the transmission frame was earlier declared idle by the SU. The throughput for these two subbands is

$$R_1^{'} = \frac{T-\tau}{T}\left\{\left(1-P_{\mathrm{d},q}\right)C_{13,q} + \left(1-P_{\mathrm{f},j}\right)C_{12,j}\right\} \tag{5.18}$$

  where $q \neq j$. The terms $C_{12,j}$ and $C_{13,q}$ are the expectations of the conditional subband capacities conditioned on the arrival and departure of the hop signal and are a modification of the busy subband capacity $C_{1,q}$ defined in (5.9). The expectation of the capacities are

$$\mathbb{E}\left[C_{12,j}\left(a'\right)\right] = \frac{1}{M-N}\sum_{a'=1}^{M-N}\log_2\left(1+\frac{\gamma_{\mathrm{s},j}}{1+\left(\frac{T-\tau-a'}{T-\tau}\right)\gamma_{\mathrm{p},j}}\right) \tag{5.19}$$

  and

$$\mathbb{E}\left[C_{13,k}\left(d'\right)\right] = \frac{1}{M-N}\sum_{d'=1}^{M-N}\log_2\left(1+\frac{\gamma_{\mathrm{s},k}}{1+\left(\frac{d'}{T-\tau}\right)\gamma_{\mathrm{p},k}}\right). \tag{5.20}$$

- **Transmission Case 2:** In Fig. 5.2b there are two subbands of interest. The PU signal hops to a new subband during the ED sensing period. However, it is present throughout the transmission period of the new subband the PU signal arrived at, i.e $0 < a \leq N$ and $a' = d' = 0$. The

throughput for the two subbands is

$$R_1^{''} = \frac{T-\tau}{T}\left\{\left(1-P_{\mathrm{d},q}^{\mathrm{dep}}\right)C_{0,q} + \left(1-P_{\mathrm{d},j}^{\mathrm{arr}}\right)C_{1,j}\right\} \tag{5.21}$$

where $q \neq j$ and the terms $C_{0,q}$ and $C_{1,j}$ are given in (5.8) and (5.9) respectively. $P_{\mathrm{d},q}^{\mathrm{dep}}$ and $P_{\mathrm{d},j}^{\mathrm{arr}}$ are the detection probabilities given in (5.17) and (5.16) respectively and averaged over the intervals $0 < d \leq N$ and $0 < a \leq N$.

The throughput through the idle subbands in both transmission Cases 1 and 2 is

$$R_0^{'} = \frac{T-\tau}{T}\sum_{i\notin\Xi} C_{0,i}(1-P_{\mathrm{f},i}). \tag{5.22}$$

Note that Ξ is the set of active channels and $i \neq j \neq q$ in (5.21) and (5.22). Hence, the overall throughput for both cases of misalignment is given by

$$R'(\tau) = \left(R_1^{'} + R_0^{'}\right)P_{\mathrm{case1}} + \left(R_1^{''} + R_0^{'}\right)P_{\mathrm{case2}} \tag{5.23}$$

where $P_{\mathrm{case1}} = {}^{(T-\tau)}/_{T}$ and $P_{\mathrm{case2}} = {}^{\tau}/_{T}$ denote the respective probabilities of obtaining Case 1 and Case 2. The quantities $R_1^{'}$, $R_1^{''}$ and $R_0^{'}$ are defined in (5.18), (5.21) and (5.22) respectively.

5.4 Unequal PU-SU Frame Length

In the preceding sections of this chapter (Sec. 5.2 and 5.3), frameworks were proposed for SU detection of a PU employing slow frequency hopping. The analysis incorporated both synchronous and asynchronous opportunistic access networks. However, the analysis assumed schemes in which the SU frame time and PU hop duration were known and equal, i.e. $T = T_{\mathrm{h}}$ in both cases. Note that when the PU hop duration is known, the SU can synchronise its sensing and transmission time frame with PU's hop duration or in the worst case a constant time offset can be maintained (when hop duration is known but the exact hop commencement time is unknown). In practice, the assumption of known PU hop duration may not always be viable since the CR may

not necessarily have knowledge of the PU hop duration.

Thus, the particular contribution in this section is the extension of analysis to the general case when the PU hop duration is unknown. In this case the task is by no means trivial and several problems could emerge. Firstly, the selected SU time frame for combined sensing and transmission could be shorter or longer than the PU hop duration. Secondly, as a result of the unequal PU and SU time intervals, the relative statistics of the SU achievable throughput, detection probability of the PU hop signal and amount of interference inflicted on the PU may change with every hop of the PU.

5.4.1 The System Model

Consider the system model illustrated in Fig. 5.1 and described in Sec. 5.2.1. Again, the PU is assumed to employ slow frequency hopping with hop duration T_{h} to access the wideband channel B divided into Q equal non-overlapping subbands. In the analysis in this section, the PU hop duration is assumed to be unknown and therefore T_{h} may not be equal to T.

Consequently, the PU hop duration may be longer or shorter than the SU time frame and T_{h} could span several SU time frames. Therefore the analysis is simplified by assuming the relationship between the lengths of the time frame intervals as

$$T = \rho T_{\mathrm{h}} \tag{5.24}$$

where $0.5 \leq \rho \leq 2$. This ensures that there is always a maximum of two PU hops within a single SU frame or vice versa. Furthermore, considering the illustrations in Fig. 5.3 and observing each hop duration independently, a direct result of the unequal SU and PU frames can be observed. The PU signal is seen to hop in or out of a subband during the SU time frame, which may result in both the PU and SU transmissions to overlap in time, thereby causing interference.

In order to make the analysis in this section even more tractable, the usage of the variables/parameters a, d, a' and d' as employed in Sec. 5.3.1 was modified to a single variable a. This modification is reasonable since contrasting Figs. 5.2 and 5.3 shows that $a = d$ and $a' = d'$. However, this assumption means that the RV a is now defined over the entire sensing and transmission

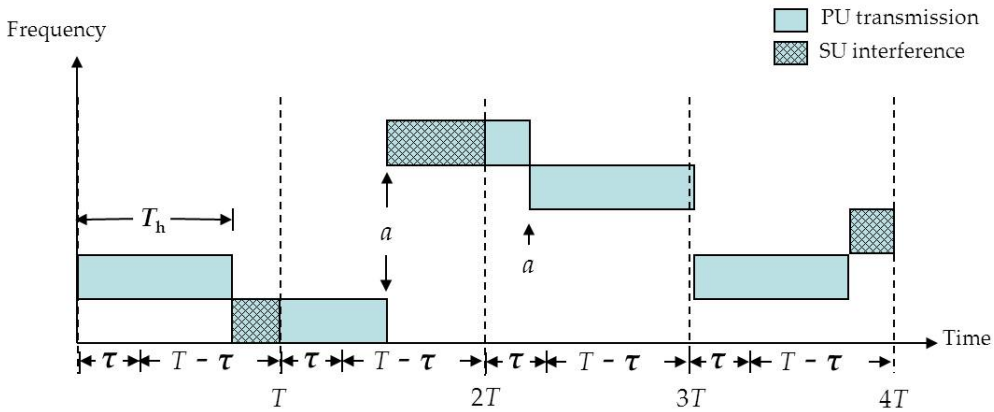

(a) Unequal SU and PU time frames, such that $T > T_h$.

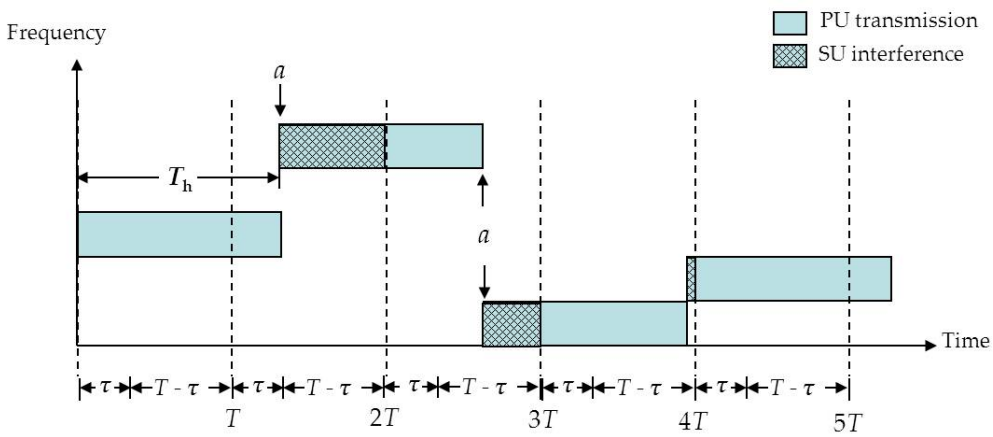

(b) Unequal SU and PU time frames, such that $T < T_h$.

Figure 5.3: Illustration of unequal PU hop duration T_h and ED sensing-transmission time slot T for a single PU network (i.e. $T \neq T_h$). τ = sensing frame of SU and $T - \tau$ = transmission frame of SU.

period such that $0 < a \leq M$. Hence, when $0 < a \leq N$, a hop (in or out) is observed during SU sensing. On the other hand, when $N < a \leq M$ then a hop is observed during the SU transmission phase.

5.4.2 Detection Analysis

5.4.2.1 Subband Detection

When sensing is conducted within any subband without any interruption due to the PU signal hopping in or out of the subband, the subband detection and false alarm probabilities under the hypotheses H_0 and H_1 remain as computed in (5.3) and (5.4). Interestingly, Fig. 5.3 illustrates other possibilities for which

the subband detection probabilities in (5.3) and (5.4) do not hold. Careful observation of Fig. 5.3, the ED will observe only partial energy from the PU hop signal during certain SU time frames. For example, between time intervals $2T$ and $3T$ in Fig. 5.3a and time intervals T and $2T$ in Fig. 5.3b, the PU signal appears to hop to a different subband while ED sensing is ongoing. Consequently, in this case the decision variable for the subband as earlier presented in (5.1) is modified to reflect this change. Similar to (5.14) and (5.15), when the hop signal is absent at the beginning of the sensing period in subband q but seems to appear while sensing is ongoing or the hop signal is present at the beginning of the sensing period, but departs before sensing is complete (e.g. between $3T$ and $4T$ in Fig. 5.3a, the ED obtains a subband decision variable

$$y_q = \sum_{n=1}^{a}(w(n))^2 + \sum_{n=a+1}^{N}(s(n)+w(n))^2 \tag{5.25}$$

and

$$y_q = \sum_{n=1}^{a}(s(n)+w(n))^2 + \sum_{n=a+1}^{N}(w(n))^2. \tag{5.26}$$

Note that (5.26) is equivalent to (5.15) with the departure sample d replaced with a in line with the new assumptions. From (5.25) and (5.26), and analogous to (5.16) and (5.17) the corresponding detection probabilities when the signal hops into subband q after the ath sample or hops out from the subband are

$$P_{\mathrm{d},q}^{\mathrm{arr}}(a) = \frac{1}{2}\mathrm{Erfc}\left(\frac{\xi_q - N - (N-a)\gamma_{\mathrm{p},q}}{2\sqrt{N+2\gamma_{\mathrm{p},q}(N-a)}}\right) \tag{5.27}$$

and

$$P_{\mathrm{d},q}^{\mathrm{dep}}(a) = \frac{1}{2}\mathrm{Erfc}\left(\frac{\xi_q - N - a\gamma_{\mathrm{p},q}}{2\sqrt{N+2a\gamma_{\mathrm{p},q}}}\right). \tag{5.28}$$

Again in (5.28), the fact that within the sensing period, the samples before and after the PU signal hop, sum up to the number of observed samples was used. Hence, (5.17) can be represented in the form (5.28).

5.4.2.2 Wideband Joint Detection

It is worth noting that obtaining the overall detection probability in (5.5) for the wideband under unequal PU-SU frame lengths, is not straightforward. This is due to the fact that the hop interval of the PU signal is unknown and unsynchronised with the SU frame. Considering a single SU time frame T, and given the presence of a single PU in the wideband, then the overall detection probability for the wideband is (5.29).

$$\begin{aligned} P_{\mathrm{D}}(a) = \frac{\tau}{T}\left\{\frac{Q-1}{Q}\left[1-\left(1-P_{\mathrm{d},q}^{\mathrm{dep}}(a)\right)\left(1-P_{\mathrm{d},j}^{\mathrm{arr}}(a)\right)\prod_{i\neq q\neq j}^{Q-2}\left(1-P_{\mathrm{f},i}\right)\right]\right\} \\ +\frac{\tau}{T}\left\{\frac{1}{Q}\left[1-\left(1-P_{\mathrm{d},q}\right)\prod_{i\neq q}^{Q-1}\left(1-P_{\mathrm{f},i}\right)\right]\right\} \\ +\frac{T-\tau}{T}\left\{1-\left(1-P_{\mathrm{d},q}\right)\prod_{i\neq q}^{Q-1}\left(1-P_{\mathrm{f},i}\right)\right\} \end{aligned} \tag{5.29}$$

This is justified in the following paragraphs. When a PU hop falls during the SU sensing slot, two cases are observed. Firstly, with a probability $1/Q$ two consecutive hops occur within the same subband and the PU signal remains in the same subband during the next hop phase. Therefore, an ED sensing any subband, observes full PU energy during the sensing period and the subband detection probability $P_{\mathrm{d},q}$ is computed as (5.4) and represented in the second term in (5.29).

Secondly, with probability $(Q-1)/Q$ the PU hops to a different subband and hence a sensing ED observes partial hops in two different subbands. In this case, the subband detection probability is given as (5.27) and (5.28) and is represented by the first term in (5.29).

When the PU hop is observed during the transmission frame of the SU, then full detection is observed in the subband the PU signal occupied during the preceding sensing phase. This event occurs with a probability $\frac{T-\tau}{T}$ and is represented as the third term in (5.29).

5.4.3 Transmission Analysis

5.4.3.1 Subband Capacity

With respect to the channel capacity, the network policy defines that each subband declared as idle could be exploited for transmission by SUs. However, in the event that there is a missed detection of the PU signal by the SU, a subband which is busy would be wrongly declared idle and SU transmission would commence. The subband transmission rate (in bps/Hz) when the qth subband is idle or busy are respectively given in [139] as

$$C_{0,q} = \log_2 (1 + \gamma_{\mathrm{s},q}) \tag{5.30}$$

and

$$C_{1,q} = \log_2 \left(1 + \frac{\gamma_{\mathrm{s},q}}{1 + \gamma_{\mathrm{p},q}} \right) \tag{5.31}$$

where $\gamma_{\mathrm{s},q}$ and $\gamma_{\mathrm{p},q}$ are the respective signal-to-noise ratios of the SU and PU in the qth subband. Interestingly, from Fig.5.3 it can be observed that due to the unequal lengths in PU and SU frames, severe misalignments occur such that a PU signal may hop to a subband occupied by the SU, before the SU frame elapses. This results in interference. For example, between time intervals T and $2T$ (or $3T$ and $4T$) in Fig. 5.3a and time intervals $2T$ and $3T$ in Fig. 5.3b, the PU signal hops to a new subband during the transmission frame of the SU (i.e. $N < a \leq M$). Note that the SU commenced transmission in the subband, because it was sensed as idle during the sensing phase. In this case, the subband capacities are

$$C_{1,j}^{\mathrm{arr}}(a) = \log_2 \left(1 + \frac{\gamma_{\mathrm{s},j}}{1 + \left(\frac{M-a}{M-N} \right) \gamma_{\mathrm{p},j}} \right) \tag{5.32}$$

and

$$C_{1,q}^{\mathrm{dep}}(a) = \log_2 \left(1 + \frac{\gamma_{\mathrm{s},q}}{1 + \left(\frac{a-N}{M-N} \right) \gamma_{\mathrm{p},q}} \right). \tag{5.33}$$

where $q \neq j$ and $N < a \leq M$. The terms $C_{1,j}^{\mathrm{arr}}$ and $C_{1,q}^{\mathrm{dep}}$ are a modification of the busy subband capacity $C_{1,q}$ defined in (5.31) and are conditioned on the sample which the PU signal hops to a different subband.

5.4.3.2 Wideband Channel Throughput

Intuitively, the SU will access a subband, either when the PU is absent or the presence of the PU was missed during sensing. The probability that the qth subband is actually idle is $1 - P_{\mathrm{f},q}$, while the probability that the presence of the PU was missed in the subband is $1 - P_{\mathrm{d},q}$. Thus, the throughput for a busy subband is

$$R_1 = C_{1,q}\,(1 - P_{\mathrm{d},q}) \tag{5.34}$$

while the throughput for all idle subbands is

$$R_0 = \sum_{i \notin \Xi} C_{0,i}(1 - P_{\mathrm{f},i}). \tag{5.35}$$

where $i \neq q$ and Ξ denotes the set of active channels. A close observation of Fig. 5.3 reveals that accurately analysing the channel throughput requires that subsequent analysis is conducted based on the relative lengths of T and T_{h}.

Shorter PU Hop Duration: When $1 < \rho \leq 2$ in (5.24) such that the PU hop duration is shorter (i.e. $T > T_{\mathrm{h}}$) as illustrated in Fig. 5.3a, then in a single SU frame T, three possible events are observed.

- Firstly, the PU is present throughout sensing of one subband, but hops to a different subband before SU transmission is complete. The throughput for the two affected subbands is

$$R_1^{(1)} = (1 - P_{\mathrm{d},q})\, C_{1,q}^{\mathrm{dep}}\,(a) + (1 - P_{\mathrm{f},j})\, C_{1,j}^{\mathrm{arr}}\,(a)\,. \tag{5.36}$$

- Secondly, the PU signal is present throughout the current SU transmission period, but had hopped during the earlier sensing period. The throughput for the two affected subbands is

$$R_1^{(2)} = \left(1 - P_{\mathrm{d},q}^{\mathrm{dep}}\,(a)\right) C_{0,q} + \left(1 - P_{\mathrm{d},j}^{\mathrm{arr}}\,(a)\right) C_{1,j}. \tag{5.37}$$

- Thirdly, the PU signal could hop twice during a particular SU frame. This means it could hop during both sensing and transmission frames

of the SU (i.e. between $3T$ and $4T$ Fig. 5.3a) or twice during the transmission.[1] Note that the constraint $1 < \rho \leq 2$ applied to Eq. (5.24) ensures that there is a maximum of two PU hops in a single SU frame T. In this scenario, the analysis rapidly becomes very complex.

The implication of simplifying the analysis through curtailing the number of hops within a single SU time frame is demonstrated next. Consider the model under analysis, it can be shown that the number of cases under each hop category are:

$$\begin{cases} 1 \text{ hop} & 2 \text{ cases} \\ 2 \text{ hops} & 2+3 \text{ cases} \\ 3 \text{ hops} & 2+3+4 \text{ cases} \\ \vdots & \vdots \\ h \text{ hops} & 2+3+4+\cdots+(h+1) \text{ cases} \end{cases} . \tag{5.38}$$

Proof: The proof is as follows.

Observe that (5.38) forms the sum of an arithmetic progression with the first term $a_1 = 2$ and the hth term $a_h = h+1$. The series itself is $\{2, 5, 9, 14 \ldots\}$. From [150, Eq. (1)], recall that the sum of an AP series is $S_h = \frac{h}{2}(a_1 + a_h)$. This can be shown by expressing the arithmetic series in 2 different ways

$$S_h = a_1 + (a_1 + d) + (a_1 + 2d) + \cdots + (a_1 + (h-2)\,d) + (a_1 + (h-1)\,d) \tag{5.39a}$$

$$S_h = (a_h - (h-1)\,d) + (a_h - (h-2)\,d) + \cdots + (a_h - 2d) + (a_h - d) + a_h. \tag{5.39b}$$

Adding (5.39a) and (5.39b) yields

$$2S_h = h\,(a_1 + a_h) \tag{5.40}$$

which reduces to (5.41) for a single PU system with 2 hops as described in the model

[1] Based on an assumption that τ is always less than $T - \tau$, then two hops cannot occur within a single sensing frame.

$$S_h = \frac{h\,(3+h)}{2} \tag{5.41}$$

where h is the number of hops observed within a single SU time frame. ■

Next the probability of each of the possible cases is derived. Consider the notation $p_{i,j,q}$ to denote the probability of a particular case occurring, where i, j, q are the first, second and third subbands the PU hop signals occupied during its two hops. Then the probability the PU hop occupied $i = 1$, then hopped to $j = 2$ and then hopped back to the initial channel is $p_{1,2,1} = \frac{Q-1}{Q} \times \frac{1}{Q}$. i.e. from the initial subband, the PU signal hops to a second subband with probability $\frac{Q-1}{Q}$. However, the signal remains in the same subband or hops back to the initial subband with probability $\frac{1}{Q}$. Hence $p_{1,2,1} = p_{1,2,2}$. If on the other hand, it hops to occupy a third subband i.e. $p_{1,2,3}$, then it does so with probability $\frac{Q-2}{Q}$, because it has only $Q-2$ possible subbands to occupy. Similarly the probabilities of the remaining cases are summarised in Table 5.1.

Case	Probability
$p_{1,1,1}$	$\frac{1}{Q^2}$
$p_{1,1,2}$	$\frac{Q-1}{Q^2}$
$p_{1,2,1}$	$\frac{Q-1}{Q^2}$
$p_{1,2,2}$	$\frac{Q-1}{Q^2}$
$p_{1,2,3}$	$\frac{(Q-1)(Q-2)}{Q^2}$

Table 5.1: Probabilities of hop scenarios

Observe that $p_{1,1,1}$ indicates three consecutive hops occupied the same subband, while only one of the possible cases resulted in a hop signal occupying three different subbands (i.e. $p_{1,2,3}$) during a single SU frame.

- **First hop within τ:** Borrowing the notation for the different possible cases, while following similar analysis for the derivation of (5.36) and (5.37), the throughput through the affected subbands (when $i \neq j \neq q$)

can be summarised by $R_{i,j,q}^{(31)}$ as

$$\begin{aligned}
R_{1,1,1}^{(31)} &= (1-P_{\mathrm{d},q})\,C_{1,q} \\
R_{1,1,2}^{(31)} &= (1-P_{\mathrm{d},q})\,C_{1,q}^{\mathrm{dep}}(a) + (1-P_{\mathrm{f},j})\,C_{1,j}^{\mathrm{arr}}(a) \\
R_{1,2,1}^{(31)} &= \left(1-P_{\mathrm{d},q}^{\mathrm{dep}}(a)\right)C_{1,q}^{\mathrm{arr}}(a) + \left(1-P_{\mathrm{d},j}^{\mathrm{arr}}(a)\right)C_{1,j}^{\mathrm{dep}}(a) \\
R_{1,2,2}^{(31)} &= \left(1-P_{\mathrm{d},q}^{\mathrm{dep}}(a)\right)C_{0,q} + \left(1-P_{\mathrm{d},j}^{\mathrm{arr}}(a)\right)C_{1,j} \\
R_{1,2,3}^{(31)} &= \left(1-P_{\mathrm{d},q}^{\mathrm{dep}}(a)\right)C_{0,q} + \left(1-P_{\mathrm{d},j}^{\mathrm{arr}}(a)\right)C_{1,j}^{\mathrm{dep}}(a) + (1-P_{\mathrm{f},i})\,C_{1,i}^{\mathrm{arr}}(a)
\end{aligned} \tag{5.42}$$

- **First hop within $T-\tau$:** When the first hop occurs within the SU transmission frame, the throughput through the subbands with PU activity can be summarised as

$$\begin{aligned}
R_{1,1,1}^{(32)} &= (1-P_{\mathrm{d},q})\,C_{1,q} \\
R_{1,1,2}^{(32)} &= (1-P_{\mathrm{d},q})\,C_{1,q}^{\mathrm{dep}}(a) + (1-P_{\mathrm{f},j})\,C_{1,j}^{\mathrm{arr}}(a) \\
R_{1,2,1}^{(32)} &= (1-P_{\mathrm{d},q})\,C_{1,q}^{d+a}(\rho) + (1-P_{\mathrm{f},j})\,C_{1,j}^{a+d}(\rho) \\
R_{1,2,2}^{(32)} &= (1-P_{\mathrm{d},q})\,C_{1,q}^{\mathrm{dep}}(a) + (1-P_{\mathrm{f},j})\,C_{1,j} \\
R_{1,2,3}^{(32)} &= (1-P_{\mathrm{d},q})\,C_{1,q}^{\mathrm{dep}}(a) + (1-P_{\mathrm{f},j})\,C_{1,q}^{\mathrm{dep}}(a) + (1-P_{\mathrm{f},i})\,C_{1,j}^{\mathrm{arr}}(a)
\end{aligned} \tag{5.43}$$

  where the subband capacities under $R_{1,2,1}^{(32)}$ are conditioned on the relative lengths of the PU and SU frames ρ. In the third line of Eq. (5.43), the term $C_{1,q}^{d+a}(\rho) = \log_2\left(1+\frac{\gamma_{\mathrm{s},q}}{1+\left(1-\frac{M}{\rho(M-N)}\right)\gamma_{\mathrm{p},q}}\right)$ stems from the fact that the PU signal hops out (for a period of $T_{\mathrm{h}} = M/\rho$) and then hops back into the subband, while $C_{1,q}^{a+d}(\rho) = \log_2\left(1+\frac{\gamma_{\mathrm{s},q}}{1+\left(\frac{M}{\rho(M-N)}\right)\gamma_{\mathrm{p},q}}\right)$ indicates that the PU signal arrived and then departed within the same SU transmission frame.

Thus, the throughput when there are two hops within the SU frame is In the third section

$$R_1^{(3)} = \sum_{j=1}^{h}\sum_{q=1}^{j+1} p_{1,j,q}\left(\frac{\tau}{T}R_{1,j,q}^{(31)} + \frac{T-\tau}{T}R_{1,j,q}^{(32)}\right) \tag{5.44}$$

Therefore, the overall throughput for the case when $T > T_{\mathrm{h}}$ is obtained from (5.36), (5.37) and (5.44) as

$$R_{sh} = \left\{ \left(R_1^{(1)} + R_0 \right) P_1 + \left(R_1^{(2)} + R_0 \right) P_2 \right\} P_{12} + \left(R_1^{(3)} + R_0 \right) P_3 \tag{5.45}$$

where $P_1 = {}^{(T-\tau)}/_{T}$, $P_2 = {}^{\tau}/_{T}$, $P_3 = {}^{T_\mathrm{h}}/_{T}$ and $P_{12} = 1 - P_3$ denote the respective probabilities of obtaining Case 1, Case 2, Case 3 and the joint probability of Cases 1 and 2. The terms $R_1^{(1)}$, $R_1^{(2)}$, $R_1^{(3)}$ and R_0 are defined in (5.36), (5.37), (5.44) and (5.35) respectively.

Longer PU Hop duration: When $T < T_\mathrm{h}$ and $0.5 < \rho \leq 1$ as illustrated in Fig. 5.3b, then events similar to (5.36) and (5.37) are observed. In addition, a third case is observed when no hop occurs throughout the SU frame (see Fig. 5.3b between 0 to T and $4T$ to $5T$). Thus, throughput is equivalent to (5.34) and the overall throughput for the case when $T < T_\mathrm{h}$ is

$$R_{long} = \left\{ \left(R_1^{(1)} + R_0 \right) P_1 + \left(R_1^{(2)} + R_0 \right) P_2 \right\} P_{12} + \left(R_1 + R_0 \right) P_3 \tag{5.46}$$

where $R_1^{(1)}$, $R_1^{(2)}$, R_1 and R_0 are defined in (5.36), (5.37), (5.34) and (5.35) respectively. The probability $P_3 = \rho$ while $P_{12} = 1 - \rho$.

5.5 Subband Throughput Optimisation

In this section, the throughput of the wideband is maximised by optimising the individual subband capacities. To achieve this, recall the overall probability of missing the detection of the PU signal in the wideband is given by (5.5). Therefore an overall network throughput optimisation problem can be defined as

$$\max_{\xi} \quad R(\xi, \tau) \tag{5.47a}$$

$$\text{s.t.} \quad P_{\mathrm{m},q}\left(\xi, \tau\right) \leq \quad P_{\mathrm{m},q}^{\max} \tag{5.47b}$$

$$P_{\mathrm{f},q}\left(\xi, \tau\right) \leq \quad P_{\mathrm{f},q}^{\max} \tag{5.47c}$$

The term $P_{\mathrm{m},q}^{\max}$ designates the upperlimit to the missed detection in each subband. This defines the interference inflicted on the PU signal when in the subband. On the other hand, $P_{\mathrm{f},q}^{\max}$ defines the maximum spectrum wastage

allowed in each subband which is equivalent to the target false alarm probability for the subband. However, $P_{\mathrm{m},q}^{\max}$ and $P_{\mathrm{f},q}^{\max}$ are controlled by the value of the ED threshold ξ. Hence, the appropriate threshold value needs to be adapted to ensure the constraints $P_{\mathrm{m},q}^{\max}$and $P_{\mathrm{f},q}^{\max}$ are satisfied in each subband. From (5.3) and (5.47c) the minimum threshold in each subband can be obtained as

$$\xi_{\min,q} = N + 2\sqrt{N}\mathrm{Erfc}^{-1}\left(2P_{\mathrm{f},q}^{\max}\right) \tag{5.48}$$

while the maximum subband threshold can be computed from (5.4) and (5.47b) as

$$\xi_{\max,q} = N\left(\gamma_{p,q}+1\right) + 2\sqrt{N\left(2\gamma_{p,q}+1\right)}\mathrm{Erfc}^{-1}\left(2\left(1-P_{\mathrm{m},q}^{\max}\right)\right) \tag{5.49}$$

Therefore the constraints in (5.47b) and (5.47c) can be satisfied by observing $\xi_{\min,q} \leq \xi_q \leq \xi_{\max,q}$. The conditions of optimality and convexity of the problem in Eq. (5.47a) was extensively discussed in [143, 144] and shown to lie within the region $0 < P_{\mathrm{m},q}^{\max} \leq 0.5$ and $0 < P_{\mathrm{f},q}^{\max} \leq 0.5$.

5.6 Results and Discussion

Expressions obtained for the multi-channel throughput and interference in Sections 5.2, 5.3 and 5.4 were plotted and then validated with simulations. In particular, the expression (5.6) was used after appropriate substitutions for the interference offered to the PU network. For all results, a multi-channel with number of subbands $Q = 8$ was assumed and SU transmission power through any idle subbands was selected such that $\gamma_{\mathrm{s},q} = 20$dB. The PU power was randomly generated for different subbands to give a range within $\gamma_{\mathrm{p},q} = -10$ to 0dB. The cost for interfering with any PU was assumed equal for all subbands and fixed at $c = 1$. By applying the constraints in Eqs. (5.47b) and (5.47c), the upperlimit for the allowable interference was fixed in each subband such that $P_{\mathrm{f},q}^{\max} = 0.1$ and the maximum spectrum wastage allowed in each subband $P_{\mathrm{m},q}^{\max} = 0.5$.

In Fig. 5.4, the achievable secondary throughput for the multi-channel was studied for when the PU hop duration and ED time frames are aligned

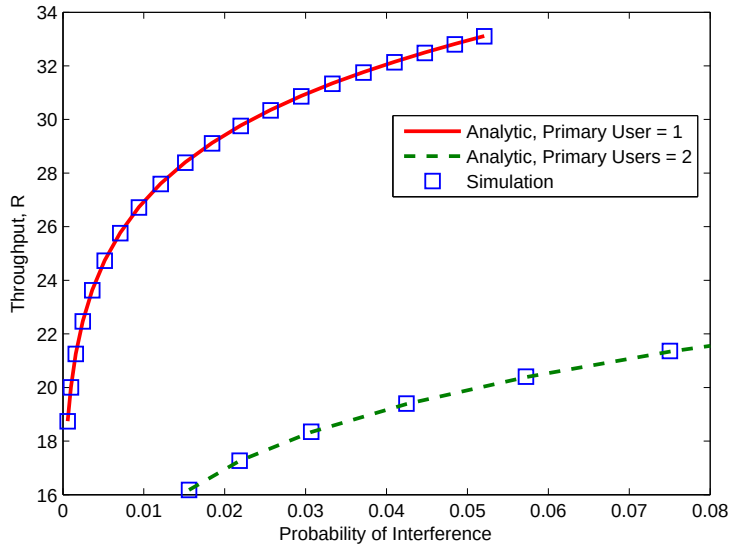

Figure 5.4: Achievable throughput against interference for aligned PU hop duration and ED time frames comparing different number of PUs K. Sensing time $\tau = 0.1T$

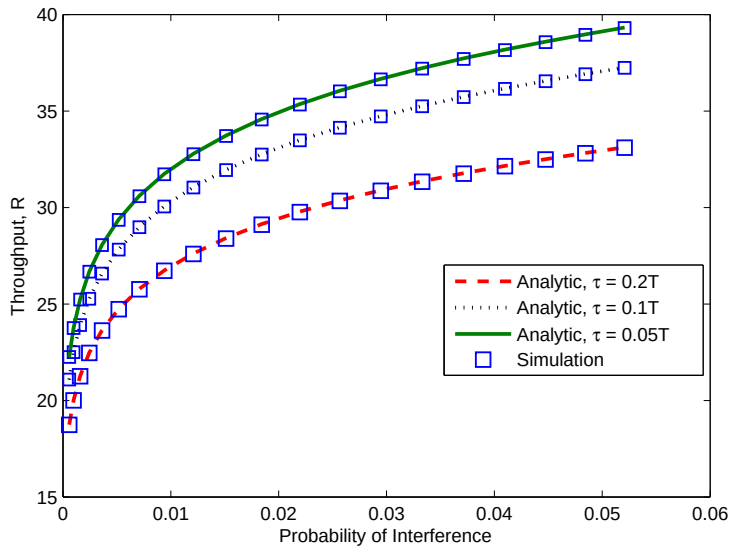

Figure 5.5: Achievable throughput against interference for aligned PU hop duration and ED time frames comparing the effect of varying the sensing time τ. Number of PU $K = 1$

at different number of PUs. The numerical throughput values were obtained from Eq. (5.11) and the interference obtained by combining Eqs. (5.6) and (5.7). It can be seen that when the number of active PUs increase within the network, there is a significant decrease in the achievable SU throughput for a fixed interference level. This indicates that when the number of PUs is increased, fewer subbands will be available for SU transmission and there is an increased likelihood that the PU will be interfered in the active channels.

Further investigations into the performance of the sensing node when the PU hop duration and ED time frames are aligned are presented in Fig. 5.5. It is observed that for a fixed number of PUs, decreasing the sensing time corresponds to an increased throughput. This result is expected, since a reduced sensing time corresponds to an increased transmission time for the PU.

Throughput performance for misaligned PU hop duration and ED time frames within the ED sensing slot is illustrated in Fig. 5.6. It can be observed that for a fixed interference level and sensing time, the achievable SU throughput decreases for larger values of misalignment. Conversely, a more surprising result is observed in Fig. 5.7 where the misalignment occurs such that the PU signal appears to hop to a new band during SU transmission. Though a close examination of Eqs. (5.19) and (5.20) indicates the effect of the misalignment a' and d' on the capacity, the curves indicate no discernible loss in achievable throughput at a fixed interference level whatever the extent of misalignment. This suggest that due to the short duration of hops, on average an unsychronised PU-SU frame results in a constant interference effect across the subbands.

In (5.45) and (5.46) the values of all subband capacities were substituted by an unconditional value after averaging out the RV. This was achieved by invoking the transformation [151, Eq. (7)], for which the proof can be found in Annex A

$$\log_2(1+x) = \log_2 e \int_0^\infty \frac{1}{z}\left(1-e^{-zx}\right)e^{-z}dz. \tag{5.50}$$

Thereafter (5.32) and (5.33) can be expressed in thIn the third sectione form of (5.50). After averaging out the RV a, both equations reduce to

$$\overline{C_{1,q}} = \log_2 e \int_0^\infty \frac{1}{z}\left(1-e^{-z\gamma_{s,q}}\right)\mathcal{M}(z)\,dz \tag{5.51}$$

where $\overline{C_{1,q}}$ is the unconditional subband capacities when the PU signal has

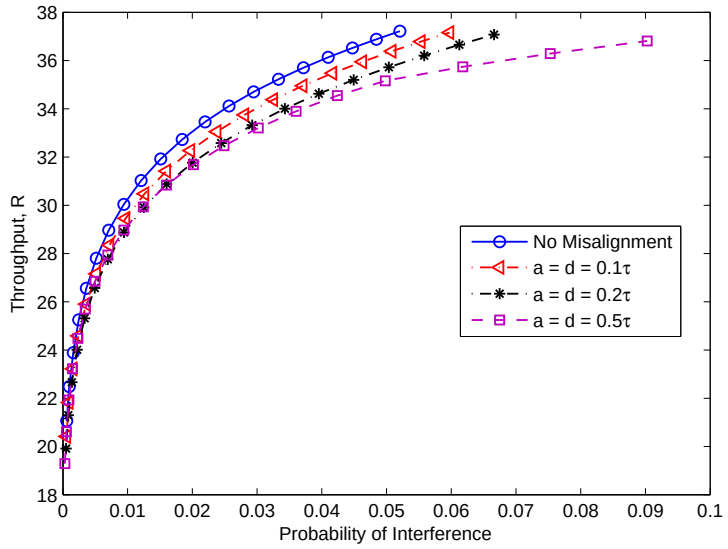

Figure 5.6: Throughput performance for misaligned PU hop duration and ED time frames illustrating the effect of misalignment within the ED sensing time $0 < a \leq \tau$. Number of PU $K = 1$. Sensing time $\tau = 0.1T$

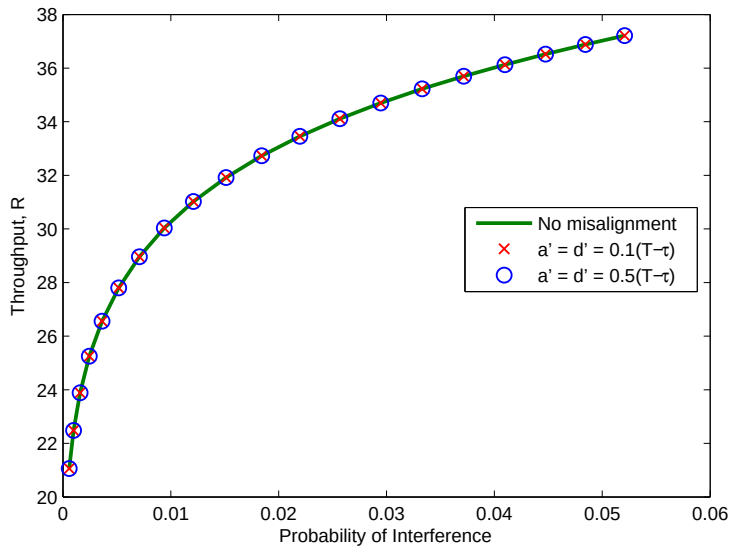

Figure 5.7: Throughput performance for misaligned PU hop duration and ED time frames showing misalignment within the ED transmission time $(T - \tau) < a' \leq T$. Number of PU $K = 1$. Sensing time $\tau = 0.1T$

hopped in or out of a subband. The term $\mathcal{M}(z)$ denotes the moment generating function. Since each subband and SU time frame are observed independently, then the sample after which the PU signal is observed to hop (i.e. RV a) follows a uniform distribution within the transmission frame $M-N$. Hence from (5.32), $\mathcal{M}(z)$ in (5.51) is

$$\begin{aligned}\mathcal{M}(z) &= \mathbb{E}\left[e^{-z\left(1+\left(\frac{M-a}{M-N}\right)\gamma_{\mathrm{p}}\right)}\right] \\ &= \int_N^M \frac{\exp\left(-z\left(1+\left(\frac{M-a}{M-N}\right)\gamma_{\mathrm{p}}\right)\right)}{M-N} da \\ &= \frac{e^{-z}-e^{-z(1+\gamma_{\mathrm{p}})}}{z\gamma_{\mathrm{p}}}. \end{aligned} \tag{5.52}$$

Similarly, from (5.33), the average $\mathbb{E}\left[\exp\left(-z\left(1+\left(\frac{a-N}{M-N}\right)\gamma_{\mathrm{p}}\right)\right)\right]$ reduces to (5.52). On the other hand, the unconditional subband detection probabilities were obtained by invoking the Jensen's inequality i.e. $f(\mathbb{E}[a]) \leq \mathbb{E}[f(a)]$, (see [132, pp. 265]), since (5.27) and (5.28) are concave and convex in a respectively. Thus bounds for (5.27) and (5.28) can be obtained directly by substituting $\mathbb{E}[a] = N/2$.

In Fig. 5.8, the achievable secondary throughput for the multi-channel when the PU hop duration is shorter than the SU frame was investigated. The SU throughput was observed to increase with sensing time for a fixed value PU-SU frame length difference ρ. Similar results are obtained in Fig. 5.9 indicating that the throughput increases with the sensing time. Additionally, there is no significant difference observed in the achievable throughput in both figures, leading to the conclusion that the relative frame length differences has no discernible effect. More so, in each figure it can be observed that when ρ is changed at a fixed sensing time, there is no observable change in SU throughput at any interference level. Furthermore, at the points when the PU-SU frames are equal, i.e. when $\rho = 1$ in Fig. 5.9 or $\rho = 0.5$ in Fig. 5.8, there is no change in the SU throughput for corresponding sensing times and interference levels, which indicates that the misalignments between the frames plays a more significant role in the achievable SU throughput (since the PU-SU frames are still considered misaligned).

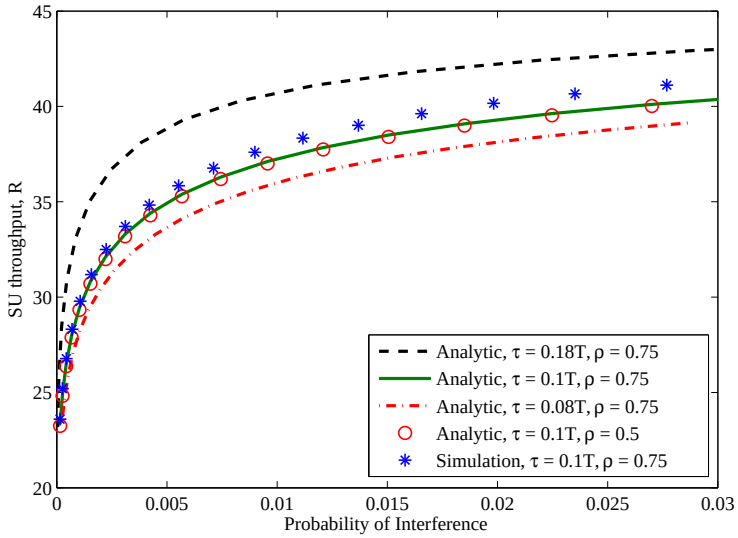

Figure 5.8: Achievable SU throughput against interference to PU. $K = 1$, $\rho = 0.75$, varying sensing time τ and $T < T_{\mathrm{h}}$.

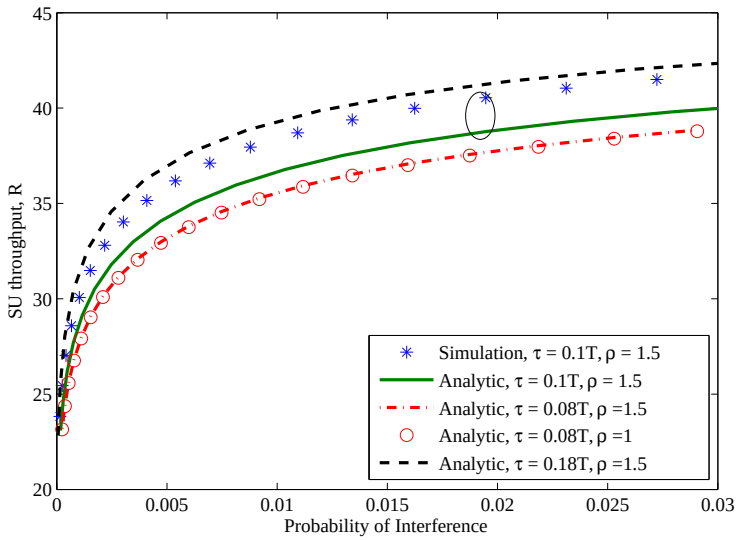

Figure 5.9: Achievable SU throughput against interference to PU. $K = 1$, varying ρ, varying sensing time τ and $T > T_{\mathrm{h}}$.

5.7 Chapter Summary

In this chapter, wideband spectrum sensing was studied for a channel with a primary system employing slow FH and an opportunistic secondary network. By adopting a channelised radiometer model, different scenarios were investigated such as when the PU hop duration and SU time frame are equal ($T_{\mathrm{h}} = T$) but commencement is either synchronised or not. In this scenario, a network with multiple PUs was considered. Accordingly, expressions were derived for the interference incurred by the PU network in the channel and the achievable secondary throughput in all scenarios examined. As expected, results indicate that additional number of PUs in the channel and increasing the sensing time, reduces the achievable secondary throughput for a fixed interference level. On the other hand, when misalignment of PU hop duration and SU time frame exists, an increased misalignment during the SU sensing frame increases interference to the PU, while any length of misalignment during the SU transmission frame has no discernible effect on the achievable secondary throughput.

Finally, the different cases when the PU hop duration and SU time frame are unequal were investigated i.e. $T_{\mathrm{h}} \neq T$. In fact, a scenario when the PU hop duration is unknown was examined. These situations present severe misalignments of the PU-SU frames and bring about detrimental effects to the achievable SU throughput. The results were compared against the case when $T_{\mathrm{h}} = T$ with misalignment, and simulation results were presented. For practical purposes, this study can be adopted to make the necessary adjustments in ED design parameters such as the detection threshold.

Chapter 6

Efficiency of Energy Detectors for CSMA based Networks

THIS chapter examines the efficiency of employing energy detectors in a multi-user network whose nodes are spatially distributed in a geographic area and employ a MAC protocol to access the channel. Explicit expressions for the analysis of imperfect physical carrier sensing MAC protocols using energy detection are presented for two protocols; namely, the mandatory physical carrier sensing protocol and a hybrid protocol incorporating the optional virtual carrier sensing.

6.1 Background

Due to the inherent random nature of ad hoc networks, avoiding interference is more intricate than in infrastructure based networks [93]. In order to improve the efficiency of shared wireless channels and minimise harmful interference, various Media Access Control (MAC) protocols have been proposed to coordinate user access in the shared medium. One of the most popular protocols is the carrier sense multiple access with collision avoidance (CSMA/CA) employed in several applications such as bluetooth piconets employing the Listen-before-Talk scheme or Wireless Local Area Networks (WLANs) and other devices employing the IEEE 802.11 standard [16,145–147].

As discussed in Sec. 2.5.2.1, an important reason for defining the virtual carrier sensing (VCS) handshake under the Distributed Coordination Function (DCF) protocol is in order to curb the *hidden node* problem. However, a

key assumption of the VCS mechanism is that all hidden nodes are within the receiving range of the victim receiver, which may not entirely be true in the presence of large interference ranges[1] or when the transmitter-receiver distance grows so that some stations are outside this range [92, 97]. Hence, it was shown that the VCS has limitations in solving the hidden node problem [92]. Meanwhile, underutilisation of transmission opportunities are observed in networks using physical carrier sensing (PCS) only mechanisms, especially when configured with a fixed threshold. This approach is mostly pessimistic such that even remote communications would generate a strong enough signal to make a node to backoff transmission [93]. Tuning and optimising the sensing threshold was seen to greatly improve the throughput performance [93], although this approach seems to be effective only in Dense CSMA networks. Furthermore, the authors in [92] examined the effectiveness of the request-to-send/clear-to-send (RTS/CTS) handshake and established its relationship to the PCS while several attempts have been made to evaluate the effectiveness of the DCF from a spatial viewpoint [92–96], a spatial and temporal viewpoint [97] or a Markovian viewpoint [91].

Generally speaking, the subject of the DCF protocol enjoys a rich amount of attention in the literature. It has been studied under several scenarios ranging from perfect networks, fading channels, saturated and non-saturated networks. Other scenarios include finite retry limits, presence of hidden terminals and multihop networks amongst others [91, 152–157]. A careful observation indicates that a number of the aforementioned studies have assumed perfect carrier sensing. The implication of this assumption is that, existing transmissions within the spatial region is detected with perfect accuracy once the received signal-to-noise ratio (SNR) is larger than a chosen threshold and below this threshold nothing is sensed at all. (In certain literature it is defined with the carrier sensing range, such that if the sensing range is within a certain distance, a detection with 100% accuracy is assumed and no detection otherwise). Hence, for an arbitrary SNR, γ and SNR threshold, ξ_{snr}, the probability of detection, P_{d} for perfect sensing is assumed to be

$$P_{\text{d}}(\gamma) = \begin{cases} 1 & \text{if } \gamma \geq \xi_{\text{snr}} \\ 0 & \text{if } \gamma < \xi_{\text{snr}}. \end{cases} \tag{6.1}$$

[1] A definition of the interference range in this context is provided in Sec. 6.2.2

Unfortunately, perfect sensing is hardly realistic and thus imperfect carrier sensing was studied for non-persistent, p-persistent and 1-persistent CSMA networks [158–163]. Moreover, in a number of the studies only simulation results are provided for the VCS mechanism [92, 97, 99, 164] or the PCS mechanism [95, 96, 165] .

Meanwhile, interference mitigation whether through the MAC protocols, as in the DCF previously discussed, or through other proposed techniques such as power control [166], directional antennas [167] or optimising the sensing parameters [93], it is pertinent to consider the particular characteristics of the detector employed. In practice, a detector having the ability to measure the energy in the channel, even without full information about the transmitting nodes in the network would be required. For this reason, the energy detector (ED) has been favoured in several literature, since it requires little or no knowledge of the transmitter modulation type, number and so on [3].

However, an important observation is that although the energy detector has been proposed for use in CSMA based networks (for e.g. [163, 168]) and the realisation that PCS cannot be perfect [158–163], to the best of the author's knowledge, no explicit expressions for this detector type have thus far been available.

Hence, in the first instance, the main contribution is to analytically study both forms of DCF protocols employed, i.e. PCS and VCS. Thereafter, explicit expressions are derived and presented for imperfect physical carrier sensing MAC protocols using energy detection required for the performance analysis of a node employing the aforementioned protocols. Moreover, for the PCS protocol, the simple sequential inhibition (SSI) process [169] is employed, which takes into account the cumulative interference generated in the network. The analysis for the SSI process in the literature are restricted to simulations because there is currently no analytical solution [169]. Hence, a tight bound to the solution is presented. Analysis is also conducted for performance metrics such as the transmission probability and throughput of a node, while the effect of CSMA inhibition zones arising due to neighbour node deactivation by the protocol and other system parameters such as the ED detection threshold, the node density and the radius of inhibition are investigated and simulation results presented alongside.

In the rest of the chapter, the system model is presented in Sec. 6.2, the

performance analysis in Sec. 6.3 and the results in Sec. 6.4.

6.2 The Model

6.2.1 Transmission and Reception

Let K independent nodes share a communication channel. Assuming each node senses the channel using energy detection, and is expected to observe a protocol where a node measures the cumulative interference present before initiation. When the received energy is below a predefined threshold ξ then the user transmits. Otherwise, the user defers. Consider an arbitrary reference receiver node at the centre of a circle of radius D, each node receives interference from all active transmitters on the plane, and these interference powers are added to the channel noise at the receiver. The received accumulated signal $x_0(t)$ at the reference receiver is

$$x_0(t) = \sum_{k=1}^{K} \delta_k s_k(t) + w(t) \tag{6.2}$$

where $w(t) \sim \mathcal{N}(0, \sigma_w^2)$ is the additive white Gaussian noise (AWGN) at the reference user with single sided power spectral density N_0. The total number of nodes in the region K, while the term δ_k is a Bernoulli random variable (RV) denoting the access-right of the kth user to transmit or not. This access-right is interpreted as

$$\delta_k = \begin{cases} 1, & y_k \leq \xi \\ 0, & y_k > \xi \end{cases} \tag{6.3}$$

where y_k is the decision variable defined in (6.6). The term $s_k(t)(k = 1, 2, \ldots K)$ in (6.2) is the signal from the kth node and is represented as

$$s_k(t) = \sqrt{p_k r_k^{-\beta}} g_k(t) e^{j2\pi f_k t} \tag{6.4}$$

where $g_k(t)$ is a low-pass zero-mean complex Gaussian random process. The term p_k is the transmission power of the kth user, while $r_k^{-\beta}$ is the distant dependent path loss function for the kth user at distance r_k and path loss exponent β. As far as the distribution of r_k is concerned, the nodes are assumed

to be uniformly distributed in a circular region of radius D with the reference user at the origin. The PDF of the distances is given by [129, 130]

$$f(r) = \begin{cases} \frac{2r}{D^2}, & 0 < r_k \leq D \\ 0, & \text{otherwise.} \end{cases} \tag{6.5}$$

6.2.2 Media Access Control

To ensure fairness in the network, a MAC coexistence protocol determines which node transmits at any given time. For the proposed model, the following MAC protocols are considered for channel access:[2]

- Protocol I: *Physical Carrier Sensing*. The channel occupancy is associated to the cumulative interference level in the network. Hence, a busy channel is reported when the energy is sensed above the sensing threshold of an energy detector.

- Protocol II: *Hybrid Physical and Virtual Carrier Sensing*. This protocol seeks to logically combine Protocol I with the VCS protocol in order to declare the occupancy state of the channel. In the VCS protocol considered, the carrier sense is sensitive to the nearest node and not to the cumulative interference. Hence, this protocol seeks to maintain a minimum distance between each node and its nearest neighbour that manifests as a virtual inhibition ball around a node within which no other node in the network is present. Moreover, as a consequence of this protocol, the cumulative interference may or may not be above the detection threshold for the channel to be declared busy.

In the context of this study, the following distance parameters of interest are defined [92]

- The *transmission range* is the range within which a packet is successfully received if there is no interference from other nodes. It is mainly determined by the transmission power and channel propagation effects.

- The *interference range* is the range within which nodes in receive mode will be "interfered with" by an unrelated transmitter and thus suffer a loss.

[2]Protocol I was referred to as the *physical model* in [170] or *energy-above-threshold* in [169].

- The *inhibition range* is the minimum range within which neighbouring nodes are separated under the virtual carrier sensing protocol. Denoted here by $r_{\min}$.

The two protocols to be examined are now elaborate upon. The VCS mechanism is explained thus [98]. Assume a transmitter-receiver node attempting to communicate from positions i and j, node i sends out an RTS frame to the intended receiver node j. Node j responds with a CTS frame granting transmission permission to i, which also includes channel usage duration. Importantly though, neighbouring nodes overhearing the RTS/CTS handshake will abide by the channel reservation of node i. However, it is expected that a neighbouring node may potentially fail to receive the RTS/CTS if outside the transmission range of i or j (for RTS or CTS respectively). Hence, this eventuality is accounted for by measuring the cumulative interference through the PCS.

It is worth noting that in the aforementioned protocols the total nodes in the network (that are potential transmitters i.e. passive and active nodes) are assumed to follow a Poisson point process (PPP). However, as a consequence of the MAC protocol, the spatial distribution of the active nodes cannot be aptly represented by the traditional PPP, but by some modifications of it. In fact, Protocols I and II result in quite dissimilar spatial distributions. Protocol I, requires an extension of the simple sequential inhibition (SSI) process [169], which takes into account the cumulative interference generated in the network and not the closest neighbour[3]. On the other hand, in the case of the VCS mechanism under Protocol II, a convenient representation is the Matern hard-core (MH) process [171], which is a dependent thinning process that describes patterns produced by the locations of centres of non-overlapping circles or spheres of radii $r_{\min}/2$. In this case r_{min} is the minimum separation between two transmitting nodes, which is assumed to be the inhibition range. A full description of the MH process is presented under the analysis section while a demonstration (via simulation) of the effect of the MH thinning is presented in Fig. 6.1.

[3]There is currently no analytical solution for the SSI process and analysis is mainly restricted to simulations [169], but as will be shown later, a convenient tight bound will be presented.

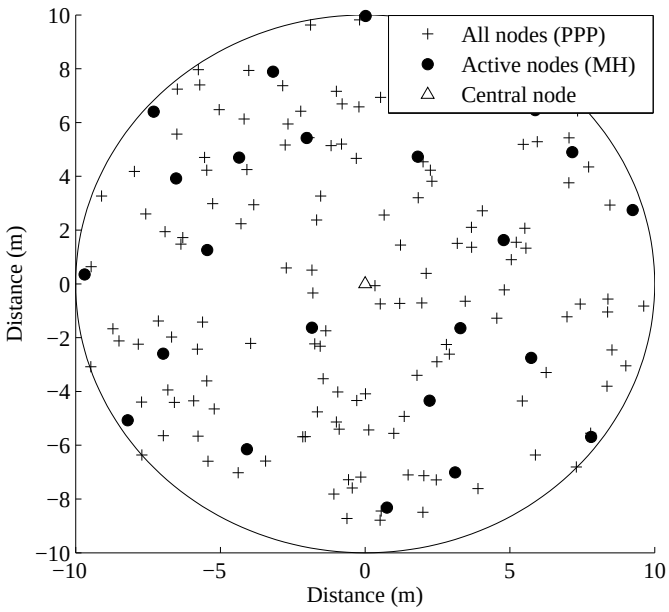

(a) Scatter diagram for the MH and PPP processes. Inhibition radius $r_{min} = 2$ and node density $\lambda = 0.5$.

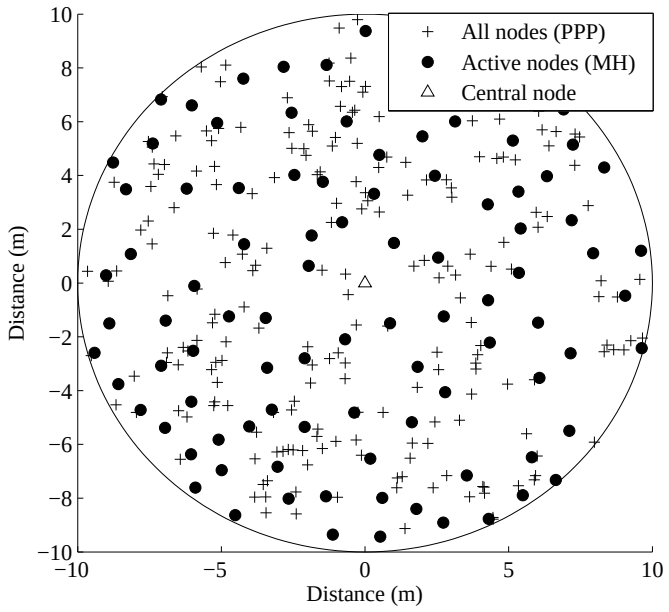

(b) Scatter diagram for the MH and PPP processes. Inhibition radius $r_{min} = 1$ and unit node density.

Figure 6.1: Illustration of the PPP and MH processes generated through simulation.

6.3 Performance Analysis

In this section, expressions are derived for the performance analysis of nodes in a network employing each of the aforementioned protocols.

The decision variable y_0 is the output of an energy detector, which is then compared against a threshold ξ to make the final decision on the state of the channel. Assuming N independent samples are received during the sensing time, then from (6.2) and (6.4) the decision variable is given by

$$y_0 = \frac{1}{N}\sum_{n=1}^{N}\left|\sum_{k=1}^{K}\sqrt{\delta_k p_k r_k^{-\beta}}g_k\left(n\right)+w\left(n\right)\right|^2 \tag{6.6}$$

where $g_k\left(n\right)$ and $w\left(n\right)$ are defined in (6.4) and (6.2) respectively. Note that the decision variable y_0 is a sum of conditional i.i.d. complex Gaussian random variables (conditioned on the distances of the interfering nodes $(r_1, r_2, \ldots, r_K)$ and their access-rights $(\delta_1, \delta_2, \ldots, \delta_K)$. This implies that y_0 is a sum of squares of zero-mean complex Gaussian RVs and follows a conditional central chi-square distribution.

6.3.1 Transmission Probability

6.3.1.1 PCS-only protocol

In a saturated network where nodes are always backlogged and ready to transmit, then the transmission probability is simply the probability that the measured energy is less than the detection threshold. Thus from (6.6) and employing a similar derivation to Lemma 3

$$\begin{aligned}\Theta &= \Pr\left\{y_0 \leq \xi\right\}\\ &= \Pr\left\{\frac{1}{N}\sum_{n=1}^{N}\left|\sum_{k=1}^{K}\sqrt{\delta_k p_k r_k^{-\beta}}g_k\left(n\right)+w\left(n\right)\right|^2 \leq \xi\right\}\\ &= \frac{1}{\Gamma\left(\frac{N}{2}\right)}\int_0^{\infty} z^{\frac{N}{4}-1}J_{\frac{N}{2}}\left(2\sqrt{z}\right)\mathcal{M}\left(\frac{z}{N\xi}\right)e^{-\left(\frac{z}{N\xi}\right)p_{\mathrm{w}}}dz\end{aligned} \tag{6.7}$$

where

$$\mathcal{M}(z) = \mathbb{E}\left[e^{-z\sum_{k=1}^{K}\delta_k p_k r_k^{-\beta}}\right]$$

is the moment generating function (MGF) and the expectation is with respect to the random variables $\{\delta_k, r_k\}$. For the sake of simplicity the transmitters are assumed to have identical transmit powers, such that $p_1 = p_2 = \cdots = p_K$. Furthermore, and without any loss of generality, powers are normalised such that $p_1 = p_2 = \cdots = p_K = 1$. Therefore, p_{w} is the noise power normalised to the transmit power.

Note that although the random variables $r_k, r_2, \ldots, r_K$ are independent, the access-right variables $\delta_1, \delta_2, \ldots, \delta_K$ are generally not independent. Hence, Jensen's inequality [132, pp. 265] was invoked in order to obtain the following bound for the conditional MGF

$$\begin{aligned}\mathcal{M}(z|r_1, \ldots, r_K) &= \mathbb{E}\left[e^{-z\sum_{k=1}^{K}\delta_k r_k^{-\beta}}|r_1, \ldots, r_K\right] \\ &\geq e^{-z\sum_{k=1}^{K}\mathbb{E}[\delta_k] r_k^{-\beta}}\end{aligned} \tag{6.8}$$

where the expectation in (6.8) is with respect to $\{\delta_1, \delta_2, \ldots, \delta_K\}$.

Assuming that all users experience identical statistical behavior. Then the expectation of the RV is $\mathbb{E}[\delta_k] = \Pr\{y_k \leq \xi\} = \Theta_k$, which is identical for all users. Therefore

$$\begin{aligned}\mathcal{M}(z) &\geq \prod_{k=1}^{K}\mathbb{E}\left[e^{-z\Theta r_k^{-\beta}}\right] \\ &\geq \prod_{k=1}^{K}\int_0^D e^{-z\Theta r^{-\beta}}\frac{2r}{D^2}dr \\ &\geq \prod_{k=1}^{K}\frac{D^2 e^{-z\Theta D^{-\beta}} - (z\Theta)^{\frac{2}{\beta}}\Gamma\left(1-\frac{2}{\beta}, z\Theta D^{-\beta}\right)}{D^2}\end{aligned} \tag{6.9}$$

where D is the radius of the spatial region in which the nodes lie. Assuming a large network, where $K \gg 1$ and are distributed in space according to a Poisson point process and $D \gg 1$, such that $0 < \frac{K}{\pi D^2} = \lambda < \infty$, then it can be shown that (6.9) reduces to (6.10), which corresponds to the MGF of a Poisson field of nodes with density λ being the average number of nodes per unit area.

$$\mathcal{M}(z) \geq$$
$$\lim_{\substack{K\to\infty,\\ D\to\infty\\ K/\pi D^2=\lambda}} \left[\frac{D^2 e^{-z\Theta D^{-\beta}} - (z\Theta)^{\frac{2}{\beta}}\Gamma\left(1-\frac{2}{\beta}, z\Theta D^{-\beta}\right)}{D^2}\right]^K$$
$$\geq \lim_{K\to\infty}\left[1-\frac{\lambda\pi(z\Theta)^{\frac{2}{\beta}}}{K}\Gamma\left(1-\frac{2}{\beta}\right)\right]^K$$
$$\geq \exp\left(-\lambda\pi(z\Theta)^{\frac{2}{\beta}}\Gamma\left(1-\frac{2}{\beta}\right)\right) \tag{6.10}$$

It is worthy of note that the Poisson process is thinned to represent only the active nodes in the network that have been granted the access-right $\delta_k = 1$. Hence, by combining (6.7) and (6.10) an upper bound to the transmission probability $\Theta = \Pr\{y_0 \leq \xi\}$ is

$$\Theta \geq \int_0^\infty \frac{z^{\frac{N}{4}-1} J_{\frac{N}{2}}(2\sqrt{z})}{\Gamma\left(\frac{N}{2}\right)} e^{-\left(\lambda\pi\left(\frac{z\Theta}{N\xi}\right)^{\frac{2}{\beta}}\Gamma\left(1-\frac{2}{\beta}\right)+\frac{p_W z}{N\xi}\right)} dz \tag{6.11}$$

and Θ can be obtained by solving the non-linear equation (6.11).

6.3.1.2 Hybrid PCS and VCS protocol

The effect of applying a minimum separation between two transmitting nodes (inhibition range) as against the energy level only is that the effect of the nearest neighbour is now considered. The MH process assumes that each node is located at the centre of non-overlapping circles or spheres of radii $r_{\min}/2$. Consider a stationary Poisson process Φ with intensity λ. A dependent thinning process is then applied, where a point c of Φ is marked with a random variable $m(c)$ uniformly distributed in $(0,1)$. The point c is retained if the circle $C(c, r_{\min})$ contains no points of Φ with marks smaller than $m(c)$ otherwise the point c is removed. Under these assumptions, the access-right variables $\{\delta_1, \delta_2, \ldots, \delta_K\}$ are still correlated but the expectation is now dependent on both the cumulative interference been above the ED threshold and the nearest

neighbour to the node located outside the inhibition range. Thus

$$\begin{aligned}\mathbb{E}\left[\delta_k\right] &= \Pr\left\{y_0 \leq \xi\right\} \Pr\left\{r_k > r_{\min}\right\} \\ &= \Theta_k \left\{ \frac{1 - e^{-\lambda \pi r_{\min}^2}}{\pi r_{\min}^2} \right\}\end{aligned} \tag{6.12}$$

where the term Θ_k denotes the probability the cumulative energy received by the kth node is above the detection threshold given in (6.11) and $\frac{1-e^{-\lambda\pi r_{\min}^2}}{\pi r_{\min}^2}$ is the palm retaining probability of a typical node under the MH process [171]. Following similar analysis to the result obtained in (6.10), the MGF can be bounded as in (6.8) and replacing $\mathbb{E}\left[\delta_k\right]$ from (6.12) a closed-form MGF for this protocol is obtained as

$$\mathcal{M}\left(z\right) = \exp\left(-\pi\lambda \left[\frac{z\Theta\left\{1 - e^{-\lambda\pi r_{\min}^2}\right\}}{\pi r_{\min}^2} \right]^{\frac{2}{\beta}} \Gamma\left(1 - \frac{2}{\beta}\right) \right). \tag{6.13}$$

Hence, by combining (6.7) and (6.13) the transmission probability under protocol II is

$$\begin{aligned}\Theta_{\text{vp}} \geq \frac{1}{\Gamma\left(\frac{N}{2}\right)} \int_0^\infty z^{\frac{N}{4}-1} J_{\frac{N}{2}}\left(2\sqrt{z}\right) e^{-\frac{p_{\text{w}} z}{\xi}} \\ \times e^{-\pi\lambda\left(\frac{z\Theta}{N\xi\pi r_{\min}^2}\right)^{\frac{2}{\beta}}\left(1-e^{-\lambda\pi r_{\min}^2}\right)^{\frac{2}{\beta}}\Gamma\left(1-\frac{2}{\beta}\right)} dz\end{aligned} \tag{6.14}$$

where $r_{\min}$ is the minimum separation between two neighbouring nodes by virtue of the VCS protocol and Θ can be computed recursively from (6.11).

6.3.2 Throughput

The throughput of the network is the number of transmissions in the channel per unit area. If the packet arrival rate is denoted as λ_{a}, then the number of transmissions in the channel is

$$S = \lambda_{\text{a}}\Theta \tag{6.15}$$

where Θ is the probability of successful transmissions and can be computed from (6.11). Note that the packet arrival rate as λ_{a} is proportional to the node density λ and for the purpose of analysis, this can simply be represented as $\lambda_{\mathrm{a}} = \varrho\lambda$, where ϱ is an arbitrary constant. The throughput for the hybrid PCS and VCS protocol is given as

$$S_{\mathrm{vp}} = \lambda_{\mathrm{a}}\Theta_{\mathrm{vp}} \tag{6.16}$$

where Θ_{vp} is the transmission probability under the hybrid scheme.

6.4 Results

In this section results are presented to demonstrate the performance of the energy detector under both coexistence protocols analysed. Unless otherwise mentioned, it is assumed that the path loss exponent $\beta = 3$, the number of observed samples by the receiving node's ED $N = 10$, the ED detection threshold $\xi = 1$ and the VCS inhibition radius between two neighbouring nodes $r_{\min} = 1$.

Note here that the traditional technique for thinning a PPP to generate the MH process requires that the selection process is a function of random marks associated to each point. However, a modified selection process is proposed here, which depends on the arrival order of the nodes. Hence, when a new node arrives, the decision to keep the node, stems from its relative distance to all other nodes present, which includes distances to active and passive nodes. This is important since the passive nodes could be regarded as potential receivers. In Figs. 6.1a and 6.1b the effectiveness of this approach is illustrated with the scatter diagrams. The effect of a change in node density on the total nodes in the region and the effect of the inhibition distances maintained between transmitting nodes when the VCS is activated are both observed. Only the nodes marked under the MH process are active. On the other hand, the SSI process for cumulative interference considers only the position of the active nodes present during the thinning process, thus ignoring the passive nodes.

In Fig. 6.2, the transmission probability of a node is observed as the detection threshold is varied. Under both protocols, for a fixed node density,

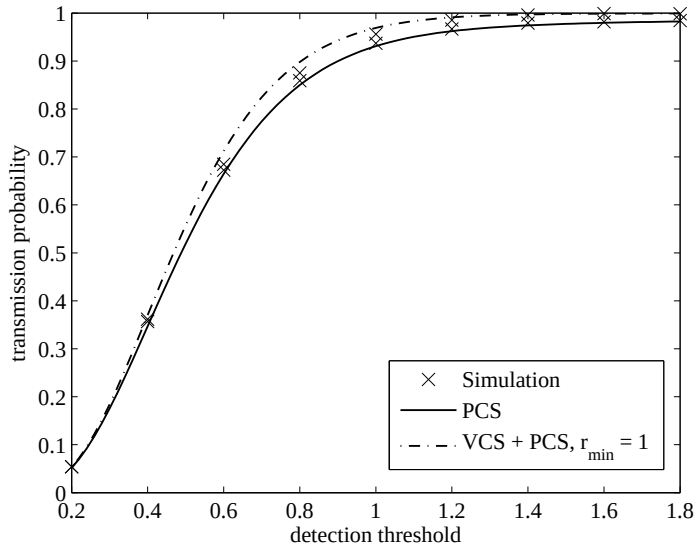

Figure 6.2: Transmission probability against detection threshold for both coexistence protocols. Node density $\lambda = 0.01$, path loss exponent $\beta = 3$ and inhibition radius for VCS $r_{\min} = 1$.

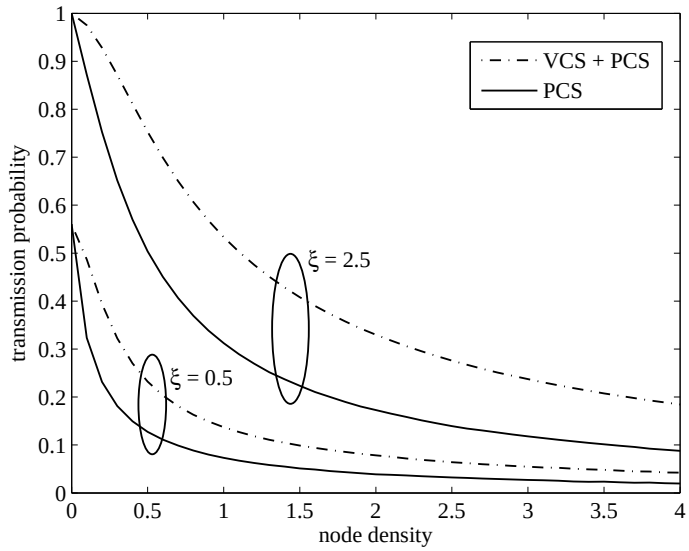

Figure 6.3: Analytical results for transmission probability against node density for both coexistence protocols at different detection thresholds ξ. Path loss exponent $\beta = 3$ and inhibition radius for VCS $r_{\min} = 1$.

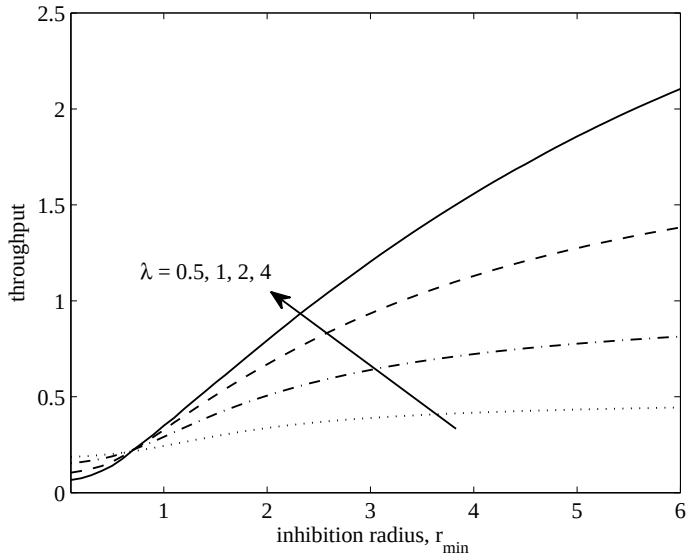

Figure 6.4: Analytical results for throughput against inhibition radius for the combined physical and virtual sensing protocol. Path loss exponent $\beta = 3$, detection threshold $\xi = 1$ and varying traffic densities.

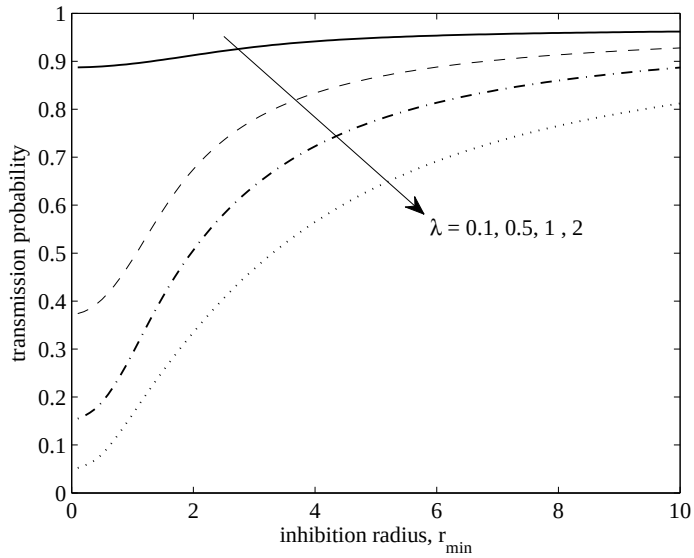

Figure 6.5: Analytical results for transmission probability against inhibition radius for the combined physical and virtual sensing protocol. Path loss exponent $\beta = 3$, detection threshold $\xi = 1$ and varying traffic densities.

increasing the detection threshold of the intending transmitter is likely to provide a higher transmission probability. This does not indicate that the performance of the ED is increased but rather a higher detection threshold indicates a willingness of the node to tolerate higher cumulative interference in the network. This needs to be traded off against the potential collisions and loss of data through interference within the network. Next, at each detection threshold, it can be observed that the protocol incorporating the optional VCS scheme provides a higher transmission probability, since the node density is lower for this scheme. More so, because the nearest nodes, which are expected to offer the highest interference to the sensing node are prohibited from transmission.

The results from Fig. 6.2 are elaborated upon in Fig. 6.3 where in this case, the transmission probability is observed for varying node densities at a fixed threshold. Comparing both figures, it can first be concluded that the performance difference between the two coexistence schemes increase as the detection threshold increases. Hence, in Fig. 6.3 the performance gap between the two protocols is larger at $\xi = 2.5$. Secondly, the transmission probability for both protocols decreases at higher node densities as expected, since an individual node would find it more difficult to gain access right to the channel.

Another issue worth mentioning is that the PCS-only protocol depends on only one threshold for the ED, while the alternate protocol is conditioned on a second threshold which is not a direct parameter for the ED. This parameter determines the inhibition radius for virtual sensing and in Figs. 6.4 and 6.5 its effect on the analysis is presented. Here it is assumed that the constant $\varrho = 1$ such that $\lambda_{\mathrm{a}} = \lambda$. In Fig. 6.4 the throughput generally increases when the inhibition radius is increased (at a fixed ED threshold). However, at very low inhibition radii (approximately $r_{\min} \lessapprox 0.7$) the throughput is higher for less density of nodes, because the network is less saturated and the fewer nodes would benefit from less inhibition. Note that this corroborates the fact that the CSMA protocol is traditionally more beneficial at higher densities [172]. Additionally, it is possible to infer this from Fig. 6.5, where the transmission probability is observed to be much higher at less network densities for very low inhibition radii. However, as the inhibition radii increase, the transmission probability for higher densities rapidly increase and converge towards

maximum, which demonstrates the benefit of the optional VCS scheme.

6.5 Chapter Summary

In this chapter, the efficiency of employing energy detectors in a multi-user network was examined. The nodes were assumed to be spatially distributed in a geographic area and employ a CSMA-like MAC protocol to access the channel. Explicit expressions were presented for the analysis of two DCF protocols that were hitherto not available within the current literature. The expressions obtained were in the form of single integrals in terms of the moment generating functions of the random intra-network SINR. Furthermore, the MGFs were derived in closed-form and the overall expressions were validated through Monte Carlo simulations. In the case of the SSI process, tight bounds to the solutions were presented. For both protocols examined, the system parameters were studied such as the energy detector detection threshold, the node density and the radius of inhibition as they affect the efficiency of the ED quantified by the transmission probabilities and throughput of the nodes.

Chapter 7

Conclusions and Future Work

7.1 Conclusions

THE study presented in this thesis has focused on the problem of spectrum sensing, which is known to be a fundamental task within any DSA-enabled wireless communication network. The literature review in Chapter 2, presents several challenges currently facing spectrum sensing techniques in general, such as detecting spread spectrum users, aggregate interference and noise uncertainty, multi-user networks, hidden terminal problems amongst others. In the subsequent chapters an attempt was made to address a few of these issues. Furthermore, the fact that the energy detector is a favoured technique for spectrum sensing due to certain advantages inherent within the technique was established. However a few of its shortcomings were also in need of further investigation. Thus, the analysis in Chapters 4, 5 and 6 mainly focused on the performance analysis of the ED in various network types.

In Chapter 3, two classes of detector types were examined. Firstly, the PLD which is a generalization of the ED and secondly, Kay's detector for unknown deterministic signals. For the PLD, the statistics for the decision variable of this detector involves the need to compute the sum of arbitrarily powered Gaussian random variables, for which simple but highly precise approximations for the PDF and CDF were presented. The technique proposed was illustrated to be more accurate than a currently existing technique for the range of values examined. The second detector investigated was analysed for performance under AWGN, Rayleigh and Nakagami fading channels, for which the relevant analytical expressions were derived and the results

contrasted against that of the classic energy detector. While, the analysis for the PLD considered the zero mean case for the primary signal, the analysis for Kay's detector was mainly for the non-zero mean case.

Chapter 4 addresses the important problem of the interference that is generated within an opportunistic spectrum access network, due to the fact that interference is inherent in a network of coexisting users. The efficiency of the ED was put to test under such interference uncertainty and in order to aid the analysis, alternative expressions were derived in terms of the MGF of the interferers' variance, which provides several advantages over the more traditional approaches. Generally, the ROC curves, error probability and effect of number of observed samples by the ED were assessed. Also, other parameters such as the effect of the detection threshold, path loss exponent and number of nodes in the network were examined.

Chapter 5 addresses two core issues. In the first instance, due to the concept of multidimensional spectrum opportunities, it is understood that in addition to spatial and spectral spectrum holes, coexisting users employing CDMA techniques can make use of spectrum opportunities in the code dimension. Secondly, a key problem highlighted with spectrum sensing was in the detection of spread spectrum users. Therefore, investigations into the efficiency of using EDs were conducted in order to exploit opportunities resulting from the use of slow frequency hopping by the PUs of the network. Several scenarios were examined arising from the amount of knowledge of the PU code sequence available to the SU, i.e., hop duration and hop commencement time. This knowledge directly affects the relative statistics of the SU's achievable throughput, detection probability of the PU hop signal and amount of interference inflicted on the PU, which may change with every hop of the PU. The framework presented for performance analysis was shown to be successful in observing the throughput of the SUs vis-a-vis the probability of interfering with the PU in the network.

Furthermore, the fact that coexistence protocols are not 100% perfect was also established and hence in Chapter 6 further investigation of the efficiency of EDs in such a network of coexisting users was studied. In particular, explicit expressions for the analysis of nodes employing energy detection are presented for two protocols, i.e. the physical carrier sensing and a hybrid physical and virtual carrier sensing protocol. Both protocols were contrasted

against each other and the benefit of the additional optional VCS in the hybrid protocol was clearly demonstrated. Further analysis was conducted for performance metrics such as the transmission probability and throughput of a node by studying parameters such as the ED detection threshold, the node density and the radius of inhibition.

7.2 Future Work

In what follows, possible research extensions to the work in this thesis are suggested.

- In Chapter 3, an alternative approach for approximating the statistics of the decision variable for the PLD under an AWGN channel was presented. It would be interesting to extend this analysis to the following
  - Fading channels
  - Detector performance under diversity reception and
  - Interference limited channels.

  As far as the analysis under interference uncertainty is concerned, the technique introduced in Chapter 4 for the ED and MFD could be adopted by expressing the equations for the P_{f} and P_{d} of the PLD in the form where the random variables are contained only in an exponent. Hence, since there are two valid approximation techniques explored in this thesis via the $\alpha - \mu$ distribution (Sec. 3.2.1.1) and gamma distribution (Sec. 3.2.1.2) and both their CDFs are in the form of the regularized upper incomplete gamma function (see Eqs. (3.7) and (3.12)), the approach could be extended to the PLD approximation under interference uncertainty.

- In Chapter 4 non-cooperating CR nodes employing contention protocols were studied, where it was assumed that the detection thresholds of various CR nodes were the same. This information could be obtained from a database stating the acceptable interference levels in the channel and other network parameters. However, detection thresholds could be determined by individual nodes depending on the prevailing channel conditions and the length/duration of sensing for that node. It should

be noted that policies could exist for maximum period for the sensing cycle. In such cases, the duration of sensing could be different across nodes and this would ultimately affect the detection threshold. It would be worthwhile investigating the effect of adaptive threshold selection on the results already obtained for fixed node thresholds.

- Another key assumption for the analysis in Chapter 4 is that zero mean signals were considered. It would be interesting to consider the non-zero mean case and accommodate other non-Gaussian signals and/or interferers. For the zero mean case, an alternate expression for the regularized upper incomplete gamma function (see Lemma 3) was required. However, when the interfering signals and/or the PU desired signal are non-zero mean, then the statistics for the decision variable of the ED becomes non-central chi-square distributed. Hence, the CDF is in terms of the generalized Marcum Q-function under both hypotheses. In order to employ a similar approach to that utilized in Chapter 4 of this thesis, it would be necessary to express the Marcum Q-function in an alternate form (similar to the form in Lemma 3) in which the random variables are contained only as a linear sum in the exponents, to ease the process of averaging out the random variables. Note that this desired form exists in the literature [173] as

$$Q_m(x,y) = \frac{1}{2\pi j}\oint_{\Gamma} \frac{e^{g(z)}}{z^m(1-z)}\mathrm{dz} \tag{7.1}$$

where $g(z) = x^2((1/z)-1)/2 + y^2(z-1)/2$ and Γ is a circular contour of radius r that encloses the origin. However, the challenge to using Eq. (7.1) is two fold; There exists singularities to the integrand at $z=0$ and $z=1$ and this solution is only valid when the number of observed samples (N) is even (note that $m = {}^{N}/_{2}$ and hence m in (7.1) must be a positive integer). Nevertheless, when the detector observes odd samples such that m is a multiple of 0.5, the transformations reported in [174, eq. (11) and (14)] for $Q_{m-0.5}(.,.)$ and $Q_{m+0.5}(.,.)$ could be used. These expressions provide tight lower and upper bounds for $Q_m(x,y)$. Moreover, this can be supported by the fact that it was further shown in [174], that as m increases, the bounds become much tighter and that the average of the two bounds is a fairly good approximation to $Q_m(x,y)$ as well.

- In addition to the important aspect of interference management through contention control, the investigated models can be investigated and improved upon by considering power control mechanisms.

- In general, the noise statistics was assumed known to the receiver and the noise was white Gaussian, which may not be true in all cases. Relaxing this assumption will make room for further analysis of noise uncertainty.

- The analysis in Chapters 4 and 6 can be extended to consider multi-hop networks. This will enable the employment of similar techniques to relays and examination of various routing protocols. Particularly, the existing analysis lends itself to several routing strategies such as shortest distance routing, $k-$nearest neighbour routing and opportunistic routing strategies. In this case, the results in Chapters 4 and 6 will form the foundation for the single hop protocol from which the multi-hop analysis would be based.

- The models in Chapters 4 and 6 could also be extended by assuming scenarios in which the interfering nodes are not Poisson distributed. Other interference distributions such as the Beta distribution could form a basis for further work. Furthermore, the fading channels assumed in Chapters 3 - 6 could be extended to investigate the effect of frequency selectivity.

- In Chapter 5, several frameworks were proposed for different PU-SU frame states with or without timing synchronisation between the frames. However, in all cases an assumption of perfect bandwidth synchronisation was made. It would be worth while extending the model to account for the presence of frequency offset between the PU-SU frames.

- Additional work could be conducted by optimising sensing parameters, through adaptive threshold selection and cooperating spectrum sensing.

- The performance analysis of multiple-input interference channels has recently received much attention. It would be interesting to characterise and model sensing algorithms to improve the performance of MISO and MIMO systems beyond the SISO case.

References

[1] FCC, "Federal communications commission spectrum policy task force: Report of the spectrum efficiency working group," Nov. 2002.

[2] IEEE, "Standard definitions and concepts for dynamic spectrum access: Terminology relating to emerging wireless networks, system functionality, and spectrum management," *IEEE Std 1900.1-2008*, pp. c1 –48, Sept. 2008.

[3] I. Akyildiz, W. Lee, M. Vuran, and S. Mohanty, "Next generation/dynamic spectrum access/cognitive radio wireless networks: A survey," *Computer Networks*, vol. 50, no. 13, pp. 2127 – 2159, 2006.

[4] M. J. Marcus, "The underlay/overlay controversy," *IEEE Wireless Commun.*, vol. 14, no. 5, pp. 4–5, 2007.

[5] B. A. Fette and B. Fette, *Cognitive Radio Technology (Communications Engineering)*. Newnes, 2006.

[6] S. Haykin, "Cognitive radio: brain-empowered wireless communications," *IEEE J. Sel. Areas Commun.*, vol. 23, no. 2, pp. 201 – 220, Feb. 2005.

[7] FCC, "Facilitating opportunities for flexible, efficient, and reliable spectrum use employing cognitive radio technologies,," *ET Docket No. 03-108, Notice of proposed rule making and order*, Feb. 2005.

[8] M. A. Abdulsattar and Z. A. Hussein, "Energy detection technique for spectrum sensing in cognitive radio: A survey," *International Journal of Computer Networks and Communications (IJCNC)*, vol. 4, no. 5, pp. 223–242, Sep. 2012.

[9] FCC, "Public Notice DA 13-1472 : Office of Engineering and Technology Announces the Approval of Google Inc.s TV Bands Database System for Operation," *in ET Docket No. 04-186*, Jun. 2013.

[10] R. V. Prasad, P. Pawelczak, J. A. Hoffmeyer, and H. S. Berger, "Cognitive functionality in next generation wireless networks: Standardization efforts," *IEEE Commun. Mag.*, vol. 46, no. 4, pp. 72 –78, Apr. 2008.

[11] O. lleri and N. B. Mandayam, "Dynamic spectrum access models: Toward an engineering perspective in the spectrum debate," *IEEE Commun. Mag.*, vol. 46, no. 1, pp. 153 –160, Jan. 2008.

[12] P. Anker, "Does cognitive radio need policy innovation?" *First Annual Conf. on Competition and Regulation in Network Industries, CRNI '08*, pp. 23 – 31, Nov. 2008.

[13] G. R. Faulhaber, "The question of spectrum: Technology, management and regime change," *Journal on Telecommunications and High Technology Law*, vol. 4, no. 1, pp. 123 – 182, 2005.

[14] T. Yucek and H. Arslan, "A survey of spectrum sensing algorithms for cognitive radio applications," *IEEE Commun. Surveys Tuts.*, vol. 11, no. 1, pp. 116 –130, Jan. 2009.

[15] A. N. Mody, M. J. Sherman, R. Martinez, R. Reddy, and T. Kiernan, "Survey of IEEE standards supporting cognitive radio and dynamic spectrum access," in *IEEE Military Commun. Conf., MILCOM '08.*, 16-19 2008, pp. 1 –7.

[16] N. Golmie, N. Chevrollier, and O. Rebala, "Bluetooth and WLAN coexistence: Challenges and solutions," *IEEE Wireless Commun.*, vol. 10, no. 6, pp. 22 – 29, Dec. 2003.

[17] C. Cordeiro, K. Challapali, D. Birru, and N. Sai Shankar, "IEEE 802.22: the first worldwide wireless standard based on cognitive radios," in *First IEEE Int. Symp. on New Frontiers in Dynamic Spectrum Access Networks, DySPAN '05.*, 8-11 2005, pp. 328 –337.

[18] C. Stevenson, G. Chouinard, Z. Lei, W. Hu, S. Shellhammer, and W. Caldwell, "IEEE 802.22: The first cognitive radio wireless regional

area network standard," *IEEE Commun. Mag.*, vol. 47, no. 1, pp. 130 –138, Jan. 2009.

[19] T. Rappaport, *Wireless Communications: Principles and Practice*, 2nd ed. Prentice-Hall, 2002.

[20] M. Aljuaid and H. Yanikomeroglu, "Investigating the validity of the gaussian approximation for the distribution of the aggregate interference power in large wireless networks," in *25th Biennial Symp. on Commun. (QBSC)*, May 2010, pp. 122 –125.

[21] R. K. Ganti and M. Haenggi, "Interference and outage in clustered wireless ad hoc networks," *IEEE Trans. Inf. Theor.*, vol. 55, no. 9, pp. 4067–4086, Sep. 2009.

[22] J. Song, Z. Feng, P. Zhang, and Z. Liu, "Spectrum sensing in cognitive radios based on enhanced energy detector," *IET Commun.*, vol. 6, no. 8, pp. 805–809, 2012.

[23] Y. Chen, "Improved energy detector for random signals in gaussian noise," *IEEE Trans. Wireless Commun.*, vol. 9, no. 2, pp. 558 – 563, Feb. 2010.

[24] R. Tandra, A. Sahai, and S. M. Mishra, "What is a spectrum hole and what does it take to recognize one?" *Proc. IEEE*, vol. 97, no. 5, pp. 824 –848, May 2009.

[25] S. Haykin, D. J. Thomson, and J. H. Reed, "Spectrum sensing for cognitive radio," *Proc. IEEE*, vol. 97, no. 5, pp. 849–877, 2009.

[26] S. Maharjan, K. Po, and J. Takada, "Experimental study of energy detector prototype for cognitive radio system," in *in IEICE Technical Report, SR2007*.

[27] D. Cabric, S. M. Mishra, and R. W. Brodersen, "Implementation issues in spectrum sensing for cognitive radios," in *Conference Record of the Thirty-Eighth Asilomar Conference on Signals, Systems and Computers, 2004*, vol. 1, Nov. 2004, pp. 772 – 776.

[28] R. A. Dillard, "Detectability of spread-spectrum signals," *IEEE Trans. Aerosp. Electron. Syst.*, vol. AES-15, no. 4, pp. 526–537, Jul. 1979.

[29] J. J. Lehtomäki and M. Juntti, "Detection of frequency hopping signals using a sweeping channelized radiometer," *Signal Process.*, vol. 85, no. 10, pp. 2030–2043, 2005.

[30] J. J. Lehtomaki, J. Vartiainen, and H. Saarnisaari, "Domain selective interference excision and energy detection of direct sequence signals," in *Proc. of the 6th Nordic Signal Process. Symp., NORSIG '04.*, 2004, pp. 216 – 219.

[31] A. Sonnenschein and P. M. Fishman, "Radiometric detection of spread-spectrum signals in noise of uncertain power," *IEEE Trans. Aerosp. Electron. Syst.*, vol. 28, no. 3, pp. 654–660, Jul. 1992.

[32] S. A. Stoops, D. Norman, and G. E. Prescott, "Simulation of radiometers for detection of spread spectrum signals," vol. 1, Apr. 1990, pp. 355–368.

[33] R. Tandra and A. Sahai, "SNR walls for signal detection," *IEEE J. Sel. Topics Signal Process.*, vol. 2, no. 1, pp. 4 –17, Feb. 2008.

[34] A. Ghasemi and E. S. Sousa, "Spectrum sensing in cognitive radio networks: requirements, challenges and design trade-offs," *IEEE Commun. Mag.*, vol. 46, no. 4, pp. 32–39, Apr. 2008.

[35] W. Wang, "Spectrum sensing for cognitive radio," in *Third Int. Symp. on Intell. Inform. Technology Application Workshops, IITAW '09.*, Nov. 2009, pp. 410 –412.

[36] Q. H. Mahmoud, *Cognitive Networks: Towards Self-Aware Networks*, Q. H. Mahmoud, Ed. John Wiley & Sons, Ltd., 2007.

[37] M. J. Marcus, "Unlicensed cognitive sharing of tv spectrum: The controversy at the federal communications commission," *IEEE Commun. Mag.*, vol. 43, no. 5, pp. 24 – 25, May 2005.

[38] FCC, "Establishment of an interference temperature metric to quantify and manage interference and to expand available unlicensed operation in certain fixed, mobile and satellite frequency bands,," *ET Docket No. 03-237, Notice of Inquiry and Notice of proposed rule making*, Nov. 2003.

[39] T. C. Clancy, "Formalizing the interference temperature model," *Wireless Communications and Mobile Computing*, vol. 7, no. 9, pp. 1530–8677, 2007.

[40] T. C. Clancy and B. D. Walker, "Spectrum shaping for interference management in cognitive radio networks," in *Proceedings 2006 Software Defined Radio Technical Conference*, Nov. 2006.

[41] B. Sklar, *Digital Communications*. Prentice Hall, 1988.

[42] J. G. Proakis, *Digital Communications*, 4th ed. McGraw-Hill, 2001.

[43] R. A. Dillard and G. H. Dillard, *Detectability of Spread-Spectrum Signals*. Norwood, MA, USA: Artech House, Inc., 1989.

[44] R. F. Mills and G. E. Prescott, "A comparison of various radiometer detection models," *IEEE Trans. Aerosp. Electron. Syst.*, vol. 32, no. 1, pp. 467–473, Jan. 1996.

[45] J. B. Tsui, *Microwave Receivers with Electronic Warfare Applications*. Malabar, FL, USA: Krieger publishing company, 1992.

[46] J. Lehtomaki, "Analysis of Energy Based Signal Detection," Ph.D. dissertation, University of Oulu, Finland, Dec. 2005.

[47] H. Urkowitz, "Energy detection of unknown deterministic signals," *Proc. IEEE*, vol. 55, no. 4, pp. 523 – 531, Apr. 1967.

[48] V. I. Kostylev and M. P. Slichenko, "Energy detection of radio signals against the background of non-gaussian noise with unknown intensity," *Radiophysics and Quantum Electronics*, vol. 52, no. 11, pp. 910 – 920, Nov. 2009.

[49] V. I. Kostylev, "Energy detection of a signal with random amplitude," in *IEEE Int. Conf. Commun., ICC '02*, vol. 3, Apr.- May 2002, pp. 1606 – 1610.

[50] F. F. Digham, M.-S. Alouini, and M. K. Simon, "On the energy detection of unknown signals over fading channels," in *Proc. IEEE Int. Conf. Commun.*, vol. 5, May 2003, pp. 3575 – 3579.

[51] ——, "On the energy detection of unknown signals over fading channels," *IEEE Trans. Commun.*, vol. 55, no. 1, pp. 21 –24, Jan. 2007.

[52] Q. Wang and D. Yue, "A general parameterization quantifying performance in energy detection," *IEEE Signal Process. Lett.*, vol. 16, no. 8, pp. 699–702, Aug. 2009.

[53] S. P. Herath and N. Rajatheva, "Analysis of equal gain combining in energy detection for cognitive radio over nakagami channels," *IEEE Global Telecommunications Conf., GLOBECOM '08*, pp. 1–5, Nov. 2008.

[54] A. Sahai, N. Hoven, and R. Tandra, "Some fundamental limits on cognitive radio," in *in Forty-second Allerton Conference on Communication, Control, and Computing*, 2004.

[55] F. Hu and S. Wang, "Energy detection for spectrum sensing in cognitive radio sensor network over fading channels," *5th Int. Conf. on Wireless Communications, Networking and Mobile Computing, WiCom '09*, pp. 1 –4, Sep. 2009.

[56] Y. D. Alemseged and H. Harada, "Spectrum sensing for cognitive radio," *IEEE Radio and Wireless Symp., RWS '09.*, pp. 356–359, Jan. 2009.

[57] D. Cabric, A. Tkachenko, and R. W. Brodersen, "Experimental study of spectrum sensing based on energy detection and network cooperation," in *Proc. of First Int. Workshop on Technology and Policy for Accessing Spectrum, TAPAS*, 2006.

[58] S. H. Hwang, J. H. Baek, and O. A. Dobre, "Spectrum sensing using multiple antenna-aided energy detectors for cognitive radio," *2009 IEEE 22nd Canadian Conference on Electrical and Computer Engineering, Vols 1 and 2*, pp. 66–69.

[59] E. H. Gismalla and E. Alsusa, "On the performance of energy detection using bartlett's estimate for spectrum sensing in cognitive radio systems," *IEEE Trans. Signal Process.*, vol. 60, no. 7, pp. 3394–3404, 2012.

[60] ——, "Performance analysis of the periodogram-based energy detector in fading channels," *IEEE Trans. Signal Process.*, vol. 59, no. 8, pp. 3712–3721, 2011.

[61] ——, "On the detection of unknown signals using welch overlapped segmented averaging method," in *IEEE Vehicular Technology Conference (VTC Fall)*, 2011, pp. 1–5.

[62] S. S. Jeong, W. S. Jeon, and D. G. Jeong, "Collaborative spectrum sensing for multiuser cognitive radio systems," *IEEE Trans. Veh. Technol.*, vol. 58, no. 5, pp. 2564 –2569, Jun. 2009.

[63] G. Ganesan and Y. Li, "Agility improvement through cooperative diversity in cognitive radio," in *IEEE Global Telecommunications Conference, GLOBECOM '05.*, vol. 5, Dec. 2005, pp. 2505 –2509.

[64] S. M. Mishra, A. Sahai, and R. W. Brodersen, "Cooperative sensing among cognitive radios," in *IEEE Int. Conf. on Commun., 2006. ICC '06.*, vol. 4, Jun. 2006, pp. 1658 –1663.

[65] T. Sung, "Cooperative spectrum sensing for cognitive radio with multiple secondary users," in *IEEE Radio and Wireless Symp., RWS '10*, Jan. 2010, pp. 693 –696.

[66] A. Ghasemi and E. S. Sousa, "Opportunistic spectrum access in fading channels through collaborative sensing," *Journal of Commun.*, vol. 2, no. 2, pp. 71 – 82, Mar. 2007.

[67] G. Ganesan and Y. Li, "Cooperative spectrum sensing in cognitive radio, part I: Two user networks," *IEEE Trans. Wireless Commun.*, vol. 6, no. 6, pp. 2204 –2213, Jun. 2007.

[68] J. Unnikrishnan and V. V. Veeravalli, "Cooperative spectrum sensing and detection for cognitive radio," in *IEEE Global Telecommunications Conference, GLOBECOM '07.*, Nov. 2007, pp. 2972 –2976.

[69] B. Shen, L. Y. Huang, C. Zhao, Z. Zhou, and K. Kwak, "Energy detection based spectrum sensing for cognitive radios in noise of uncertain power," in *2008 Int. Symp. on Commun. and Information Technologies*, pp. 630–635.

[70] S. Kyperountas, N. Correal, Q. Shi, and Z. Ye, "Performance analysis of cooperative spectrum sensing in suzuki fading channels," in *2nd Int.*

Conf. on Cognitive Radio Oriented Wireless Networks and Commun., CrownCom '07., Aug. 2007, pp. 428 –432.

[71] S. M. Kay, *Fundamentals of Statistical Signal Processing, Volume II: Detection Theory*. Indian Ed.: Dorling Kindersely, 2010.

[72] L. Gradshteyn and I. Rhyzik, *Table of Integrals, Series and Products*, 7th ed. Academic Press, 2007.

[73] S. Atapattu, C. Tellambura, and H. Jiang, "Analysis of area under the ROC curve of energy detection," *IEEE Trans. Wireless Commun.*, vol. 9, no. 3, pp. 1216–1225, Mar. 2010.

[74] M. Kaynia, "Analysis and Improvement of Wireless Ad Hoc Network Performance Through MAC and PHY Layer Design," Ph.D. dissertation, Norwegian University of Science and Technology, Nov. 2010.

[75] B. Wild and K. Ramchandran, "Detecting primary receivers for cognitive radio applications," in *First IEEE Int. Symp. on New Frontiers in Dynamic Spectrum Access Networks, DySPAN '05.*, 8-11 2005, pp. 124 –130.

[76] A. F. Molisch, *Wireless Communications*. Weat Sussex, England: John Wiley & sons Ltd., 2005.

[77] R. S. Dhillon and T. X. Brown, "Models for analyzing cognitive radio interference to wireless microphones in TV bands," in *3rd IEEE Symp. on New Frontiers in Dynamic Spectrum Access Networks, DySPAN '08.*, 14-17 2008, pp. 1–10.

[78] A. Ghasemi, "Statistical characterization of interference in cognitive radio networks," in *IEEE 19th Int. Symp. on Personal, Indoor and Mobile Radio Commun., PIMRC '08.*, 15-18 2008, pp. 1–6.

[79] A. Ghasemi and E. S. Sousa, "Spectrum sensing in cognitive radio networks: the cooperation-processing tradeoff," *Wireless Communications and Mobile Computing*, vol. 7, no. 9, pp. 1049–1060, 2007.

[80] X. Hong, C. Wang, and J. Thompson, "Interference modeling of cognitive radio networks," in *IEEE Veh. Technology Conf., VTC Spring '08.*, 11-14 2008, pp. 1851 –1855.

[81] Q. Liu and Z. Zhong, "Statistical analysis of interference in cognitive networks," in *IEEE 20th Int. Symp. on Personal, Indoor and Mobile Radio Commun., '09*, 13-16 2009, pp. 345–349.

[82] Q. Liu, Z. Zhou, C. Yang, and Y. Ye, "Outage probability analysis for cognitive radio network caused by primary users," in *Third Int. Conf. on Communications and Networking in China, ChinaCom '08.*, 25-27 2008, pp. 1222 –1225.

[83] Q. Yang, X. An, and K. S. Kwak, "Outage probability analysis for cognitive radios with reception diversity," in *Int. Workshop on Cross Layer Design, IWCLD '07*, 20-21 2007, pp. 37 –40.

[84] P. von Rickenbach, S. Schmid, R. Wattenhofer, and A. Zollinger, "A robust interference model for wireless ad-hoc networks," in *19th IEEE Int. Parallel Distrib. Process. Symp.'05.*, 4-8 2005, p. 8 pp.

[85] P. von Rickenbach, R. Wattenhofer, and A. Zollinger, "Algorithmic models of interference in wireless ad hoc and sensor networks," *IEEE/ACM Trans. Netw.*, vol. 17, no. 1, pp. 172 –185, Feb. 2009.

[86] M. Vu, N. Devroye, and V. Tarokh, "On the primary exclusive region of cognitive networks," *IEEE Trans. Wireless Commun.*, vol. 8, no. 7, pp. 3380 –3385, Jul. 2009.

[87] A. Goldsmith, *Wireless Communications*. Cambridge University Press, N.Y., 2005.

[88] R. L. Pickholtz, D. L. Schilling, and L. B. Milstein, "Theory of spread-spectrum communications–a tutorial," *IEEE Trans. Commun.*, vol. 30, no. 5, pp. 855–884, 1982.

[89] R. Steele and L. Hanzo, *Mobile Radio Communications*, 2nd ed. John Wiley & Sons, London, 1999.

[90] L. Kleinrock and F. A. Tobagi, "Packet switching in radio channels: Part I - carrier sense multiple-access modes and their throughput-delay characteristics," *IEEE Trans. Commun.*, vol. 23, no. 12, pp. 1400–1416, 1975.

[91] G. Bianchi, "Performance analysis of the IEEE 802.11 distributed coordination function," *IEEE J. Sel. Areas Commun.*, vol. 18, no. 3, pp. 535–547, 2000.

[92] K. Xu, M. Gerla, and S. Bae, "How effective is the IEEE 802.11 RTS/CTS handshake in ad hoc networks," in *IEEE Global Telecommun. Conf., GLOBECOM '02*, vol. 1, Nov. 2002, pp. 72 – 76.

[93] J. Zhu, X. Guo, L. L. Yang, and W. S. Conner, "Leveraging spatial reuse in 802.11 mesh networks with enhanced physical carrier sensing," in *IEEE Int. Conf. on Commun., ICC*, vol. 7, Jun. 2004, pp. 4004 – 4011.

[94] H. Ma, H. M. K. Alazemi, and S. Roy, "A stochastic model for optimizing physical carrier sensing and spatial reuse in wireless ad hoc networks," in *IEEE Int. Conf. on Mobile Adhoc and Sensor Systems Conf., MASS*, Nov. 2005, pp. 615–622.

[95] ——, "A stochastic model for optimizing physical carrier sensing and spatial reuse in wireless ad hoc networks," in *IEEE Int. Conf. on Mobile Adhoc and Sensor Systems Conf. (MASS)*, 2005.

[96] H. Zhai and Y. Fang, "Physical carrier sensing and spatial reuse in multirate and multihop wireless ad hoc networks," in *IEEE INFOCOM*, 2006.

[97] F.-Y. Hung and I. Marsic, "Effectiveness of physical and virtual carrier sensing in ieee 802.11 wireless ad hoc networks," in *IEEE Wireless Commun. and Networking Conf., WCNC'07*, 2007, pp. 143–147.

[98] P802.11, "IEEE Standard for Information Technology- Telecommunications and Information Exchange Between Systems- Local and Metropolitan Area Networks- Specific Requirements- Part 11: Wireless LAN Medium Access Control (MAC) and Physical Layer (PHY) Specifications," IEEE Standard 802.11, Jun. 1999.

[99] L. Liu, S. M. Kuo, and M. Zhou, "Virtual sensing techniques and their applications," in *IEEE Int. Conf. on Networking, Sensing and Control, ICNSC '09*, 2009, pp. 31–36.

[100] C.-K. Toh, *Ad Hoc Mobile Wireless Networks: Protocols and Systems*, 2nd ed. Prentice Hall, N.J., 2002.

[101] R. Ware and F. Lad, "Approximating the distribution for sums of products of normal variables," *University of Canterbury, England, Tech. Rep. UCDMS*, vol. 15, 2003.

[102] S. Nadarajah, "A review of results on sums of random variables," *Acta Applicandae Mathematicae: An International Survey Journal on Applying Mathematics and Mathematical Applications*, vol. 103, no. 2, pp. 131–140, 2008. [Online]. Available: http://dx.doi.org/10.1007/s10440-008-9224-4.

[103] F. Yilmaz and M.-S. Alouini, "Sum of weibull variates and performance of diversity systems," in *Int. Conf. on Wireless Commun. and Mobile Computing (IWCMC)*, 2009, pp. 247–252.

[104] J. C. S. S. Filho and M. D. Yacoub, "Simple precise approximations to weibull sums," *IEEE Commun. Lett.*, vol. 10, no. 8, pp. 614–616, 2006.

[105] D. Da Costa, M. D. Yacoub, and J. C. S. S. Filho, "Highly accurate closed-form approximations to the sum of $\alpha - \mu$ variates and applications," *IEEE Trans. Wireless Commun.*, vol. 7, no. 9, pp. 3301–3306, 2008.

[106] J. C. S. S. Filho and M. D. Yacoub, "Highly accurate $\eta - \mu$ approximation to the sum of M independent nonidentical hoyt variates," *IEEE Antennas Wireless Propag. Lett.*, vol. 4, pp. 436–438, 2005.

[107] ——, "Highly accurate $\kappa - \mu$ approximation to sum of M independent non-identical ricean variates," *Electron. Lett.*, vol. 41, no. 6, pp. 338–339, 2005.

[108] ——, "Nakagami-m approximation to the sum of M non-identical independent nakagami-m variates," *Electron. Lett.*, vol. 40, no. 15, pp. 951–952, 2004.

[109] I. S. Ansari, F. Yilmaz, and M.-S. Alouini, "On the sum of squared $\eta - \mu$ random variates with application to the performance of wireless communication systems," *arXiv preprint arXiv:1210.0100*, Sep. 2012.

[110] M. D. Yacoub, "The $\alpha - \mu$ distribution: A general fading distribution," in *The 13th IEEE Int. Symp. on Personal, Indoor and Mobile Radio Commun. (PIMRC)*, vol. 2, 2002, pp. 629–633.

[111] M. K. Simon and M. S. Alouini, *Digital Communication over Fading Channels: A Unified Approach to Performance Analysis*, 1st ed. Wiley, 2000.

[112] M. Abramowitz and I. A. Stegun, *Handbook of Mathematical Functions with Formulas, Graphs, and Mathematical Tables*, ninth dover printing, tenth gpo printing ed. New York: Dover, 1964.

[113] A. P. Prudnikov, Y. A. Brychkov, and M. O. I., *Integrals and Series*. Gordon and Breach, 1990, vol. 3.

[114] A. U. Makarfi and K. A. Hamdi, "Interference analysis of energy detection for spectrum sensing," *IEEE Trans. Veh. Technol.*, vol. 62, no. 6, pp. 2570–2578, Jul. 2013.

[115] ——, "Efficiency of energy detection for spectrum sensing in the presence of non-cooperating secondary users," in *IEEE Global Communications Conference, GLOBECOM*, Dec. 2012, pp. 4939–4944.

[116] ——, "Efficiency of energy detection for spectrum sensing in a poisson field of interferers," in *IEEE Wireless Commun. and Networking Conf. (WCNC)*, Apr. 2012, pp. 1023–1028.

[117] L. Wei and O. Tirkkonen, "Cooperative spectrum sensing of OFDM signals using largest eigenvalue distributions," in *IEEE 20th Int. Symp. on Personal, Indoor and Mobile Radio Commun.*, 13-16 2009, pp. 2295 –2299.

[118] S. Kusaladharma and C. Tellambura, "On approximating the cognitive radio aggregate interference," *IEEE Wireless Commun. Lett.*

[119] ——, "Aggregate interference analysis for underlay cognitive radio networks," *IEEE Wireless Commun. Lett.*, vol. 1, no. 6, pp. 641–644, 2012.

[120] K. W. Sung, M. Tercero, and J. Zander, "Aggregate interference in secondary access with interference protection," *IEEE Commun. Lett.*, vol. 15, no. 6, pp. 629–631, Jun. 2011.

[121] Z. Chen, C.-X. Wang, X. Hong, J. Thompson, S. Vorobyov, X. Ge, H. Xiao, and F. Zhao, "Aggregate interference modeling in cognitive radio networks with power and contention control," *IEEE Trans. Commun.*, vol. 60, no. 2, pp. 456–468, Feb. 2012.

[122] Y. Zeng, Y.-C. Liang, A. T. Hoang, and E. C. Y. Peh, "Reliability of spectrum sensing under noise and interference uncertainty," in *IEEE Int. Conf. on Commun. Workshops '09*, Jun. 2009, pp. 1–5.

[123] E. Biglieri, "Effect of uncertainties in modeling interferences in coherent and energy detectors for spectrum sensing," in *IEEE Int. Symp. on Inform. Theory (ISIT)*, Aug. 2011, pp. 2418 –2421.

[124] J. Nieminen, R. Jantti, and L. Qian, "Primary user detection in distributed cognitive radio networks under timing inaccuracy," in *IEEE Symposium on New Frontiers in Dynamic Spectrum, DYSPAN'10*, Apr. 2010, pp. 1 – 8.

[125] S. H. Song, K. Hamdi, and K. B. Letaief, "Spectrum sensing with active cognitive systems," *IEEE Trans. Wireless Commun.*, vol. 9, no. 6, pp. 1849–1854, Jun. 2010.

[126] H. Inaltekin, S. B. Wicker, M. Chiang, and H. V. Poor, "On unbounded path-loss models: effects of singularity on wireless network performance," *IEEE Journal on Selected Areas in Commun.*, vol. 27, no. 7, pp. 1078–1092, Sep. 2009.

[127] N. H. Mahmood, F. Yilmaz, M. S. Alouini, and G. E. Oien, "On the ergodic capacity of legacy systems in the presence of next generation interference," in *proc. 2011 8th Int. Symp. on Wireless Commun. Systems (ISWCS)*, Nov. 2011, pp. 462 – 466.

[128] A. Nuttall, "Some integrals involving the Q_m function (corresp.)," *IEEE Trans. Inf. Theor.*, vol. 21, no. 1, pp. 95 – 96, Jan. 1975.

[129] Y. M. Shobowale and K. A. Hamdi, "A unified model for interference analysis in unlicensed frequency bands," *IEEE Trans. Wireless Commun.*, vol. 8, no. 8, pp. 4004 – 4013, Aug. 2009.

[130] E. S. Sousa and J. A. Silvester, "Optimum transmission ranges in a direct-sequence spread-spectrum multihop packet radio network," *IEEE J. Select. Areas Commun.*, vol. 8, no. 5, pp. 762–771, Jun. 1990.

[131] J. Ahmed and K. A. Hamdi, "On the coexistence of uncoordinated ad-hoc networks," in *IEEE Global Telecommunications Conference, GLOBECOM*, Dec. 2010, pp. 1–5.

[132] S. Ross, *A First Course in Probability*, 1st ed. Macmillan, 1976.

[133] P. C. Pinto and M. Z. Win, "Communication in a poisson field of interferers–part i: Interference distribution and error probability," *IEEE Trans. Wireless Commun.*, vol. 9, no. 7, pp. 2176 – 2186, Jul. 2010.

[134] S. M. Ross, *Introduction to Probability Models*, 7th ed. Academic Press, 2000.

[135] D. Bhargavi and C. R. Murthy, "Performance comparison of energy, matched-filter and cyclostationarity-based spectrum sensing," in *IEEE Eleventh Int. Workshop on Signal Process. Advances in Wireless Commun. (SPAWC)*, Jun. 2010, pp. 1 –5.

[136] R. Tandra and A. Sahai, "Snr walls for feature detectors," in *2nd IEEE International Symposium on New Frontiers in Dynamic Spectrum Access Networks, (DySPAN)*, Apr. 2007, pp. 559 – 570.

[137] E. Biglieri, "Spectrum sensing under uncertain channel modeling," *J. Commun. and Networks*, vol. 14, no. 3, pp. 225 – 229, Jun. 2012.

[138] ——, "Effect of uncertainties in modelling interference in spectrum sensors," *Electron. Lett.*, vol. 47, no. 13, pp. 776 –778, Jun. 2011.

[139] A. U. Makarfi and K. A. Hamdi, "Wideband spectrum sensing framework for multiple slow frequency hopping primary users," in *proc. IEEE Wireless Commun. and Networking Conf. (WCNC)*, Apr. 2012, pp. 2653 – 2658.

[140] ——, "Wideband sensing of slow FH primary users with unknown hop duration," in *proc. IEEE Wireless Commun. and Networking Conf. (WCNC)*, Apr. 2013, pp. 3370–3375.

[141] Z. Quan, S. Cui, H. Poor, and A. Sayed, "Collaborative wideband sensing for cognitive radios," *IEEE Signal Processing Mag.*, vol. 25, no. 6, pp. 60 –73, Nov. 2008.

[142] L. Khalid, K. Raahemifar, and A. Anpalagan, "Cooperative spectrum sensing for wideband cognitive OFDM radio networks," in *proc. 70th IEEE Veh. Technol. Conf. VTC Fall*, Sep. 2009, pp. 1 –5.

[143] Z. Quan, S. Cui, A. H. Sayed, and H. V. Poor, "Optimal multiband joint detection for spectrum sensing in cognitive radio networks," *IEEE Trans. Signal Process.*, vol. 57, no. 3, pp. 1128–1140, Mar. 2009.

[144] P. Paysarvi-Hoseini and N. Beaulieu, "Optimal wideband spectrum sensing framework for cognitive radio systems," *IEEE Trans. Signal Process.*, vol. 59, no. 3, pp. 1170 –1182, Mar. 2011.

[145] B. Zhen, Y. Kim, and K. Jang, "The analysis of coexistence mechanisms of bluetooth," in *proc. 55th IEEE Veh. Technol. Conf., VTC Spring*, vol. 1, May 2002, pp. 419 – 423.

[146] A. C. C. Hsu, D. S. L. Wei, C. C. J. Kuo, N. Shiratori, and C. J. Chang, "Enhanced adaptive frequency hopping for wireless personal area networks in a coexistence environment," in *proc. IEEE Global Telecommun. Conf. GLOBECOM '07.*, Nov. 2007, pp. 668 – 672.

[147] S.-H. Lee, H.-S. Kim, and Y.-H. Lee, "Mitigation of co-channel interference in bluetooth piconets," *IEEE Trans. Wireless Commun.*, vol. 11, no. 4, pp. 1249 – 1254, Apr. 2012.

[148] D. Torrieri, *Principles of Military Communication Systems*. MA: Artech, 1981.

[149] T. Wang, Y. Chen, E. L. Hines, and B. Zhao, "Analysis of effect of primary user traffic on spectrum sensing performance," in *proc. Fourth Int. Conf. on Commun. and Networking in China, ChinaCOM*, Aug. 2009, pp. 1 – 5.

[150] L. B. W. Jolley, *Summation of Series*, 2nd ed. Dover, N.Y., 1961.

[151] K. A. Hamdi, "Capacity of mrc on correlated rician fading channels," *IEEE Trans. Commun.*, vol. 56, no. 5, pp. 708–711, May 2008.

[152] P. Chatzimisios, A. C. Boucouvalas, and V. Vitsas, "IEEE 802.11 packet delay: A finite retry limit analysis," in *IEEE Global Telecommun. Conf., GLOBECOM '03*, vol. 2, 2003, pp. 950–954.

[153] P. Latkoski, Z. Hadzi-Velkov, and B. Popovski, "Extended model for performance analysis of non-saturated IEEE 802.11 DCF in erroneous channel," in *IEEE Int. Conf. on Mobile Adhoc and Sensor Systems (MASS)*, 2006, pp. 783–788.

[154] E. J. Leonardo and M. D. Yacoub, "Exact formulations for the throughput of ieee 802.11 dcf in hoyt, rice, and nakagami-m fading channels," *IEEE Trans. Wireless Commun.*, vol. 12, no. 5, pp. 2261–2271, 2013.

[155] A. Pal and A. Nasipuri, "Performance analysis of IEEE 802.11 distributed coordination function in presence of hidden stations under non-saturated conditions with infinite buffer in radio-over-fiber wireless LANs," in *18th IEEE Workshop on Local Metropolitan Area Networks (LANMAN)*, 2011, pp. 1–6.

[156] D. Malone, K. Duffy, and D. Leith, "Modeling the 802.11 distributed coordination function in nonsaturated heterogeneous conditions," *IEEE/ACM Trans. Netw.*, vol. 15, no. 1, pp. 159–172, 2007.

[157] V. Pourahmadi, S. H. Jamali, and R. Safavi-Naieeni, "Saturated throughput analysis of the IEEE 802.11b DCF mode in a slow rayleigh fading channel," in *13th IEEE Int. Conf. Netw.*, vol. 1, 2005.

[158] S. G. Glisic, R. Rao, and L. Milstein, "The effect of imperfect carrier sensing on nonpersistent carrier sense multiple access," in *Supercomm Technical Sessions, SUPERCOMM in IEEE Int. Conf. on Commun., ICC '90*, vol. 3, 1990, pp. 1266–1269.

[159] S. G. Glisic, "1-persistent carrier sense multiple access in radio channels with imperfect carrier sensing," *IEEE Trans. Commun.*, vol. 39, no. 3, pp. 458–464, 1991.

[160] T. H. Kim, J. Ni, R. Srikant, and N. H. Vaidya, "On the achievable throughput of CSMA under imperfect carrier sensing," in *Proc. IEEE INFOCOM*, 2011, pp. 1674–1682.

[161] ——, "Throughput-optimal CSMA with imperfect carrier sensing," pp. 1–15, 2013.

[162] I. Ramachandran and S. Roy, "Analysis of throughput and energy efficiency of p-persistent CSMA with imperfect carrier sensing," in *IEEE Global Telecommun. Conf., GLOBECOM '05*, vol. 6, 2005, pp. 3428–3432.

[163] J. Sheng and K. S. Vastola, "Physical carrier sensing outage in single hop IEEE 802.11 ad hoc networks with slowly moving stations," in *IEEE Wireless Commun. and Networking Conf., WCNC'08*, 2008, pp. 1350–1355.

[164] F. Ye and B. Sikdar, "Distance-aware virtual carrier sensing for improved spatial reuse in wireless networks," in *IEEE Global Telecommun. Conf., GLOBECOM '04*, vol. 6, 2004, pp. 3793–3797.

[165] H. Ma and S. Roy, "Simple and effective carrier sensing adaptation for multi rate ad-hoc mesh networks," in *IEEE Int. Conf. on Mobile Adhoc and Sensor Systems Conf. (MASS)*, 2006, pp. 795–800.

[166] J. P. Monks, V. Bharghavan, and W.-M. W. Hwu, "A power controlled multiple access protocol for wireless packet networks," in *Proc. IEEE INFOCOM*, vol. 1, Apr. 2001, pp. 219–228.

[167] Y.-B. Ko, V. Shankarkumar, and N. F. Vaidya, "Medium access control protocols using directional antennas in ad hoc networks," in *Proc. IEEE INFOCOM*, vol. 1, Mar. 2000, pp. 13–21.

[168] L. Fu, S. C. Liew, and J. Huang, "Effective carrier sensing in csma networks under cumulative interference," *IEEE Trans. Mobile Comput.*, vol. 12, no. 4, pp. 748–760, 2013.

[169] A. Busson and G. Chelius, "Point processes for interference modeling in CSMA/CA ad-hoc networks," in *Proc. of the 6th ACM symposium on Performance evaluation of wireless ad hoc, sensor, and ubiquitous networks*, ser. PE-WASUN '09. New York, NY, USA: ACM, 2009, pp. 33–40. [Online]. Available: http://doi.acm.org/10.1145/1641876.1641884

[170] P. Gupta and P. R. Kumar, "The capacity of wireless networks," *IEEE Trans. Inf. Theory*, vol. 46, no. 2, pp. 388–404, 2000.

[171] D. Stoyan, W. S. Kendall, and J. Mecke, *Stochastic Geometry and its Applications*, 2nd ed. Wiley, 2002.

[172] G. Ferrari and O. K. Tonguz, "MAC protocols and transport capacity in ad hoc wireless networks: Aloha versus PR-CSMA," in *IEEE Military Communications Conference, MILCOM*, vol. 2, 2003, pp. 1311–1318.

[173] C. Tellambura, A. Annamalai, and V. K. Bhargava, "Closed form and infinite series solutions for the mgf of a dual-diversity selection combiner output in bivariate nakagami fading," *IEEE Trans. Commun.*, vol. 51, no. 4, pp. 539 – 542, Apr. 2003.

[174] R. Li and P.-Y. Kam, "Computing and bounding the generalized marcum q-function via a geometric approach," in *2006 IEEE Int. Symp. on Information Theory*, 2006, pp. 1090–1094.

Appendix A

Mathematical Transformations

This appendix is presented for quick reference. It summarises the main transformations of mathematical expressions employed in this thesis that led to the efficient computation of the averages of random variables encountered in the analysis. These transformations are presented under two sections, namely; novel transformations conducted under this research and those transformations employed in this thesis but existing within the literature.

A.1 Summary of Novel Transformations

Here a summary of the novel transformations derived and employed in this study are presented

- From Lemma 1, the Marcum $Q-$function, with $m = 0.5$ can be expressed as

$$Q_{\frac{1}{2}}\left(\sqrt{2\gamma}, \sqrt{\frac{\lambda}{N}}\right) = \frac{1}{2}\left\{\text{Erfc}\left(\frac{\sqrt{\lambda} - \sqrt{2N\gamma}}{\sqrt{2N}}\right) + \text{Erfc}\left(\frac{\sqrt{\lambda} - \sqrt{2N\gamma}}{\sqrt{2N}}\right)\right\}.$$

  The proof is at (3.35) - (3.37).

- The error function of the form $\text{Erf}\,(y \pm b)$ can be expressed as Eq. (3.38) given in Lemma 2. For any $y > 0$ then

$$\text{Erf}\,(y \pm b) = \pm\text{Erf}\,(b) + \frac{2}{\sqrt{\pi}}\int_0^y \exp\left(-\left(x^2 \pm 2bx + b^2\right)\right) dx$$

  where the proof is outlined in (3.39) - (3.42).

- The regularised upper incomplete gamma function can be expressed in the form presented in Lemma 3

$$\frac{\Gamma\left(N/2, \xi/\vartheta\right)}{\Gamma\left(N/2\right)} = 1 - \frac{1}{\Gamma\left(\frac{N}{2}\right)} \int_0^\infty z^{\frac{N}{4}-1} J_{\frac{N}{2}}\left(2\sqrt{z}\right) \exp\left(-\frac{z\vartheta}{\xi}\right) dz$$

  where $J_v\left(.\right)$ is the vth order Bessel function of the first kind. The proof can be found at (4.13) - (4.18).

- In Lemma 4, an alternative expression to the complementary error function of the form $\text{Erfc}\left(\xi\sqrt{\frac{N}{x}}\right)$ is presented. For any variable $x > 0$, then

$$\text{Erfc}\left(\xi\sqrt{\frac{N}{x}}\right) = 1 - \frac{1}{\pi}\int_0^\infty \frac{\sin\left(2\xi\sqrt{zN}\right)}{z} e^{-zx} dz.$$

  The proof is at (4.67)-(4.69).

A.2 Other Important Transformations

The transformation at Eq. (5.50) was presented in [151, Eq. (7)]. For any $x > 0$, then

$$\log_2\left(1+x\right) = \log_2 e \int_0^\infty \frac{1}{z}\left(1 - e^{-zx}\right) e^{-z} dz. \tag{A.1}$$

The proof is reproduced as follows. For all $x \geq 0$, recall the identity [112, Eq. (4.1.25)]

$$\ln\left(1+x\right) = \sum_{n=1}^{\infty} \frac{1}{n}\left(\frac{x}{1+x}\right)^n, \quad x \geq 0. \tag{A.2}$$

Then invoking the identity [72, Eq. (8.312.2)]

$$x^n = \int_0^\infty \frac{s^{n-1}}{\Gamma\left(n\right)} e^{-\frac{s}{x}} ds, \quad n, x > 0$$

(A.2) becomes

$$\begin{aligned}\ln(1+x) &= \sum_{n=1}^{\infty} \frac{1}{n} \int_0^{\infty} \frac{s^{n-1}}{\Gamma(n)} e^{-s\frac{1+x}{x}} ds \\ &= \int_0^{\infty} \left\{ \sum_{n=1}^{\infty} \frac{1}{n} \frac{s^{n-1}}{\Gamma(n)} \right\} e^{-s\frac{1+x}{x}} ds \\ &= \int_0^{\infty} \left\{ \frac{1}{s}\left(e^s - 1\right) \right\} e^{-s\frac{1+x}{x}} ds \end{aligned} \tag{A.3}$$

where the last line of (A.3) is obtained using the fact that $\Gamma(n) = (n-1)!$ and $e^s = \sum_{n=1}^{\infty} \frac{s^n}{n!}$. Thereafter, $s = zx$ is substituted to obtain

$$\ln(1+x) = \int_0^{\infty} \frac{1}{z}\left(1 - e^{-zx}\right) e^{-z} dz$$

which can easily be rearranged to the form of (A.1) as required.